STELLAR ASTROPHYSICS: A STUDY OF STELLAR PHYSICS WITH PARTICULAR REFERENCE TO LOW MASS STARS

Guo Quan Luo

A Thesis Submitted for the Degree of PhD
at the
University of St Andrews

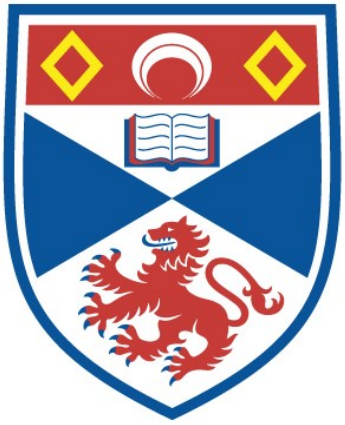

1991

STELLAR ASTROPHYSICS

A STUDY OF STELLAR PHYSICS WITH PARTICULAR REFERENCE TO LOW MASS STARS

BY

GUO QUAN LUO

A Thesis presented for the Degree of Doctor of Philosophy

in the University of St Andrews

May 1991

ProQuest LLC.
789 East Eisenhower Parkway
P.O. Box 1346
Ann Arbor, MI 48106 – 1346

CERTIFICATE

I hereby certify that the candidate has fulfilled the conditions and regulations appropriate to the degree of Ph.D. of the University of St. Andrews and that he is qualified to submit this thesis in application for that degree.

T. R. CARSON

(Supervisor)

DECLARATION

I, Guo Quan Luo, hereby certify that this thesis, which is approximately 30,000 words in length, has been written by me, and that it has not been submitted in any previous application for a higher degree.

I was admitted as a research student under Ordinance No.12 on the January 1988 and as a candidate for the degree of Ph.D. on the January 1989; the higher study for which this is a record was carried out in the University of St Andrews between 1988 and 1991.

G. Q. LUO

In submitting this thesis to the University of St Andrews I understand that I am giving permission for it to be made available for use in accordance with the regulations of the University Library for the time being in force, subject to any copyright vested in the work not being affected thereby. I also understand that the title and abstract will be published, and that a copy of the work may be made and supplied to any bona fide library or research worker.

G. Q. LUO

ACKNOWLEDGEMENTS

I would like to express my thanks to the following :

Dr T. R. Carson, my supervisor, for his suggesting the project of the low mass stars, his valuable advice and guidance, his generously permitting me to use his code of stellar structure and evolution as well as the molecular opacity data, and also for his patience with correction of my thesis. Professor W. Sibbett , Chairman of the Physics and Astronomy department, for the facilities made available to me, which have helped the project run smoothly. The British Council and Chinese government for the award of a research studentship.

Thanks are also due to Dr C. S. Jeffery and Professor D. W. N. Stibbs for their reading my writing and many helpful comments. Mr J. R. Stapleton, the research students and staff of the Astronomy group for their helping me with the use of Starlink computer. The staff at the St. Andrews University Computer Centre for their assistance in the use of computing facilities.

I also wish to thank Mrs. U. Carson, Dr. R. M. Amin, and other friends for their spiritual support and encouragement to my life and study.

Abstract

In this thesis we investigate the importance of various elements of the input physics and other parameters which affect the structure and evolution of models of low mass stars.

Of the elements of input physics, the nuclear generation rates, the electron screening effect on thermo-nuclear reactions, and the conductive opacities are adopted from the formulation or data tables by other contributors. The low temperature opacities are taken from the data calculated by Carson and Sharp, as well as those by Alexander.

In our study, we establish a sophisticated model for the determination of the equation of state. It is formulated by a new method based on the theory of the grand canonical ensemble. The interatomic interactions, which are responsible for the nonideal effects and pressure ionization, are treated carefully in the equation of state. In addition, and consistent with the equation of state, we also evaluate the radiative opacity according to the average atom model for heavy elements and the hydrogen-like model for hydrogen and helium. Negative hydrogen absorption and free electron scattering are also included. A computing code is constructed to calculate the radiative opacity data which are required in the study of low mass stars.

To investigate the importance of each element of the input physics, we exclude it or replace it with an alternative for the model calculations. The parameters of the stellar code , such as the element abundances, the surface condition and the mixing length ratio are as well investigated by alternative values or formulation. In the computation, all elements of input physics, except the energy generation rates, are incorporated into the main code by means of data tables. A bicubic interpolation is used for their input.

Our numerical calculations cover the zero age main sequence of the stars ranging from a solar mass down to the hydrogen burning minimum mass. The calculated results of the zero age models for the Standard Population I and Population II indicate good agreement

with the observed data for the objects with effective temperatures above 3000 K, or with masses greater than 0.15 M_{sun}. Below this limit, in agreement with other theoretical work, there is still a small discrepancy between the theoretical models and the observed data.

The investigations of the effects of the input physics and model parameters show that some of them affect considerably the minimum mass limit for hydrogen burning on the lower main sequence. The low temperature opacities, the nonideal effects in the EOS and the conductive opacities lead to a limiting mass ranging from 0.08 M_{sun} to 0.15 M_{sun} although they do not affect the models with masses above 0.15 M_{sun} obviously. The investigations also show that the massive models of the lower main sequence (i.e. those with mass near the sun) are dependent very much on the element abundances and the mixing length ratio while the lower mass models are not. The lower main sequence models are found to be insensitive to the surface condition (photospheric model or atmospheric model) used.

We also perform the calculation of the evolutionary models of the lower main sequence from the zero age up to an age of 10^{10} years. A perfect theoretical model of the solar evolution is obtained when the atmospheric model is used as surface condition, the element abundances are chosen to be 0.70/0.28/0.02 and the mixing length ratio to be 1.5. The investigations show that the element abundances are the most important parameters in the determination of the solar models. The mixing length ratio is the second most important one being much more important than the physical model used as surface condition. The evolutionary models of the masses below 0.8 M_{sun} are found to have only small changes in their properties within 10^{10} years. None of them can deplete their central hydrogen in that time.

We find one problem in that the models with masses around 0.1 M_{sun} have oscillating solutions for both the zero age models and evolutionary models. According to our investigation, the nonideal effects in the EOS can be responsible. These oscillating solutions imply the existence of more than one stable configuration for stellar masses.

Contents

Chapter I Introduction

1.1 Low mass stars

Stars in which the p-p chain dominates the energy generation are usually referred to as the lower main sequence. Typically, their central temperatures are below $2*10^7$ K and their masses below 2 M_{sun} (solar mass unit). We limit our study in this thesis for those stars with masses below one solar unit because they are most concerned with our interests, such as the nonideal effects, molecular opacities, etc.

The structure of a low mass star is described theoretically as a radiative core at the centre, where hydrogen burning produces energy, surrounded by a convective envelope which extends to the base of the photosphere. The size of the radiative core becomes smaller as the stellar mass decreases. The stellar interior becomes completely convective when the mass of the star is below about 0.3 M_{sun}. These results have been demonstrated by the pioneering work being carried out by Limber (1958), Hayashi and Nakano (1963), and Ezer and Cameron (1967).

The low mass stars have a minimum mass for them to achieve a state of thermal equilibrium by burning hydrogen, which is shown by Kumar (1963 a,b). Although most studies show a value of about 0.08 M_{sun} for the minimum mass, its determination is sensitive to the uncertainties of the input physics employed for the model calculation. For example, the study by Dorman et al. (1989) showed that there are two minimum masses by the use of two equations of state. The hydrogen burning minimum mass is also a sensitive function of the hydrogen content. This is examined by Rappaport and Joss (1984) who use a simple stellar evolution code to show that the minimum mass can be as small as 0.035 M_{sun} for a hydrogen-poor composition.

The stars with masses below the hydrogen burning minimum mass are called brown

dwarfs. They can never achieve a state on the main sequence while they evolve from the early stages of contraction, through deuterium burning, to the very late stages of degenerate cooling at ages comparable to that of the Galaxy. This is displayed by Nelson et al.. (1985, 1986a, 1986b) who employ a polytropic model to simulate the contraction evolution of very low mass stars and brown dwarfs. Accurate evolution models are calculated by D'Antona and Mazzitelli (1985) for their evolution of these objects. They find that the minimum mass is around 0.075-0.070 M_{sun} and the brown dwarfs can spend a Hubble time at luminosities between 10^{-4} L_{sun} and 10^{-5} L_{sun}.

1.2 Study of low mass stars

There are three points responsible for the interest in the study of low mass (LM) stars. First of all, significant observational progress has been made during the past decade so that more and more information about the properties of LM stars is provided. Second, the existence of dark objects in the galactic disk, which has been confirmed by Bahcall (1984a, b), is concerned with the very low mass objects. The study of them has to be based on the present knowledge of LM stars. In addition, a number of properties of dense gases at low temperatures are demonstrated in the LM stars. Unlike most of massive stars whose interiors and envelopes can be treated as ideal gases, cool and dense gases are found in the envelopes of LM stars, and even in their interiors. Therefore, the study of the cool and dense gas is required to obtain knowledge of their physical properties.

In astronomical observation, new observing techniques from both the ground and space have afforded much recent progress. They include results on the halo population as well as the first observation of the nearest globular cluster with the Hubble Space Telescope. Space observations may spatially resolve tens of thousands of M dwarfs near the main sequence mass limit.

The theoretical study of LM stars is concerned with a question whether "brown dwarfs"

with substellar masses really exist in substantial number. To confirm this, D'Antona and Mazzitelli (1983) and Kroupa et al. (1990) studied in detail the stellar initial mass function and stressed the importance of the mass-luminosity relation in the determination of the low-luminosity mass function. Meanwhile, a great number of studies have been carried out in the theoretical investigation of properties of LM stars. For example, VandenBerg et al. (1983) computed the LM star models for a wide range in metallicity. Neece (1984) investigated some uncertainties from input physics in the calculation of main sequence models of LM stars. D'Antona and Mazzitelli (1985) performed computation of the evolution of objects having masses around the minimum mass. Rappaport and Joss (1984) investigated the effect of element abundances on the minimum main sequence mass. More recently, Dorman et al. (1989) calculated theoretical models and investigated the effect of the equation of state on the model calculation.

Of these studies, the improvements incorporated mainly include more accurate evaluation of low temperature radiative opacities and the equation of state. Most of them start the model calculation from about a half of solar mass or even a lower mass. Some of them give comparison with the observed data in the H-R diagram. We summarize these studies by the following points:

1> The element abundances affect the hydrogen burning minimum mass considerably,

2> The uncertainties in the input physics for the model calculation are mainly the low-temperature opacities and the determination of the equation of state,

3> The uncertainty in the computation code is the treatment of the convection and the radiative diffusion approximation in the stellar atmosphere,

4> In comparison with the observed data, there is a noticeable discrepancy near the end of the lower main sequence.

1.3 Present research on the LM stars

The aim of this thesis is to make a theoretical study of the properties of LM stars. The

aspects covered include the following.

1> To calculate the equation of state with the inclusion of nonideal effects, mainly that of pressure ionization.

2> To calculate the radiative opacity using a hydrogen-like model and the average atom model. The effect of pressure ionization on the opacity calculation is included.

3> To examine the importance of the electron screening effect on thermo-nuclear reactions and the conductive opacities in the determination of LM star models.

4> To investigate the effects on LM star models of the mixing length ratio, the surface boundary condition, and element abundances.

5> To investigate the effects on LM star models of low temperature molecular opacities and pressure ionization in the equation of state.

6> To calculate main sequence models for LM stars with masses from 1 M_{sun} down to the hydrogen burning minimum mass, as well as a sequence of evolved models.

Of the above subjects, two require to be introduced as they constitute a major part of our work.

1.3.1 Calculation of the equation of state with an inclusion of nonideal effects

Graboske, et al. (1969) have presented the results of a systematic study of the thermodynamic properties of nonideal multi-component mixture of gases, in which the equation of state for stellar envelopes is obtained by a free energy minimisation method. Magni and Mazzitelli (1979) and Fontaine, et al. (1977) have also used this method to calculate thermodynamic functions for astrophysical application. Their contributions were employed by D'Antona and Mazzitelli (1985) and Neece (1984) to study the main sequence models and evolution sequence models of the LM stars where nonideal effects due to particle interactions were found to play a significant role. Carson (1985) has used the free energy minimisation method in the calculation of stellar opacity.

Hummer, et al. (1988), Mihalas, et al. (1988) and Dappen, et al. (1988), also based on the free energy minimisation method, calculated the equation of state for a gas mixture under stellar envelope conditions. They introduced occupation probabilities in the internal partition function to take into account the pressure ionization due to particle interactions. A hydrogen-helium plasma was investigated, including the phenomena of pressure dissociation and ionization. In our study, we formulate a new method based on the statistical theory of the grand canonical ensemble to obtain an equation of state which explicitly gives atomic configuration probabilities.

It has been known that pressure ionization is caused by interatomic interactions when the interatomic distance is near or about atomic size. However, even modern physics finds it difficult to deal with such interactions in both physical and mathematical models. In astrophysical applications, simple physical models have to be developed in order to avoid involvement of complicated models. Therefore, we treat the interatomic interactions involved in the equation of state simply by three physical effects: the statistical effect of finite size of atoms, the perturbation of bound electron energy levels and the perturbation of free electron energy levels.

1.3.2 Formulation of the radiative opacities by the Average Atom model

The Average Atom (AA) model can be a practical method for calculating the opacity of the heavy elements. This is because even now it is still difficult to determine the atomic energies and detailed configurations by quantum theory, and therefore the simple atomic model has to be used to describe the heavy elements (see Cox 1965, Carson 1976, Huebner 1985). In the AA model, the Fermi-Dirac formula has been used to determine the average population of the electrons (see Mayer 1948, Cox 1965) and the binomial distribution is used to construct the atomic configurations by Carson, Mayers and Stibbs (1968). The relativistic Hartree-Fock-Slater calculation is employed by Rozsnyai (1972) to

calculate more accurate atomic data for the AA model, and detailed configurations are constructed according to the Fermi-Dirac formula by Goldberg, Rozsnyai and Thompson (1986). We know that the AA model is based on the atomic shell structure and the independent approximation that the electron distribution in one atomic shell is supposed to be independent of those in other shells. The Fermi-Dirac formula can describe the distribution of free electrons as fermions but is too crude to describe that of the electrons in the atomic shells. The reason is that the bound electrons are populated in the special degenerate states of the atomic shell, different from the free electrons. In our study, therefore, we use the grand canonical ensemble to obtain a set of self-consistent equations for the AA model which determine the electron populations in the atomic shells and the atomic configuration probabilities.

In our formulation of radiative opacity by the AA model, the detailed electron configurations of heavy elements are constructed in terms of the electron occupation probabilities of atomic shells. They are necessary for accurate opacity calculations and also for the prediction of expected spectral patterns. The absorption coefficients for heavy elements, due to the bound-free and bound-bound transitions, are calculated for detailed electron configuration. However, the splitting of spectral lines due to the angular momentum states, which was studied by Rozsnyai (1989) and Goldberg, Rozsnyai and Thompson (1986) , is not under consideration here.

The average energies of electronic levels are calculated simply according to the Ritz variation method presented by Carson and Hollingsworth (1968), instead of the Relativistic Hartree-Fork-Slater calculation presented by Rozsnyai (1972) or the Thomas-Fermi model of the atom by Carson, Mayers and Stibbs (1968). The energy difference of any two configurations in absorption transitions is also calculated according to the Ritz variation method, as well as the corresponding effective nuclear charges. But the Slater screening constants in the Ritz variation method are corrected by introducing correcting coefficients

for each electronic level of each element according to the one-electron energies of atoms taken from the experimental data of Slater (1955). This correction is believed to be able to make the Ritz variation method a good approximation in the calculations of the AA model. All atomic data used in the calculation of absorption coefficients, including cross-sections, oscillator strengths, matrix elements and line broadening, etc, are calculated by hydrogen-like wave functions specified by the effective nuclear charges obtained.

1.4 Others

1.4.1 System of atomic units

The atomic units (a.u.) are appropriate to the subject of atomic structure. We employ the system of atomic units for our theoretical formulation as well as numerical computation. In the system of atomic units certain dimensional constants are set equal to unity so that they conveniently disappear from many formulae. These constant are

Rest mass of the electron	$m_e = 1$ a.u. of mass,
Magnitude of the charge of the electron	$e = 1$ a.u. of charge,
Radius of the first Bohr orbit	$a_0 = 1$ a.u. of length.

Derived from these constants we have

Quantum angular momentum	$h/2\pi = 1$ a.u. of action,
Speed of light	$c = 137$ a.u. of speed,
the unit of energy	$e^2/a_0 = 1$ a.u. of energy.

As a result of the a.u. of energy, the angular frequency ω is defined by

1 a.u. of frequency = 1 a.u. of energy = 27.2 eV,

and the temperature T by

1 a.u. of temperature = 1 a.u. of energy = 27.2 eV = $3.158*10^5$ K.

1.4.2 Element abundances

Of the element abundances, the mass fractions of hydrogen and helium may vary according

to the stellar objects to be studied, and the mass fraction of the heavy elements also changes with them. However, the individual fractions of the heavy elements over their total abundance have to be specified. The specification of these fractions is important in the calculation of radiative opacities.

For the calculation of both the equation of state and the radiative opacities in our study, we adopt the element abundance data provided by Cameron (1970) to obtain the individual mass fractions of heavy elements relative to their total abundance. These are listed in Table 1.1 for twelve heavy elements.

Table 1.1 : Heavy element abundances

Element	Z	Number abundance	Mass fraction
C	6	1.18(7)	0.192
N	7	3.74(6)	0.076
O	8	2.15(7)	0.465
Ne	10	3.44(6)	0.094
Na	11	6.00(4)	0.002
Mg	12	1.06(6)	0.035
Al	13	8.50(4)	0.003
Si	14	1.00(6)	0.038
S	16	5.00(5)	0.022
Ar	18	1.17(5)	0.006
Ca	20	7.21(4)	0.004
Fe	26	8.30(5)	0.064

1.5 Outline of the thesis

The thesis is organized as following: In Chapter II, III and IV we present the formulation and investigation of each element of input physics. The computational theory and method are given in Chapter V. The study of LM star models is presented in Chapter VI and VII. Finally we conclude our work in Chapter VIII.

Chapter II The Equation of State with Nonideal Effects

Introduction

Stellar envelopes and interiors are generally described as gases in local thermal equilibrium. Their physical conditions may then be expressed in terms of the equation of state (EOS) (see Section 2.1). There are several methods generally used to generate the EOS (see Section 2.2). Here we use a new method, based on the theory of the grand canonical ensemble(see Section 2.4). A simple model is made to simulate the nonideal effects (see Section 2.3) which are included in the determination of the EOS. Two determinations of the EOS are investigated in Section 2.5.

2.1 Equations of state and thermodynamic quantities

The equation of state is the relation of the pressure P, or the energy density U, to the temperature T and the density ρ. P and U may theoretically be found as functions of ρ and T, expressed as $P=P(T,\rho,\{X_i\})$ and $U=U(T,\rho,\{X_i\})$, if given the elemental abundances $\{X_i\}$. All of the thermodynamic quantities may then be calculated from these two functions. In astrophysical applications, for example, the specific heat at constant volume C_v, the specific heat at constant pressure C_P and the adiabatic gradient ∇_{ad} are defined by

$$C_v = \left(\frac{\partial U}{\partial T}\right)_v ,$$

$$C_P = C_V + \frac{P X_T^2}{T \rho X_\rho} ,$$

$$\nabla_{ad} = \frac{\gamma - 1}{\gamma X_T} ,$$

with

$$X_T = \left(\frac{\partial \ln P}{\partial \ln T}\right)_\rho ,$$

$$X_\rho = \left(\frac{\partial \ln P}{\partial \ln \rho}\right)_T ,$$

$$\gamma = C_P/C_V .$$

2.2 Methods to generate EOS

There are two common methods used to generate the EOS in astrophysical applications. One is based on the Saha equation and ideal gas model (see Cox and Giuli 1968). But it cannot take into account inter-particle interactions and thus fails for a nonideal gas in the case of high density. The other is the minimization of the free energy, which was initially introduced by Graboske et al. (1968) to study the thermodynamic properties of nonideal multi-component mixtures of gases. Afterwards, Magni and Mazzitelli (1979) and Fontaine et al. (1977), etc, used this method to calculate thermodynamic functions for astrophysical applications. In this method, thermodynamic terms and interaction terms are included in the Helmholtz free energy and the statistical equilibrium state is calculated by minimizing the free energy in composition space.

In the present study, we introduce a method based on the theory of the grand canonical ensemble to generate the EOS. In this method, an electron partition function for a multi-component gas is used to obtain a conservation equation of electron number, which is solved for the electron degeneracy parameter and thus thermodynamic quantities can be calculated from the partition function. The main interatomic interactions are included in the electron partition function to represent pressure ionization and its nonideal effects. This method will be presented in Section 2.4.

2.2.1 EOS based on the Saha equation

The simplest way to generate the EOS is to use the Saha equation. It defines the ratio of the

numbers of particles in a chemical reaction according to the conservation of chemical potentials. For an ionization reaction

$$A \Leftrightarrow A^+ + e ,$$

the ratio of particle numbers is determined by

$$\frac{N_A^+}{N_A} = \frac{g_A^+}{g_A} \exp(-\lambda - X/T) ,$$

with the statistical weights g, the ionization energy X, the temperature T, the electron degeneracy parameter λ. For a chemical reaction

$$AB \Leftrightarrow A + B ,$$

the particle number ratio is given by

$$\frac{N_A N_B}{N_{AB}} = \frac{g_A g_B}{g_{AB}} \exp(-X/T) \left[\frac{M_A M_B}{M_{AB}} \frac{T}{2\pi}\right]^{3/2} ,$$

where the M are the masses of the particles, and X is the chemical reaction energy.

Both formulae are forms of the Saha equation. In the calculation of the EOS in stellar matter, they are used to calculate the fraction of species of each element, and thus to find out the number density of free electrons n_f. Then the total pressure P_{tot} can be calculated, including the radiative pressure P_r, the free electron pressure P_f, and the atom and ion pressure P_{ai}, i.e.

$$P_{tot} = P_r + P_f + P_{ai} .$$

In the same way, the internal energy is equal to

$$U_{tot} = U_r + U_f + U_{ai} + U_{ie} ,$$

but with one more term for the ionization energy U_{ie}. The relations of the total pressure P_{tot} and the internal energy density U_{tot} with the temperature T and the mass density ρ

define the EOS, and are used to calculate all thermodynamic quantities.

Although the Saha equation has often been applied in astrophysical cases, it cannot be used to treat interacting gases where pressure ionization and nonideal effects appear. Another disadvantage is that its application to a complex system cannot preserve thermodynamic consistency because it ignores the dependence between subsystems. It can be proved that thermodynamic consistency is preserved provided that all thermodynamic quantities are calculated from the same partition function.

2.2.2 EOS generated by the free energy minimization method

The free energy minimization method (FEMM) is a powerful way to generate the dissociation and ionization equilibrium of multi-component interacting gases and their thermodynamic quantities. Here we briefly summarize the method presented by Mihalas et al. (1988).

The FEMM is based on the theory of the canonical ensemble. First of all, the Helmholtz free energy F of the system is calculated from the canonical partition function Z_C, which is the trace of the operator $\exp(-\hat{H}/T)$ with the energy operator $\hat{H}$ over all possible states of the gas, i.e.,

$$Z_C = \mathrm{Tr} \exp(-\hat{H}/T) ,$$

and

$$F = -T \log_e Z_C .$$

The states of the gas are determined by the states of all particles in the gas as well as the perturbation of their states due to the inter-particle interactions. The free energy is found to be a function $F(T,V,\{N_i\})$ of the temperature T, the volume of the system V, and the number of each type of particles N_i.

In order to determine the equilibrium state of the system, the free energy F is minimized with respect to all variations $\{\delta N_i\}$. They are subject to the constraints of number conservation, charge neutrality and the stoichiometeric relation, which describe possible dissociation and ionization processes in the gas.

After the determination of the equilibrium state, all of the other thermodynamic quantities are also calculated from the free energy $F(T,V,\{N_i\})$. The total pressure of the gas is given by

$$P = -\left[\frac{\partial}{\partial V} F(V,T,\{N_i\})\right]_{T,\{Ni\}},$$

and the internal energy by

$$U = F - \left[\frac{\partial}{\partial T} F(V,T,\{N_i\})\right]_{V,\{Ni\}}.$$

Although the FEMM can give a theoretical and systematic description of the thermodynamic properties of interacting gases, there still remain some difficulties in its astrophysical application. One is concerned with some inter-particle interactions which represent a difficult subject in physics. Although some physical approximations have been employed in astrophysical studies, a failure of the FEMM is found for pressure ionization in the case of high density ($\rho > 10^{-2}$ g/cm^3) and low temperature ($T < 10^5$ K) (see Fontaine et al. 1977).

2.3 Nonideal effects in EOS

2.3.1 Application in Astrophysics

The study of white dwarfs and the lower main sequence is concerned with nonideal effects. In these objects, there exist conditions of relatively low temperature and high density where inter-particle interactions can be comparable to or stronger than thermal energy. The

inclusion of inter-particle interactions leads to nonideal effects in the EOS, and causes the EOS to differ from that of an ideal gas.

The EOS with the inclusion of nonideal effects has found important applications in astrophysics. For instance, Copeland et al. (1970), Grossman and Graboske (1971), Neece (1984), D'Antona and Mazzitelli (1985) employ it for the lower main sequence while Fontaine et al. (1974), D'Antona and Mazzitelli (1975), and Lamb and Van Horn (1975) have used it for white dwarfs and other degenerate stars.

2.3.2 Physical description

In dense gases, interatomic interactions are concerned with complicated physical processes. Even modern physics finds it very difficult to make a quantitive description for a simple species in various states, e.g. a solid state, a liquid state, or its phase transition. In astrophysical study, therefore, simplified models have to be used to incorporate into the EOS the nonideal effects due to interatomic interactions.

Dense gases are regarded as completely ionized plasmas when there is no bound atomic system. The interactions in such plasmas have been well described by some sophisticated models, e.g. the Thomas-Fermi model, the Thomas-Fermi-Dirac model and the Debye screening model. The results of these studies find many applications in the study of white dwarfs. However, the dense gases involved in low mass stars are mostly in a neutral state or in a state under pressure ionization. In this case, most atomic systems still exist or are undergoing ionization due to high pressure. In the study of low mass stars, therefore, it is important to develop a model which can represent how atoms become ionized under high pressures.

In many studies of the EOS concerning nonideal effects, such as that by Fontaine et al. (1977), and that by Magni and Mazzitelli (1979), pressure ionization is supposed to occur in a defined way. Consequently, the physical effects of pressure ionization cannot be

incorporated into the partition function of the system. This must ignore the contribution of pressure ionization to thermodynamic functions and give rise to an inconsistency among them. The problem is solved by an introduction of occupation probability in a recent study by Hummer and Mihalas (1988). In their study, occupation probabilities are included in the internal partition function of atomic systems to represent pressure ionization. A hard sphere model is employed and a number of Coulomb interactions are taken into account to obtain a formula of occupation probability.

In our EOS, three interactions are included to explain nonideal effects. The interaction among particles, which may be interpreted by the hard sphere model, leads to an occupation probability for the atomic system. The interaction of the bound electron with free electrons causes a perturbation of the energy level of the bound electron. The interaction between free electrons and ions produces a perturbation of free electron energy levels.

2.3.3 Statistical effects of finite size of atoms

An atomic system has a finite size. When the interatomic distance is near or smaller than the atomic size, the interactions among nuclei and electrons can be strong enough to destroy the atomic system. This is equivalent to a process of ionization, since the electrons are no longer bound to nuclei, and the process is therefore called pressure ionization.

The hard sphere model is the simplest way to treat the interactions among neutral particles. By using this model, Fermi (1924) obtained a configuration free energy for the van der Waals equation of state. His result was employed by Hummer (1988) to find out the probability of the existence of an atomic system with a radius r_j

$$w(a_j) = \exp[-(4\pi/3) \sum_k n_k(r_j+r_k)^3] ,$$

where the sum is over all types of perturber particles with radii r_k and number densities n_k.

Very easily, we can obtain a similar result by using the nearest neighbour model. It gives a probability for a sphere of a radius r without any perturber in it to be $\exp[-(4\pi/3)r^3 n_a]$ in a gas with the perturber number density n_a. If we suppose that the atomic system is destroyed when the interatomic distance is shorter than twice of its radius r_n, then we have a probability for its existence

$$w(a_n) = \exp[-(4\pi/3)\,(2r_n)^3\, n_a]\,,$$

which we may call the occupation probability of the atom. The atomic sphere is defined by a radius equal to the mean radius of electron orbit r_n.

2.3.4 Perturbation of bound electron energy levels

The interaction of the bound electron with free electrons raises the energy levels of the bound electron. Suppose that the free electrons , with a number density n_e, are distributed uniformly throughout the whole space of the gas. Due to their Coulomb interactions, a bound electron in a orbit of radius r has a perturbation energy

$$\Delta E(r) = \frac{4\pi}{3} n_e\, r^3 / r = \frac{4\pi}{3} n_e\, r^2\,.$$

Then a bound electron in the state $|nl\rangle$ has its energy levels shifted upwards approximately by an amount

$$\Delta E_n = \frac{4\pi}{3} n_e \langle nl|\, r^2\, |nl\rangle\,.$$

In a hydrogen-like atom with a nuclear charge Z, the matrix element of r^2 is given by

$$\langle nl|\, r^2\, |nl\rangle = \frac{n^2}{2Z^2}\,[5n^2+l-1.0\,(l+1.0)]\,,$$

where n and l are the principal and momentum quantum numbers.

In fact, the uniform distribution is not suitable for the free electrons near the nuclei. The

Coulomb attraction can cause the free electrons to be more densely distributed near the nuclei than far from the nuclei. This effect can always increase the shift of the bound electron energy levels. Because the consideration of this effect would involve more complicated physical models, we adopt the assumption of the uniform distribution for free electrons.

2.3.5 Perturbation of free electron energy levels

There are a number of interactions between free electrons and charged nuclei, which play significant roles especially for a fully ionized plasma. At low densities, the interaction is described well by a static screened Coulomb potential (Cox and Giuli,1968). In the region of very high densities, it can be treated by some more sophisticated models, such as the Thomas-Fermi model or the Thomas-Fermi-Dirac model with an inclusion of exchange effects. Because the charged nuclei attract the free electrons, their Coulomb interactions can always shift the energy levels of free electrons downwards with respect to the bound electron energy levels.

In our study , we simply use a statistically averaged energy ΔE_f to represent the downward shift of the energy level of one free electron. The result presented by Carson and Hollingsworth (1968) gives an average potential produced by the interaction between the free electrons and the charged nuclei, i.e.

$$V = 0.1499 \left[\sum_i \alpha_i (Q_i/a_i)^{1/2} \right]^2 .$$

The number fraction of atoms of type Z_i is α_i, the charge of the nuclei is Q_i, and the radius of the ion sphere a_i is defined by $(4\pi/3)a_i^3 n_e = Q_i$ with the free electron number density n_e.

The average potential V can be written as

$$V = 0.1499 \left(\frac{4\pi}{3} n_e\right)^{1/3} \left[\sum_i \alpha_i Q_i / Q_i^{2/3} \right]^2 ,$$

where Q_i have a minimum value of unity, and $\sum_i \alpha_i Q_i$ is equal to the ratio of the free electron number density n_e to the total atom number density n_a. Therefore we obtain an approximate formula for

$$V = 0.1499 \left(\frac{4\pi}{3} n_e\right)^{1/3} \left(\frac{n_e}{n_a}\right)^2 .$$

Consequently, the perturbation of the free electron energy levels is represented by a downward shift

$$\Delta E_f = - V.$$

2.4 EOS generated by the theory of the grand canonical ensembles

In this section we formulate a new method based on the statistical theory of the grand canonical ensemble to generate an equation of state. Since the atomic configuration probability is determined only by the distribution of electrons in both bound and free states, we can use the grand partition function of electrons to include all states of electrons as well as interatomic interactions. Following this idea, we obtain a conservation equation for the electron number, which is solved for the electron degeneracy parameter λ as well as for the atomic configuration probabilities. Then all of the thermodynamic quantities are calculated from the same partition function, which certainly guarantees thermodynamic consistency.

2.4.1 The conservation equation for the electron number

2.4.1.1 The stellar gas

We utilize the theory of the grand canonical ensemble to treat stellar gases in the LTE (local thermodynamic equilibrium) condition. A system of a stellar gas is defined by a temperature $T=1/\beta$, a volume V and number of atoms of each element N_i. The total number of atoms N_a is a sum of N_i over all elements. The corresponding number densities are

defined by $n_a = N_a/V$ and $n_i = N_i/V$.

First of all, we define a system which consists only of the bound electrons and free electrons. To establish such a system in a stellar gas, the radiation and nuclei have to be separated from it. This is done in the following ways. (1) The radiation is treated as a photon gas, independent of the others. (2) The nuclei are treated as classical particles since their interaction with bound electrons is contributed to the bound states of electrons. (3) The interactions of the nuclei with free electrons are also included in the energy states of the free electrons, and the interactions among neutral particles are described by the hard sphere model . Therefore, we only need to consider the distribution of electrons in both bound and free states.

2.4.1.2 Electron partition function

We start with an electron partition function (denoted by EPF) for the system. Since the electron distribution involves the number distribution of electrons in different states, it is better to resort to the theory of the grand canonical ensemble which includes the number operator in the partition function. In statistical physics, the grand canonical partition function is defined by

$$Z_G = \mathrm{Tr}\exp(\lambda\hat{N}-\beta\hat{H}) .$$

Since the partition function for the electrons is concerned, the number operator $\hat{N}$, the energy operator $\hat{H}$ and the degeneracy parameter λ should be those of the electrons. In a representation of the eigenstates with the electron energies and numbers $\{E_i, N_i\}$, in which $\exp(\lambda\hat{N}-\beta\hat{H})$ is diagonal, Z_G is obtained by summing $\exp(\lambda\hat{N}-\beta\hat{H})$ over all eigenstates and performing its product over all subsystems. The subsystem can be one atomic system, or one element, or one phase space cell which can hold one electron.

2.4.1.3 EPF for bound states

We consider the electrons bound to the nuclei. The EPF in an atomic configuration of element i with m bound electrons and eigenvalue E_{imj} for state j is given by

$$Z_{imj} = < m, E_{imj}| \exp(\lambda\hat{N}-\beta\hat{H}) \ | m, E_{imj}>$$

$$= \exp(\lambda m-\beta E_{imj}) .$$

Here it is noted that the configuration energy E_{imj} is the total energy of all bound electrons in the configuration. The perturbation of bound electron energy levels should also be included in E_{imj} by an energy shift ΔE_n. For instance, the configuration energy of a hydrogen-like atom in the state $|n>$ is written as

$$E_{imj} = -\frac{Z^2}{2n^2} + \Delta E_n \ .$$

The first term is the configuration energy of the unperturbed atom while the second term is due to the perturbation of the bound electron. For a configuration with multiple electrons, the total energy is shifted by the perturbation of all bound electrons in the atom.

The statistical effect of the finite size of atoms is incorporated into the EPF by multiplying by an occupation probability w_{imj}, expressed in terms of $\phi_{imj} = -\log_e(w_{imj})$. Thereby, summing Z_{imj} over all eigenstates {j} and all possible numbers of bound electrons {m} gives the EPF in one atom of the element i, i.e.

$$Z_b(i) = \sum_m \sum_j Z_{imj} \, w_{imj}$$

$$= \sum_m \sum_j \exp(\lambda m-\beta E_{imj}-\phi_{imj}) \ .$$

The EPF for the bound states of all atoms of all elements is obtained by performing a product of $Z_b(i)$ over all atoms of all elements, i.e.

$$Z_b = \prod_i [Z_b(i)]^{N_i},$$

with the number of atoms N_i of element i. Its logarithm has a form

$$\log_e Z_b = \sum_i N_i \log_e [\sum_m \sum_j \exp(\lambda m - \beta E_{imj} - \phi_{imj})] ,$$

with a sum over all elements.

2.4.1.4 EPF for free states

We also need the EPF for the free states. Since there are two eigenstates for a free electron in a unit cell of phase space, i.e. there can be one electron or none, we then have for the EPF per unit cell with energy ε

$$Z_1 = \langle m,m\varepsilon|\exp(\lambda \mathbf{N} - \beta \mathbf{H})|m,m\varepsilon\rangle \qquad \text{with } m=0,1$$

$$= 1 + \exp(\lambda - \beta\varepsilon) .$$

The EPF for all free states is given by finding a product of Z_1 over the whole free phase space, that is

$$Z_f = \prod_{<free>} Z_1 .$$

Its logarithmic form is

$$\log_e Z_f = \sum_{<free>} \log_e [1 + \exp(\lambda - \beta\varepsilon)] .$$

The sum here has to be converted into an integration over the whole phase space available to the free electron

$$\sum_{<free>} = \frac{V g_e}{(2\pi)^3} \int_0^\infty 4\pi p^2 \, dp ,$$

with a statistical weight g_e=2 for two states of electron spin and the electron momentum p.

The energy of a free electron ε includes its kinetic energy and its potential energy including the interaction with other charged particles. If we represent this interaction by a statistically averaged energy decreased by ΔE_f, then the energy of the free electron is equal to

$$\varepsilon = \frac{p^2}{2} - \Delta E_f .$$

2.4.1.5 Atomic configuration probability

Now we have got the EPF, Z_b and Z_f, in both bound and free states. According to statistical physics, the total number of electrons in the system is defined by

$$\sum_i N_i Z_i = \frac{\partial}{\partial \lambda} \log_e(Z_f Z_b)$$

$$= \frac{\sqrt{2}\, V}{\pi^2 \beta^{3/2}} F_{1/2}(\lambda+\beta\Delta E_f) + \sum_i N_i \frac{\sum_m m \sum_j \exp(\lambda m - \beta E_{imj} - \phi_{imj})}{\sum_m \sum_j \exp(\lambda m - \beta E_{imj} - \phi_{imj})}$$

$$= N_f + \sum_i N_i \sum_m \sum_j p_{imj} ,$$

where $F_{1/2}(\lambda)$ is the Fermi-Dirac integral. The left hand side is from the conservation of electron number while the right hand side represents a statistical distribution of electrons in LTE conditions. So it can be called the conservation equation for the electron number. This equation can be solved for the electron degeneracy parameter λ when given N_i, Z_i, β, V, E_{imj}, ΔE_f and ϕ_{imj}.

In the conservation equation, the first term on the right hand side is the number of free electrons, and the second one is the number of electrons bound with nuclei. The second term thus defines a probability for a configuration of element i with m bound electrons and

eigenvalue E_{imj} to be

$$p_{imj} = \frac{\exp(\lambda m - \beta E_{imj} - \phi_{imj})}{\sum_m \sum_j \exp(\lambda m - \beta E_{imj} - \phi_{imj})} .$$

The Saha and Boltzmann equations are found to be special cases of this formula with the inclusion of an occupation probability.

2.4.2 Thermodynamic quantities and nonideal effects

After acquiring the electron partition function (EPF) and the electron degeneracy parameter λ by solving the conservation equation for the electron number, all of the thermodynamic quantities involved in the EPF can be calculated. Since we have included in the EPF the interatomic interactions, such as the quantum interaction on the bound electrons, the interaction of free electrons with charged particles and the statistical effect of finite size of atoms, their nonideal effects can be obtained from the EPF.

2.4.2.1 Gas pressure from electrons

The contribution to pressure from the EPF in the bound states is determined by means of

$$P_b = \frac{1}{\beta}\frac{\partial}{\partial V}\log_e Z_b$$

$$= \sum_i N_i \sum_m \sum_j p_{imj}\left[-\frac{\partial E_{imj}}{\partial V} - \frac{1}{\beta}\frac{\partial \phi_{imj}}{\partial V}\right]$$

$$= \sum_i n_i \sum_m \sum_j p_{imj}\left[n_a \frac{\partial E_{imj}}{\partial n_a} + \frac{n_a}{\beta}\frac{\partial \phi_{imj}}{\partial n_a}\right] ,$$

where the relations $n_i V = N_i$ and $n_a V = N_a$ are used, and both N_i and N_a remain constant in the system. We see that when the energy of atomic configuration E_{imj} or the occupation probability factor ϕ_{imj} is a function of the density, the non-zero terms give the nonideal

effects due to the interatomic interactions.

The pressure from the EPF for free states is given by

$$P_f = \frac{1}{\beta}\frac{\partial}{\partial V}\log_e Z_f$$

$$= \frac{2}{3}\frac{N_f}{\beta V}\frac{F_{3/2}(\lambda+\beta\Delta E_f)}{F_{1/2}(\lambda+\beta\Delta E_f)} + N_f\frac{\partial\Delta E_f}{\partial V} ,$$

$$= \frac{2}{3}\frac{n_f}{\beta}\frac{F_{3/2}(\lambda+\beta\Delta E_f)}{F_{1/2}(\lambda+\beta\Delta E_f)} - n_f n_a\frac{\partial\Delta E_f}{\partial n_a} ,$$

where the free electron number density $n_f = N_f/V$. It can be seen that the downwards shifted energy ΔE_f of the free electron due to its interactions with charged nuclei leads to terms for nonideal effects.

2.4.2.2 Internal energy

The internal energy from the EPF for the bound states is

$$U_b = -\frac{\partial}{\partial\beta}\log_e Z_b$$

$$= \sum_i N_i \sum_m \sum_j p_{imj}\left[E_{imj} + \beta\frac{\partial E_{imj}}{\partial\beta} + \frac{\partial\phi_{imj}}{\partial\beta}\right] ,$$

and the internal energy from the EPF for free states

$$U_f = -\frac{\partial}{\partial\beta}\log_e Z_f$$

$$= \frac{N_f}{\beta}\frac{F_{3/2}(\lambda+\beta\Delta E_f)}{F_{1/2}(\lambda+\beta\Delta E_f)} - N_f\left[\Delta E_f + \beta\frac{\partial\Delta E_f}{\partial\beta}\right].$$

They indicate that the dependence of E_{imj}, ϕ_{imj} and ΔE_f on the temperature causes nonideal terms.

2.4.2.3 Radiation and nuclei

The EOS should include contributions from radiation and nuclei as well. However, since they are separated from the particle interactions, the nuclei can be treated as ideal classical particles and the radiation can be described by the Bose-Einstein statistics. Their thermodynamic quantities can be simply added to those from the configurations of electrons.

2.4.3 Inclusion of molecular hydrogen

There are many ways to incorporate molecular hydrogen (H_2) states into the equation of state. However, a reasonable method is to include the molecular states of hydrogen in the same partition function. This is because the calculation of thermodynamic quantities from the same partition function can preserve thermodynamic consistency. In the same way as in Section 2.4.1 and 2.4.2, we rewrite the EPF including molecular hydrogen, and then use it to obtain the conservation equation of electron number as well as thermodynamic quantities.

2.4.3.1 The electron partition function

Suppose in the gas there are N_{HM} hydrogen (H) atoms in molecular states. Then the relation between the EPF for molecular hydrogen Z_{H2} and the number of H atoms in molecular states

$$N_{HM} = N_{BM} = \frac{\partial}{\partial \lambda} \log_e Z_{H2},$$

where N_{BM} is the number of electrons bound in the H_2 molecules, gives

$$Z_{H2} = \exp[\, \lambda N_{HM} \,].$$

Considering there are N_H-N_{HM} H atoms in atomic states, where N_H is the total number of

H atoms, the EPF for all bound states is rewritten as

$$Z_b = \sum_{i=2} [\ ] * \left[\sum_m \sum_j \exp(\lambda m - E_{1mj} - \phi_{1mj})\right]^{N_H - N_{HM}} * \exp(\lambda N_{HM}).$$

The first factor is contributed from the elements other than hydrogen, the second factor from the hydrogen atoms in atomic states, and the third one from the hydrogen atoms in molecular states.

2.4.3.2 The conservation equation for the electron number

Following the same method as in Section 2.4.1, the conservation equation for the electron number is rewritten as

$$\sum_i N_i Z_i = N_f + \sum_{i=2} [\ ] + (N_H - N_{HM})\, p_{HI} + N_{HM}\ .$$

The term p_{HI} represents the probability of hydrogen atoms in neutral states and is given by

$$p_{HI} = \frac{\sum_m m \sum_j \exp(\lambda m - \beta E_{1mj} - \phi_{1mj})}{\sum_m \sum_j \exp(\lambda m - \beta E_{1mj} - \phi_{1mj})},$$

with m=1 for neutral states of hydrogen atom and m=0 for ionized states.

The number of H atoms in molecular states N_{HM} is calculated from the dissociation equilibrium constant K(T) defined by

$$K(T) = \frac{P_{HI}^2}{P_{H2}} = \frac{n_{H2}^2 (kT)^2}{n_{H2} kT}$$

$$= \frac{n_{H2}^2 T^2}{n_{H2} T} * \frac{(5.29*10^{-9})^3}{4.36*10^{-11}} \qquad \text{(in a.u.)},$$

with the number of hydrogen molecules n_{H2} and their pressure P_{H2}, and the number

density of neutral hydrogen atoms n_{HI} and their pressure P_{HI}. The constant K(T) depends only on the temperature T and can be expressed by a polynomial form presented by Vardya (1960), i.e.

$$\log_{10} K(T) = 12.5335 - 4.92516\theta + 0.05619\theta^2 - 0.00327\theta^3 ,$$

where θ is defined by $\theta = 5040/T$ (in K). The value 4.92516 is very dependent on the dissociation energy 4.477 eV of H_2.

In terms of K(T), we have for the number of hydrogen atoms in molecular states

$$N_{HM} = 2\,N_{H2} = \frac{2N_{HI}^2 T}{VK(T)*2.945*10^{14}},$$

where the volume of the gas V relates the number density n and the number N by $N_{H2}=n_{H2}V$ and $N_{HI}=n_{HI}V$. Taking into account the perturbation of the energy levels of the bound electrons in the H_2 molecule by ΔE_b and the occupation probability $w=\exp(-\phi)$, we have

$$N_{HM} = 2\,N_{H2} = \frac{2N_{HI}^2 T*\exp(-\Delta E_b/T-\phi)}{VK(T)*2.945*10^{14}}.$$

By solving this equation with the number of hydrogen atoms N_{HI} in neutral states

$$N_{HI} = (N_H - N_{HM})\, p_{HI} ,$$

we find

$$N_{HM} = N_H + VA - \sqrt{(N_H+VA)^2-N_H^2} ,$$

or

$$n_{HM} = n_H + A - \sqrt{(n_H+A)^2-n_H^2} ,$$

with

$$A = \frac{K(T)*2.945*10^{14}}{4Tp_{HI}\exp(-\Delta E_b/T-\phi)}.$$

We see that N_{HM} depends on T, N_H, p_{HI}, K(T), ΔE_b and ϕ, thus can be incorporated into the conservation equation of electron number.

2.4.3.3 Thermodynamic quantities

Following the same method as in Section 2.4.2, the pressure and internal energy can be calculated from the EPF given in Section 3.4.3.1. Although the inclusion of molecular hydrogen complicates the case, we may use an approximate condition that only the ground state of neutral atomic hydrogen is taken into account when considering molecular hydrogen. Then we get the pressure from the EPF in bound states

$$P_b = \sum_{i=2} [\cdots\cdots] + (n_H - n_{HM}) \sum_m \sum_j p_{1mj} \left[n_a \frac{\partial E_{1mj}}{\partial n_a} + \frac{n_a}{\beta} \frac{\partial \phi_{1mj}}{\partial n_a} \right]$$

$$+ (E_{111} + \phi_{111}/\beta) \left(n_{HM} - n_a \frac{\partial n_{HM}}{\partial n_a} \right),$$

and the internal energy

$$U_b = \sum_{i=2} [\ \ ] + (N_H - N_{HM}) \sum_m \sum_j p_{1mj} \left[E_{1mj} + \beta \frac{\partial E_{1mj}}{\partial \beta} + \frac{\partial \phi_{1mj}}{\partial \beta} \right]$$

$$+ (-\beta E_{111} - \phi_{111}/\beta) \frac{\partial N_{HM}}{\partial \beta}.$$

In both formulae, the first terms are contributed from the elements other than hydrogen, the second terms from hydrogen in atomic states, and the third ones from hydrogen in molecular states. The symbol "111" denotes the ground state of neutral hydrogen. The derivative terms can be calculated in the same way as in Section 2.4.2.1.

2.4.4 Inclusion of heavy elements

In the formulation of the EOS we include twelve heavy elements whose mass fractions are listed in Table 1.1. Since the heavy elements are important sources of free electrons only at low temperatures, we only need to take into account their neutral states and first ionization states. Their atomic data, consisting of the ionization energies and the statistical weights, are taken from those given by Allen (1973). According to the formula of the atomic configuration probability, we find that the free electron number from heavy elements is determined by

$$N_f(H) = \sum_i \frac{1}{1 + \exp[\lambda - \beta(\Delta E_i - X_i) - \phi_i]\, g_i} \quad ,$$

with a sum over all heavy elements, the first ionization energy X_i, the perturbation of bound electron energy levels ΔE_i, the occupation probability ϕ_i and the statistical weight g_i of the neutral state.

2.4.5 Atomic data

The atomic data required for the calculation of the EOS are the atomic configuration energies E_{imj} and the mean radius of electron orbit a_n. For HI and HeII, their configuration energies are simply determined by a hydrogenic formula while for HeI its unperturbed energies are calculated by using the effective nuclear charges formulated by Magni and Mazzitelli (1979). For all configurations we use the ionization energy X_n and effective nuclear charge Z_n to determine the mean radius of an electron orbit in terms of a hydrogenic formula $a_n = Z_n/(2X_n)$. For instance, a hydrogen molecule with an ionization energy X_n=0.1648 a.u. of energy, thus has a mean radius of its electron orbit radius r_n=3.034 a.u. =1.605 Å if its effective nuclear charge is supposed to be Z_n=1.

2.5 Modified EOS

2.5.1 Modification of the EOS

The EOS established in the preceding section has been employed in the calculations of the LM star models, which are presented in Chapter VI and VII. We found that there was still some discrepancy between the theoretical results and the observed data for the objects with effective temperatures below 3000 K. Ignoring the uncertainties due to other elements of the input physics, we could suppose that the nonideal effects giving rise to pressure ionization in the EOS is responsible. To test this, we modified the EOS by changing the formulation of pressure ionization in the investigation of LM star models. We found (see Chapter VI) that a weakening of pressure ionization can shift the effective temperatures to lower values so as to lead to even better agreement with the observed data.

In the modification of EOS, we remove the perturbation of the bound electron energy levels. We also reduce the effect of the hard sphere model on pressure ionization by reducing the interatomic distance for an atom to be destroyed to half of the atomic radius.

2.5.2 Comparison of two determinations of EOS

2.5.2.1 Pressure ionization

Since the modified EOS shifts the LM star models to cooler effective temperatures, we are interested in its difference from the EOS established in the preceding section, which we call the standard EOS. We present the fraction of hydrogen atoms in molecular states H_2 in Figure 2.1, and the fraction in neutral states HI in Figure 2.2. In Figure 2.3 and 2.4 are presented respectively the fraction of helium atoms in neutral states HeI and in first ionized states He^+. The data from the two determinations of the EOS are plotted in a density range between 10^{-8} g/cm^3 and 10^4 g/cm^3 and for three specified temperatures.

First, let us see the data from the standard EOS. Figure 2.1 and 2.2 show that the pressure dissociation of H_2 takes place at the density between 10^{-2} g/cm^3 and 1.0 g/cm^3 while that

of HI takes place between 10^{-1} g/cm^3 and 10 g/cm^3. In Figure 2.3 and 2.4 we see that the pressure ionization of helium takes place in the density range from 10 g/cm^3 to 10^3 g/cm^3. These results basically agree to those obtained by Mihalas et al. (1988) although they employ different formulation for the pressure ionization from ours.

Thus we see that pressure ionization does influence the models of lower main sequence stars. However, we believe that a more sophisticated physical model is required to be developed for the interatomic interactions to explain the pressure ionization of dense gases.

2.5.2.2 Pressure from nonideal effects

Finally, let us consider the contribution to the pressure from the bound electrons. Usually, the internal structure of atoms is thought not to contribute to the gas pressure. But in the case of high density, the interaction between atoms gives rise to their contribution. We call it a pressure from nonideal effects or a nonideal pressure .

In our formulation of the EOS employing the electron partition function, we found that this contribution can be incorporated in the EPF of the bound states. To investigate its importance, we calculated the ratio of the pressure from nonideal effects to the total pressure. The ratios from both the standard EOS and the modified EOS are plotted in Figure 2.5. For the standard EOS, the nonideal pressure dominates the total pressure at the density around 1.0 g/cm^3 for the temperature T=10^4 K. Its contribution is reduced at higher densities, because of the pressure ionization of atoms, and is also reduced as the temperature is increased, owing to the thermodynamic (normal) ionization. For the modified EOS, its important range is at higher densities than those for the standard EOS.

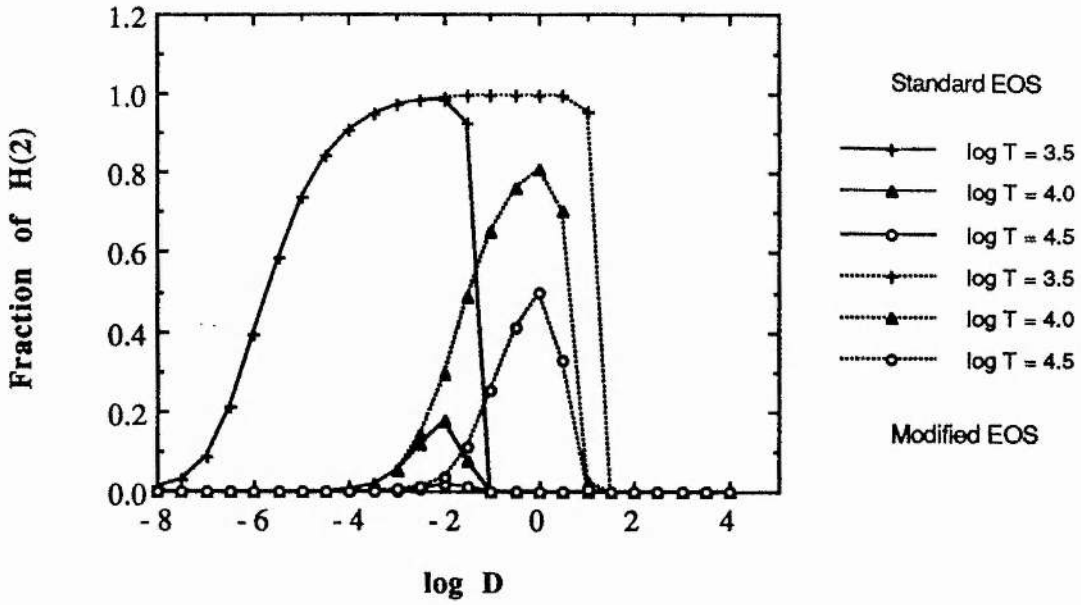

Figure 2.1 : Fractions of hydrogen atoms in molecular states for three temperatures in a density range of 10^{-8} - 10^{4} g/cm^3. Comparison of the data between the standard EOS and the modified EOS.

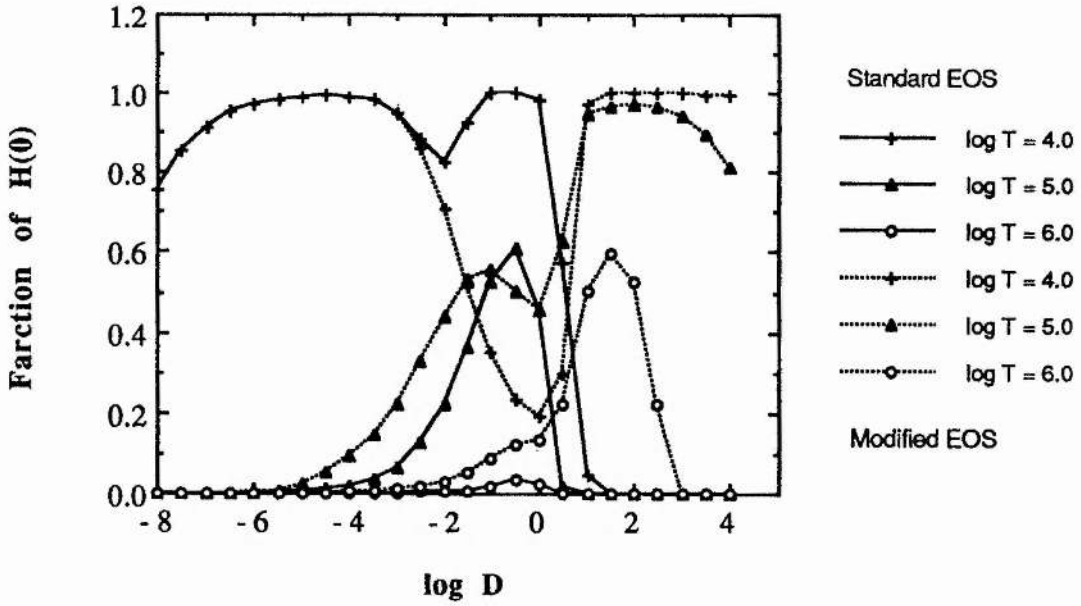

Figure 2.2 : Fractions of H atoms in neutral states, otherwise as in Figure 2.1.

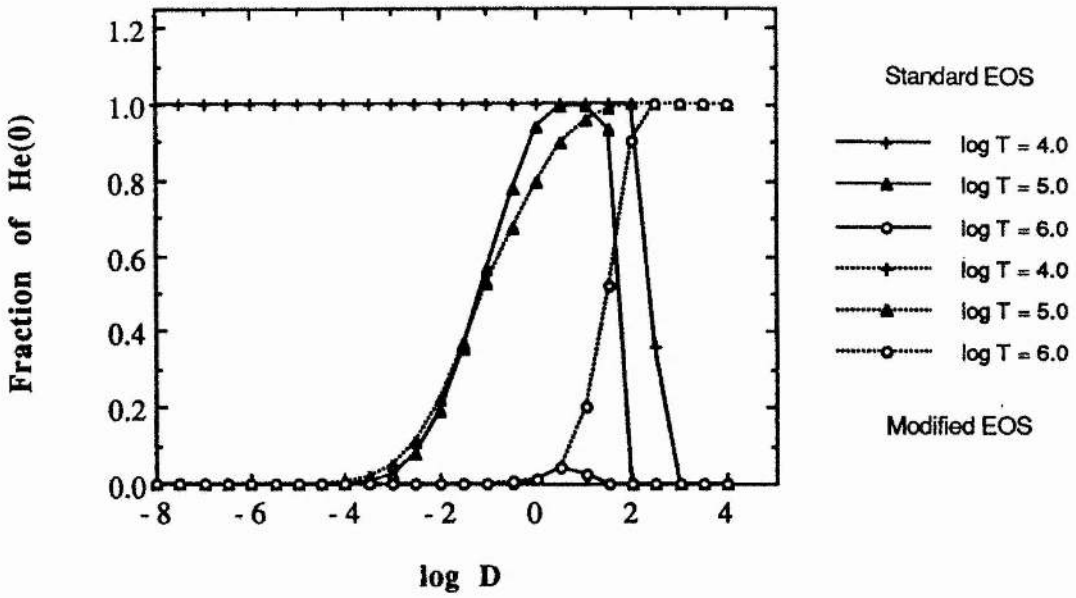

Figure 2.3 : Fractions of helium atoms in neutral states, otherwise as in Figure 2.1.

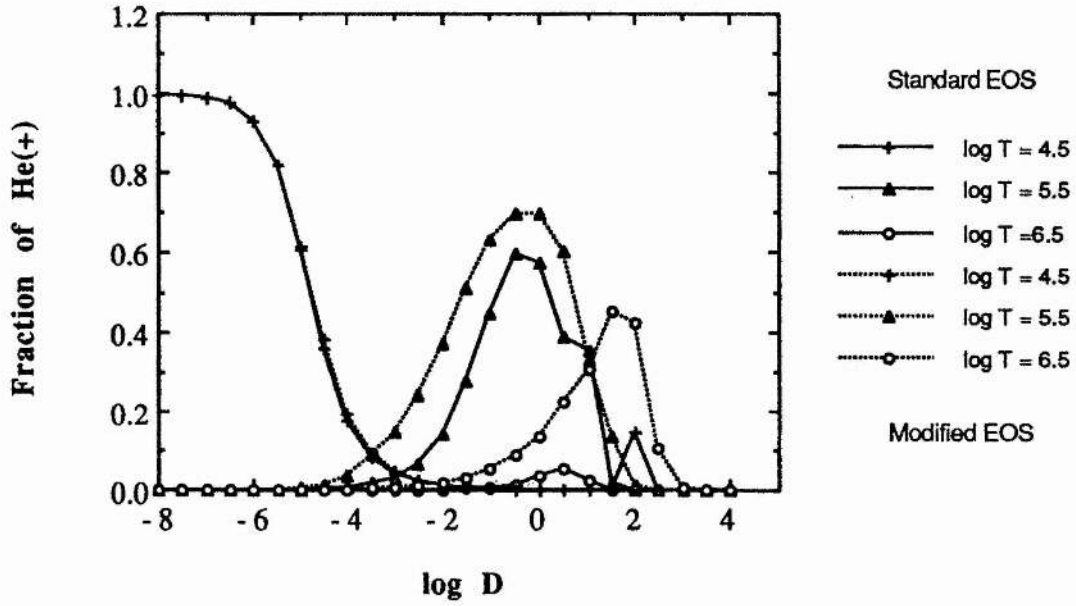

Figure 2.4 : Fractions of He atoms in the first ionized states., otherwise as in Figure 2.1.

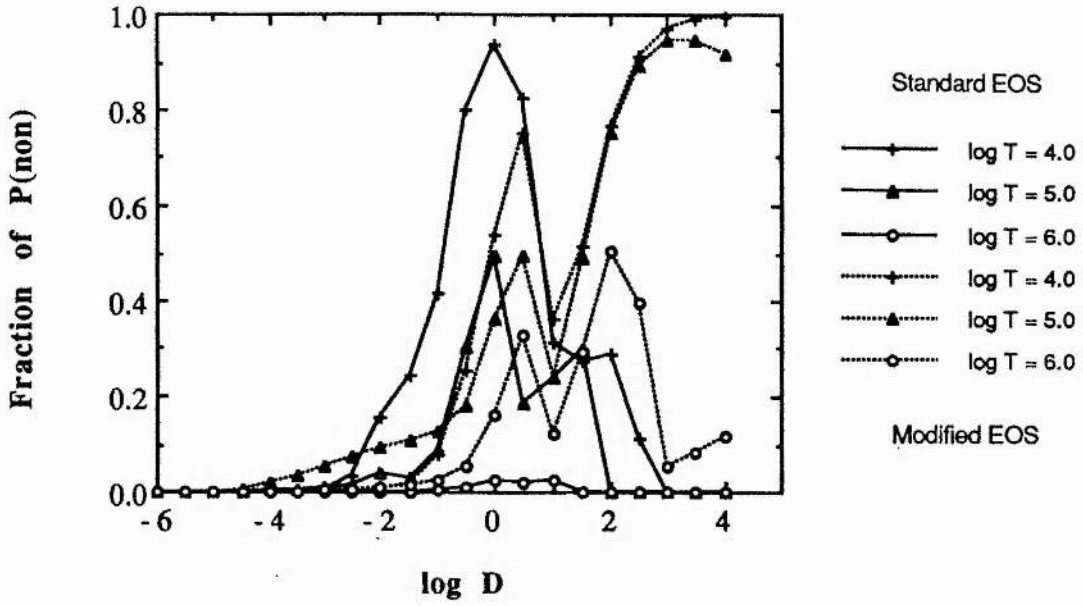

Figure 2.5 : Ratios of the pressure from nonideal effects to the total pressure, otherwise as in Figure 2.1.

Chapter III The Radiative Opacity

Introduction

An important factor governing the rate at which photons travel through stellar gases is the frequency dependent opacity. In stellar interiors and envelopes, the condition of local thermodynamic equilibrium allows one to describe the energy transport by an average quantity, i.e., the Rosseland mean opacity (see Section 3.1). The opacity is a measure of the electromagnetic interactions between photons and electrons, ions, or atomic systems. The processes of interaction are absorption and scattering of photons by those particles (see Section 3.2 and 3.3). In our study we calculate the opacity based on the hydrogen-like model for hydrogen and helium, and the average atom model for the heavy elements (see Section 3.4 and 3.5). The opacity data are computed for three compositions in Section 3.6, while in Section 3.7 we investigate the importance of each process of absorption and scattering as well as the heavy elements in the opacity calculation.

3.1 Rosseland mean opacity

3.1.1 Energy transport

It has been known that there are three basic mechanisms of energy transport in stars. They are radiation, conduction and convection, in which the energy is carried by photons, particles, and aggregates of particles, respectively. The mechanism by which the energy is carried depends on the local physical condition of the stellar gas. The conduction is a principal mode of energy transport at extremely high density when the electrons become highly degenerate. The convection dominates the energy transport when the temperature gradient is very great. Under most conditions in stars, however, energy transport by radiation is possible.

3.1.2 Radiation transport.

The rate of energy transport by radiation is limited by the interactions of photons with stellar gases. Different physical mechanisms can be used to explain this process. One of the examples is the use of the Boltzmann equation presented by Frank-Kamenetskii (1959) and Chiu (1968). The other one may also be seen from the argument by Frank-Kamenetskii (1959), following which the radiative transport is regarded as a result of diffusion of radiant energy according to the law of diffusion,

$$\mathbf{F} = -D \nabla E ,$$

where **F**, E and D are the energy flux, the energy density and the diffusion coefficient. According to the kinetic theory, the diffusion coefficient is expressed in the form

$$D = \lambda c/3 ,$$

with the photon's speed c and its mean free path λ.

3.1.3 Radiative opacity

The mean free path of photons λ quantifies the interaction of photons with stellar matter. Specifying their interactions with the particle of the type i with the number density n_i, by an absorption cross-section σ_i, the mean free path of the photons is written as

$$\lambda = [\sum_i n_i \sigma_i]^{-1}.$$

Usually, a radiative opacity κ is employed, instead of λ, to explain their interaction in terms of

$$\lambda = 1/\rho\kappa ,$$

with the mass density ρ. So the expression for radiative opacity is obtained

$$\kappa = \frac{1}{\rho} \sum_i n_i \sigma_i \ .$$

3.1.4 Rosseland mean opacity

From the above formulae, the energy flux per unit frequency is given by

$$\frac{dF}{d\omega} = - \frac{c}{3\rho\kappa(\omega)} \frac{d}{dr} \left[\frac{dE}{d\omega} \right] ,$$

where $\kappa(\omega)$ is the frequency-dependent opacity, which may be called absorption opacity. In the conditions of a stellar interior or envelope, the black body radiation formula is used to describe the energy density distribution through the Planck function for the temperature T, i.e.

$$\frac{dE}{d\omega} = \frac{1}{\pi^2 c^3} \frac{\omega}{\exp(\omega/T)-1} \ .$$

Then the integration over frequency leads to a relation of the total radiation flux to the temperature gradient, i.e.

$$F = - \frac{4acT^3}{3\rho\kappa} \frac{dT}{dr} ,$$

where the Stefan-Boltzmann constant is $a=\pi^2/15c^3$ in atomic units. A harmonic mean opacity κ, which is called the Rosseland mean opacity, is defined by

$$\frac{1}{\kappa} = \frac{15}{4\pi^4} \int du \ \frac{u^4 e^u}{\kappa(u)(e^u-1)^2} ,$$

with the reduced frequency $u=\omega/T$.

3.2 Interaction between radiation and the gas

3.2.1 Physical description

The interactions of radiation with a gas cause absorption and scattering of photons by particle systems. They take place when the particle system makes a transition from one state |a> to another one |b>, according to quantum mechanics. The transition rate is calculated by means of the quantization of the radiation field together with the particle system (see Heitler 1959, Harris 1975). Under a dipole approximation, the transition rate may be expressed as a probability per unit incident flux of photons, i.e., an absorption or scattering cross-section of photons with frequency ω

$$\sigma_{ab}(\omega) = \frac{4\pi^2 \omega}{3c} |\langle a|\mathbf{r}|b\rangle|^2 \, \delta(\omega_b - \omega_a \pm \omega) \, .$$

It requires the knowledge of the energies of the quantum system in the states |a> and |b>, i.e., ω_a and ω_b, and the position operator matrix element $\langle a|\mathbf{r}|b\rangle$.

The particle systems can be atoms, ions, molecules, or electrons, and thus the atomic absorption, molecular absorption and electron scattering take place. The state of the particle system determines the form of its interaction with photons. For instance, if both initial state and final state in the transition are bound, then we have bound-bound absorption. We can also have bound-free absorption and free-free absorption. Rayleigh scattering and Compton scattering take place respectively when the electrons in the scattering process are bound in the atom and in free states.

3.2.2 Hydrogenic approximation

The determination of the absorption cross-section requires the knowledge of the wave functions of the atomic system as well as its eigenvalues. However, it is very difficult to calculate the atomic data for complex atoms, except for the hydrogen-like atoms and some simple ones. An easy way is to treat all atomic systems like a hydrogen-like atom. This method has been used by Cox et al. (1965), Carson (1976) and Huebner (1985), etc., in the radiative opacity calculation.

In terms of the hydrogenic approximation, the wave function for an active electron in any atomic system is defined by an effective nuclear charge Z_k. A hydrogenic formula

$$E_k = - Z_k^2/2n_k^2$$

is employed to determine the effective nuclear charge Z_k if given the ionization energy E_k of the active electron from the specified state $|k>$ with a principal quantum number n_k. As a result, the absorption cross-section for any atomic system can be calculated by the formulae for the hydrogen-like atom.

3.2.3 Correction to absorption by stimulated emission

In addition to the absorption of photons by atomic systems, there are also other two processes. One of them, spontaneous emission, releases photons isotropically so as not to contribute to the total absorption. Another one, stimulated emission releases photons in the same direction as the absorption of photons so that it reduces the total absorption effect.

In thermodynamic equilibrium with a temperature T, the ratio of the probability for an atomic system to exist in an upper state relative to the probability of its existing in a lower state is $\exp(-\omega/T)$, where ω is the difference of energy of the two states and hence of the photons involved in the transition. Consequently, the absorption cross-section has to be corrected by a factor $[1-\exp(\omega/T)]$. The stimulation correction is not applied to the scattering since there is no stimulated emission in scattering processes.

3.3 Absorption and scattering processes

In this section, we state the main processes of absorption and scattering which are included in our calculation of radiative opacity. We present the formulae for the cross-sections of absorption and scattering in a way for easy computation.

3.3.1 Free-free absorption by hydrogen-like atoms

The free electrons in the Coulomb field can interact with radiation and change their states by absorbing photons. In a gas with the free electron number density n_e and a pure Coulomb potential of an ion with a nuclear charge Z, the absorption cross-section of the photons with frequency ω by the electrons with energy ε is given by quantum mechanics, i.e.,

$$\sigma_{ff}(\omega) = \left[\frac{16\pi^3}{3\sqrt{6}\ c}\ \frac{Z^2 n_e}{\omega^3\sqrt{\varepsilon}}\right] g_{ff}(\omega,\varepsilon)\ .$$

The first term in the bracket is the Kramers' semi-classical cross-section, and the second $g_{ff}(\omega,\varepsilon)$ is a quantum mechanical correction factor, called the Gaunt factor.

In thermodynamic equilibrium, a thermal average of the cross-section is obtained by using the Maxwell-Boltzmann distribution of electron velocity, giving

$$\sigma_{ff}(\omega) = \left[\frac{32\pi^2\sqrt{\pi}}{3\sqrt{6}\ c}\ \frac{Z^2\ n_e}{\omega^3\sqrt{T}}\right] g_{ff}^{T}(\omega,\varepsilon)\ .$$

The determination of the thermal average of the Gaunt factor $g_{ff}^{T}(\omega,\varepsilon)$ requires knowledge of quantum mechanics. A detailed study is given by Karzas and Latter (1961). In a recent study by Carson (1988a), the calculation of Coulomb free-free Gaunt factors is performed to produce a table for application in stellar opacity calculation.

3.3.2 Bound-free absorption by hydrogen-like atoms

The bound-free absorption takes place when an atomic system absorbs a photon and releases a free electron. For a hydrogen-like atom, its absorption cross-section is given by

$$\sigma_{bf}(\omega,i) = \left[\frac{8\pi}{3\sqrt{3}\ c}\ \frac{Z^4}{\omega^3\ n_i^5}\right] g_{bf}(i,\varepsilon_j)$$

for a transition of the electron from the bound state $|i\rangle$ with the energy $-E_i$ to a continuum

state with a kinetic energy ε_j. The frequency of the photons absorbed is defined by

$$\omega = \varepsilon_j + E_i.$$

The bound-free Gaunt factor $g_{bf}(i,\varepsilon_j)$ depends on the kinetic energy of the released electron and the bound state $|i\rangle$. It is determined by means of quantum mechanics, as shown in the studies by Goldwire (1968) and Menzel (1969). Carson (1988b) obtains a set of analytical formulae for the Coulomb Gaunt factors for hydrogen-like atoms. They include all partial wave electric dipole transitions for specified initial levels (up to n=5 for all l) and arbitrary final levels, thus giving a convenient table for use in radiative opacity calculations.

3.3.3 Line absorption by hydrogen-like atoms

3.3.3.1 Absorption cross-section

The line absorption, or bound-bound absorption, takes place when an atomic system makes a transition between two bound states. For a hydrogen-like atom with a transition from the state $|a\rangle$ to $|b\rangle$, the absorption cross-section of the photons with frequency ω is formulated as

$$\sigma_{ab}(\omega) = \frac{2\pi^2}{c} f_{ab} F_{ab}(\omega) .$$

The oscillator strength f_{ab} and the line profile function $F_{ab}(\omega)$ can be calculated according to quantum mechanics.

3.3.3.2 Oscillator strength

The oscillator strength is a correction factor to the classical result. It is determined by the wave functions of the eigenstates $|a\rangle$ and $|b\rangle$ involved in the transition and their energy difference $\omega_{ab}=E_b-E_a$ by the formula

$$f_{ab} = \frac{2}{3} \omega_{ab} \frac{\mathrm{Max}(l_a, l_b)}{2l_a+1} \delta(l_a-l_b\pm1) \, (r_{ab})^2 .$$

The angular momentum quantum numbers l_a and l_b specify the energy state |a> and |b> together with the principal quantum numbers n_a and n_b. The matrix element r_{ab} is calculated from the wave functions, i.e., r_{ab}=<a|r|b> with the radial coordinate r.

The wave functions of a hydrogen-like atom are well known and defined by the nuclear charge and quantum numbers. This is why the hydrogenic approximation is applied to the description of complex atoms. Although the matrix element r_{ab} in a Coulomb field can be calculated numerically from the specified wave functions, there are analytical formulae given recently by Carson (1988a).

3.3.3.3 Line Broadening

A number of broadening processes contribute to the determination of the line profile for bound-bound absorption. They include radiation damping, Doppler effect, Stark effect and electron impact. Of these processes, the broadening by radiation damping can always be neglected since its effect can never be comparable to the other processes. The Doppler broadening plays an important role in the case of low density and high temperature because its broadening effect only depends on the temperature. It can sometimes be ignored since at the high temperatures and low densities there are very few atomic systems existing. In the conditions of the stellar interior and envelope, the pressure broadening, i.e., from Stark effect and electron impact, are most dominant in the determination of the line profile.

In our opacity calculation we adopt the result by Griem(1959, 1960) for the line broadening by the Stark effect and electron impact. In his study, the broadening by ions is treated by using the quasi-static theory and the impact broadening of overlapping lines is applied to describe the effect of electrons on the line profile. The Holtsmark profile is obtained from the combination of these two kinds of broadening.

3.3.3.4 Line profile function

The following formulae are obtained from the results of Griem (1960). For hydrogen-like atoms, the line profile for a transition from the state |a> to |b> is defined by

$$J_{ab}(\omega) = \frac{2\pi c}{F_0 \omega^2} \frac{T(\beta,\gamma)}{K_{ab}} .$$

The Holtsmark normal field strength is $F_0=2.61 n_e^{2/3}$ with the electron number density n_e. The coefficient K_{ab}, which relates the wavelength shift to the perturbing field strength, is given by

$$K_{ab} = (72)^{1/3} \pi c \frac{(n_a n_b)^4}{Z^5 (n_b^2 - n_a^2)} ,$$

with the nuclear charge Z, and principal quantum numbers n_a and n_b for the states |a> and |b>.

The function $T(\beta,\gamma)$ defines the profile broadened by both ions and electrons. The variable β specifies the Stark effect and is defined by

$$\beta = \frac{2\pi c}{F_0 K_{ab}} \left| \frac{1}{\omega} - \frac{1}{\omega_{ab}} \right| ,$$

where ω_{ab} is the energy difference between the states |a> and |b>. The variable γ is related to the electron impact effect and defined by

$$\gamma = \Delta\omega \frac{2\pi c}{\omega_{ab}^2 F_0 K_{ab}} .$$

The electron damping constant $\Delta\omega$ is given by

$$\Delta\omega = \frac{(8\pi)^{1/2}}{9} \frac{n_e}{Z^2 T^{1/2}} \left[n_a^5 + n_b^5 \right] I(Y_{min}) ,$$

with an integral

$$I(Y_{min}) = \int_{Ymin}^{\infty} \frac{e^{-Y}}{Y} dY$$

$$\approx -\log_e Y_{min} - 0.577,$$

for $Y_{min} \ll 1$, and

$$Y_{min} = \frac{4\pi}{3} n_e \left[\frac{n_b^2}{ZT}\right]^2 .$$

In limit cases, the function $T(\beta,\gamma)$ can be reduced to simple forms. For large β ($\beta>20$), it reduces to

$$T(\beta,\gamma) = 1.5\beta^{-5/2} + \frac{\gamma}{2}\beta^{-2} ,$$

which corresponds to the broadening of the Stark effect. The electron impact effect dominates the line broadening for large γ ($\gamma>10$). Thus, a dispersion profile

$$J(\omega) = \frac{1}{\pi} \frac{\Delta\omega}{(\Delta\omega)^2+(\omega-\omega_{ab})^2}$$

is used instead of the Holtsmark profile. In the case of $\gamma<10$ and $\beta<20$, the values of $T(\beta,\gamma)$ are given in the table presented by Griem(1960).

3.3.4 Absorption by negative hydrogen

Continuous absorption by negative hydrogen ions (H^-) is a major opacity source in a cool stellar atmosphere, especially in a metal-rich gas. The negative hydrogen ions interact with radiation through bound-free transitions and free-free transitions, i.e.,

$$H^- + \text{photon} \Leftrightarrow H + e$$

and

$$H + e + \text{photon} \Leftrightarrow H + e.$$

A detailed study of the free-free absorption and bound-free absorption was given by Doughty et al. (1966) and Doughty and Fraser (1966). They listed the numerical calculation results in the form of tables. Tsuji (1966) also carried out a study of its absorption coefficients and presented analytical formulae for practical use. A recent study by John (1988) reviews continuous absorption of H^- and gives the analytical formulae which permit separate bound-free and free-free absorption coefficients to be generated at a wide range of temperatures and wavelengths. His resulting data are claimed to be accurate to better than 1 % or 2 %.

3.3.5 Free electron scattering

Electrons themselves can interact with photons, which causes a number of scattering processes. Because of the small mass of the electrons, their interaction with photons is much stronger than that of the nuclei. The scattering of photons by the electrons bound in atomic systems is called Rayleigh scattering while that by the free electrons is called Thomson scattering and Compton scattering. In fact, Thomson scattering is the low energy limiting case of Compton scattering.

The cross-section for Compton scattering must be computed quantum mechanically and turns out to be dependent on the frequency of the incoming photons. The expression for the cross-section, known as the Klein-Nishina formula, is

$$\sigma_{es}(\omega) = \frac{8\pi}{3c^4}\,\frac{3}{4}\left\{\frac{1+\alpha}{\alpha^3}\left[\frac{2\alpha(1+\alpha)}{1+2\alpha}-\frac{1}{\alpha}\ln(1+2\alpha)\right]+\frac{1}{2\alpha}\ln(1+2\alpha)-\frac{1+3\alpha}{(1+2\alpha)^2}\right\}$$

with $\alpha=\omega/c^2$.

At the extreme energy limit $\alpha<<1$, it reduces to the Thomson scattering cross-section, i.e.

$$\sigma_{es} = 8\pi/3c^4 ,$$

which is independent of the photon frequency.

3.3.6 Other processes

There are some other processes which become important opacity sources in some limiting cases. At very high temperature (e.g., $T>10^9$ K), the high energy of photons may create a positron-electron pair in the Coulomb field. They increase the number of scatterers so as to became an important source of the opacity. At low temperatures, the Rayleigh scattering by the electrons in the bound systems, e.g., atoms and molecules, also contributes to the opacity. In addition, molecular formation allows band absorption which becomes a dominant source of the opacity at temperatures below 3500 K.

3.4 Opacity calculation

3.4.1 Frequency-dependent opacities

The frequency-dependent opacities $\kappa(\omega)$ are required in the calculation of the Rosseland mean opacity. They are determined by the absorption opacities $\kappa_{ab}(\omega)$ and the scattering opacities $\kappa_{sc}(\omega)$ in terms of

$$\kappa(\omega) = \kappa_{sc}(\omega) + \kappa_{ab}(\omega)*(1- e^{\omega/T}) .$$

Here the correction factor from the stimulated emission is incorporated into the absorption opacity.

The determination of the frequency-dependent opacities $\kappa(\omega)$ needs the knowledge of the occupation number density of each type of absorbers and scatterers, denoted by n_j. If the corresponding cross-section is given by σ_j, then the resulting opacity $\kappa(\omega)$ is calculated by a sum over all types of absorbers and scatterers, i.e.,

$$\kappa(\omega) = \frac{1}{\rho} \sum_j n_j \sigma_j,$$

with the mass density ρ.

3.4.2 Free electron scattering opacity

The scattering opacity is simply determined by their number density n_e and scattering cross-section $\sigma_{es}(\omega)$ by means of

$$\kappa_{es}(\omega)=\frac{1}{\rho} n_e \sigma_{es}(\omega) .$$

3.4.3 Negative hydrogen absorption opacity

From the study by Tsuji (1966) we have the absorption cross-section $\sigma_{nh}(\omega)$ of photons per neutral hydrogen atom by negative hydrogen H^-. So the absorption opacity by H^- is calculated from the number density of neutral hydrogen atoms n_{H0} by means of

$$\kappa_{nh}(\omega) = \frac{1}{\rho} n_{H0} \sigma_{nh}(\omega) .$$

The determination of the number density of H^- ions has been included in this formula so that no knowledge of H^- ionization is required. In the case of high density, however, the pressure ionization of H^- has to be incorporated into the opacity calculation. The ratio of the number density of H^- ions to that of neutral H atoms has a form

$$\frac{n_{H^-}}{n_{H0}} = \frac{g_{H^-}}{g_{H0}} \exp(\lambda+X/T-\Delta E_b/T-\phi) ,$$

where λ is the electron degeneracy, X is the ionization energy, ΔE_b is the perturbation energy of the electrons bound in H^-, and $\exp(-\phi)$ is the occupation probability constrained by the finite size of H^-. Therefore, a correction factor $\exp(-\Delta E_b/T-\phi)$ has to be applied to $\kappa_{nh}(\omega)$.

3.4.4 Atomic absorption opacity by H-like atoms

The processes of absorption by free-free, bound-free and bound-bound transitions of atomic systems make contributions to the opacity. For a hydrogen-like atom, its energy states are specified by the principal and angular momentum quantum numbers n and l. The

equation of state in the LTE condition determines the probability of the atomic systems in each of their energy states, and is denoted by p(n,l).

If there are M types of H-like atoms in the gas and their number densities are specified by $\{n_i\}$, the atomic opacity is calculated by a sum over all of them and their energy states. This gives the bound-bound absorption opacity

$$\kappa_{bb}(\omega) = \frac{1}{\rho} \sum_{i}^{M} n_i \sum_{nl} p(n,l) \sum_{n'l'} \sigma_{bb}(n,l,n'l',\omega) ,$$

the bound-free absorption opacity

$$\kappa_{bf}(\omega) = \frac{1}{\rho} \sum_{i}^{M} n_i \sum_{nl} p(n,l) \sigma_{bf}(n,l,\omega) ,$$

and the free-free absorption opacity

$$\kappa_{ff}(\omega) = \frac{1}{\rho} \sum_{i}^{M} n_i \sigma_{ff}(n,l,\omega) .$$

In the above formulae, the sum is performed over all initial states by n and l, over all final states by n' and l'.

3.4.5 Atomic absorption opacity by complex atoms

Except for atomic systems with only one electron, which can be treated as H-like atoms, all of the other heavy elements are complex atoms. The general formulae to calculate their opacity are analogous to those for H-like atoms, but the energy states are specified in a general form of $|a\rangle$ for the initial state and $|b\rangle$ for the final one. Then their absorption opacity is given by

$$\kappa_{bb}(\omega) = \frac{1}{\rho} \sum_{i}^{M} n_i \sum_{a} p(a) \sum_{b} \sigma_{bb}(a,b,\omega) ,$$

$$\kappa_{bf}(\omega) = \frac{1}{\rho} \sum_{i}^{M} n_i \sum_{a} p(a) \sigma_{bf}(a,\omega) ,$$

and

$$\kappa_{ff}(\omega) = \frac{1}{\rho} \sum_{i}^{M} n_i \ \sigma_{ff}(\omega) \ .$$

In a practical calculation of their opacity, however, it is a very complex project to determine their energy states and absorption cross sections. In our study, we adopt an average atom model and develop it for the opacity calculation for heavy elements.

3.5 Average atom model for opacity calculation

We use the Grand Canonical Ensemble to derive new formulae to determine the average population of electrons and the distribution probabilities of electrons in atomic shells in the AA model.

3.5.1 Average atom model

The periodic table of the chemical elements indicates the shell structure of the atoms of heavy elements. For partially ionized atoms, the shell structure can remain a good approximation of the atoms since the ionization energy of an electron in a full shell is much greater than that in other cases. Consequently, it may be assumed that the ionizations of electrons in an atom occur shell by shell. On the basis of such a consideration, we make approximations that the distribution of electrons in each shell is independent of that in other shells and that the interactions between electrons in different shells are approximated by the average population of electrons in each shell. In the same shell, however, the interaction between electrons cannot be approximated by the average population because the electron number in the shell is strongly affected by their interaction if the shell is just being ionized. Therefore, the population of electrons in one shell should be solved simultaneously with their interactions, which determine the energies of those electrons in the shell.

3.5.2 Description by grand canonical ensemble

According to the AA model, all atoms of each element are described by one average atom in which there exist a series of atomic shells (nl) and the bound electrons can be populated and specified by hydrogenic wave functions (of one electron atom) with eigenvalue E_{nl}. Consider a system with one unit volume V=1 in which there are i=1,...,M types of elements and the number of atoms of each element is N_i , and suppose the system is under the LTE conditions specified by the temperature $T=1/\beta$ and the electron degeneracy parameter λ.

In order to obtain the distribution probability of electrons in the average atom and the free phase space, we start with the electron partition function (referred to EPF) in the system. The EPF per unit phase space of the free electron is $Z_1=1+\exp(\lambda-\beta\varepsilon)$ with the energy of the electron ε. In the average atom, the distribution of electrons in one shell is supposed to be independent of those in other shells and the possible numbers of bound electrons in the shell can be m = 0,1,2,...,g_{nl} (which is the statistical weight) Therefore the EPF in one atomic shell (nl) is written as

$$Z_{nl} = \sum_{m=0}^{g_{nl}} \exp[m(\lambda-\beta E_{nl}(m))] ,$$

where $E_{nl}(m)$ is the average energy of one electron with m electrons bound in the shell. According to the independent approximation of the electron distribution in different shells, the EPF in the whole average atom is equal to the product of the EPF in all shells. Therefore, the total grand partition function of the electrons in the system can be written as

$$Z_G(\beta,\lambda) = \prod_{<free>} [1+\exp(\lambda-\beta\varepsilon)] * \prod_i [\prod_{nl} Z_{nl}]^{Ni}$$

where the first product goes over the whole phase space of the free electrons, the second product over all elements, and the third one over the atomic shells of one average atom. The power of N_i accounts for the EPF in all atoms of the element i.

3.5.3 Average population and distribution probability of electrons

Statistical physics gives for the total number of electrons in the system

$$\sum_{i}^{M} N_i Z_i = \frac{\partial}{\partial \lambda} \log_e Z_G(\beta,\lambda)$$

$$= \sum_{<free>} \frac{1}{\exp(-\lambda+\beta\varepsilon)+1} + \sum_{i} N_i \sum_{nl} \frac{\partial}{\partial \lambda} \log_e Z_{nl}$$

$$= \sum_{<free>} x_e + \sum_{i} N_i \sum_{nl} x_{nl}$$

It is actually the conservation equation of electron number. The first term defines the occupation number of free electrons per unit phase space as x_e, which is given by the Fermi-Dirac formula. This term is actually the total number of free electrons which is obtained by summing over the whole phase space of free electrons (see Chapter II).

The second term defines the average population of electrons bound in each atomic shell (nl). They are obtained by using Z_{nl}, i.e.,

$$x_{nl} = \frac{\partial}{\partial \lambda} \log_e Z_{nl}$$

$$= \frac{\sum_{m=1}^{g_{nl}} \exp[m(\lambda-\beta E_{nl}(m))]*m}{\sum_{m=0}^{g_{nl}} \exp[m(\lambda-\beta E_{nl}(m))]}$$

$$= \sum_{m=1}^{g_{nl}} p_{nl}(m)*m$$

where $E_{nl}(m)$ is the average energy of the electron in the shell when there are m electrons populated in the shell.

We find that the probability of finding m electrons in the shell (nl) is defined by

$$p_{nl}(m) = \frac{\exp[m(\lambda-\beta E_{nl}(m))]}{\sum_{m=0}^{g_{nl}} \exp[m(\lambda-\beta E_{nl}(m))]} .$$

This formula defines the distribution probability of electrons in the atomic shells after the degeneracy parameter λ and the average energies of the electrons in each shell $E_{nl}(m)$ are solved from the self-consistent equations.

We notice the difference in physics between the Fermi-Dirac formula and the above formula from the statistical description of the AA mode. If it is supposed that there are g_{nl} (statistical weight) sub-shells in the atomic shell (nl) and the distribution of the electrons in each sub-shell is independent of other sub-shells, then the EPF in the atomic shell (nl) is equal to the product of the EPF in all sub-shells of the shell, that is

$$Z_{nl} = [1+\exp(\lambda-\beta E_{nl})]^{g_{nl}} .$$

Consequently, the Fermi-Dirac formula which determines the average population of electrons is recovered, but we cannot obtain the occupation probabilities of atomic shells by electrons. However, the independent approximation used above is too crude since the electrons in the same shell have the same energy, and therefore their distributions are strongly dependent on each other. In the new AA model, the EPF takes into account the dependence of the electron distributions in the same shell and thus gives an approximation of higher level than the Fermi-Dirac formula. Furthermore, the consideration of the dependence allows for the occupation probabilities of atomic shells by electrons, which is then used to determine directly the probability of the atomic configuration. If the dependences of the electron distributions in all shells of the atom are taken into account, the grand canonical ensemble can give the probabilities of atomic configurations. This has been presented in Section 2.4.1.5..

3.5.4 Determination of electron distribution probability

In the general case, the electron distribution probability $p_{nl}(m)$ can be found after the electron number conservation equation is solved for the electron degeneracy λ. Now $p_{nl}(m)$ depends on λ and the electron energies $E_{nl}(m)$ in the atomic shells while $E_{nl}(m)$ depends on the electron distributions. They thus lead to a set of self-consistent equations which can be solved for $p_{nl}(m)$.

In our opacity calculation, the electron degeneracy λ is obtained from the determination of the EOS. If the occupation probability $w_{nl} = \exp(-\phi_{nl})$ and the energy level perturbation ΔE_{nl} of the active electron in atomic shells are taken into account for interatomic interactions, the expression for the electron distribution probability is then written as

$$p_{nl}(m) = \frac{\exp[m(\lambda-\beta E_{nl,A}-\beta\Delta E_{nl}-\phi_{nl})]}{g_{nl}} \Big/ \sum_{m=0} \exp[m(\lambda-\beta E_{nl,A}-\beta\Delta E_{nl}-\phi_{nl})] .$$

3.5.5 Frequency dependent opacities

3.5.5.1 Opacity calculation with atomic configuration accounting

The electron distribution probabilities in atomic shells are used to construct detailed atomic configurations. Under the assumption that the electron distribution in one shell is independent of other shells, the probability of the configuration $A=\{m_{n'l'}\}$ in which there are $m_{n'l'}$ electrons populating in the shells $(n'l')$ is written as

$$P(A) = p(\{m_{n'l'}\}) = \prod_{n'l'} p_{n'l'}(m_{n'l'}) .$$

P(A) is normalised over all existing configurations of the atom, i.e.,

$$\sum_{<A>} P(A) = \prod_{n'l'} [\sum_{m_{n'l'}} p_{n'l'}(m_{n'l'})] = 1 .$$

When the detailed atomic configurations are taken into account, the total opacity from

bound-free transitions of the bound electrons is calculated by the summation over all existing configurations by A, over all atomic shells by n and l, and over all elements by i, i.e.,

$$\kappa_{bf}(\omega) = \frac{1}{\rho} \sum_{i} N_i \sum_{nl} \sum_{A} P(A) * m_{nl}(A) * \sigma_{bf}(\omega, Z_{nl}(A), E_{nl}(A)) ,$$

where $m_{nl}(A)$ is the number of electrons in the shell (nl) of the configuration A. The bound-free cross-section σ_{bf} for an active electron is calculated from the hydrogenic wave function defined by the effective nuclear charge $Z^*_{nl}(A)$ and the energy $E_{nl}(A)$ of the active electron in the shell (nl) of the configuration A.

Similarly, the total opacity from the bound-bound transitions of electrons are calculated by a sum over the existing configurations, i.e.,

$$\kappa_{bb}(\omega) = \frac{1}{\rho} \sum_{i} N_i \sum_{nl} \sum_{n'l'} \sum_{A} P(A) * m_{nl}(A) * \sigma_{bb}(\omega, \omega_0, Z_{nl}(A), Z_{n'l'}(A), E_{nl}(A), E_{n'l'}(A)) ,$$

where a summation over upper shells (n'l') is required for the bound-bound transitions. The effective nuclear charges of active electrons in both low shells (nl) and upper shells (n'l') are required to define the hydrogenic wave functions. They are used to calculate corresponding oscillator strengths and line profiles, and thence to determine the absorption cross-section σ_{bb}. The energy difference of the active electron between the low level and upper level $\omega_0 = E_{n'l'}(A) - E_{nl}(A)$ is used to approximate the absorption energy of the line centre.

3.5.5.2 Opacity calculation by average populations of electrons

If the average populations of electrons x_{nl} are used to approximate the detailed atomic configurations, a relation

$$\sum_{A} P(A) * m_{nl}(A) = x_{nl}$$

can be used to simplify the opacity calculation by the AA model. We then have the total opacity from the bound-free absorption calculated by

$$\kappa_{bf}(\omega) = \frac{1}{\rho} \sum_i N_i \sum_{nl} x_{nl} * \sigma_{bf}(\omega, Z_{nl}(A), E_{nl}(A)) ,$$

and the total opacity from the bound-bound absorption by

$$\kappa_{bb}(\omega) = \frac{1}{\rho} \sum_i N_i \sum_{nl} \sum_{n'l'} x_{nl} * \sigma_{bb}(\omega,\omega_0, Z_{nl}(A), Z_{n'l'}(A), E_{nl}(A), E_{n'l'}(A)) .$$

3.5.6 Atomic data

The calculation based on the AA model needs as the atomic data: the energies of the electrons in the atomic shells and their (one electron) wave functions, which are required to calculate the average populations, atomic configuration probabilities and radiative absorption cross-sections. So far, the relativistic Hartree-Fock-Slater calculation presented by Rozsnyai (1972) is one possible method to obtain these atomic data, as is the Thomas-Fermi model, used by Carson, Mayers and Stibbs (1968) in the calculations of stellar opacity. In the present opacity model, we choose the Ritz variational method presented by Carson and Hollingsworth (1968) to calculate the energy levels of electrons. Furthermore we assume that the wave functions of electrons are of hydrogen-like form defined by corresponding effective nuclear charges.

It is well known that the hydrogenic Slater screening constants, which are used in calculating effective charges, cannot reasonably describe the interaction between the multiple electrons in an atom, especially when most electrons are still bound. This can be seen from the comparison of theoretical calculations of the one-electron energy with the experimental data obtained by Slater (1955). The screening constants play a better role when the atom is nearly neutral. We therefore introduce corrections to the hydrogenic Slater screening constants in order to fit the experimental data of the neutral atoms, and

thus retain the screening constants $s_{nl,n'l',Z}$ for each element.

According to the Ritz variational method, the effective nuclear charge $Z_{nl}(A)$ felt by the electron in the shell (nl) of the configuration A is given by

$$Z_{nl}(A) = Z - \sum_{n'l' \neq nl} (s_{nl,n'l',Z} * m_{n'l'}) - s_{nl,nl,Z}[m - \mathrm{Min}(1, m_{nl})]$$

where Z is the nuclear charge of the element and $m_{n'l'}$ is the electron population in the shell (n'l') of the configuration $A=\{m_{nl}\}$. The corresponding energy of the active electron is determined by a hydrogenic form

$$E_{nl}(A) = -\frac{Z_{nl}^2(A)}{2n^2} .$$

3.5.7 Computation

In the computation of the AA model with detailed configuration-accounting for the opacity, the difficulty is the great cost of computing time due to the great number of atomic configurations involved. We adopt the following methods to overcome it.

In the AA model, the atomic shells with the first six principal quantum numbers (n=1,...,6) and all their angular momentum quantum states are included in the calculations of the bound-free absorption opacity and those with the first ten principal quantum numbers are included for the line absorption. They consequently involve a great number of atomic configurations which cost a lot of computing time. In order to make the AA model practical in the opacity calculation, we have to ignore those atomic configurations with relatively small probabilities. The molecular fraction, which is defined as the product of the atom number fraction of the element and the configuration probability, is employed to specify the most important atomic configurations. They are expected to contribute to the photon-ionization absorption and line absorption. Usually, we need to specify a minimum molecular fraction in order to limit the total number of the included atomic configurations to

below a couple of hundreds. The specified molecular fraction limit depends on the temperature and mass density.

The number of absorption lines is large because of the great number of the atomic configurations. Because the distribution of absorption lines is very dense in the photon frequency space, it is necessary to make the frequency mesh very fine for the integration of absorption coefficients. Usually, thousands of points in the photon energy space are required to be taken for the line absorption, and hundreds for the continuous absorption. For the sake of computing time, we allow the calculation to include only main part of a line profile and ignore the far wings. The integration for each line is started from the line centre towards the two wings and is cut off if the contribution to the absorption coefficient is smaller than one hundredth of the continuous absorption coefficient. This is a very good approximation since the line profile decreases rapidly towards the two wings. Also the contribution from the bound-free absorption is included only when the absorption coefficient at the absorption edge is greater than one hundredth of the continuous absorption coefficient integrated. These two specifications together with that of including only the most important configurations can accelerate the computing very considerably.

3.5.8 Investigation of AA model

It had been thought that the AA model can only be used to calculate the opacities at high temperatures where most electrons are free and the AA model is a good description of the heavy element atoms. Since we have developed the AA model by using a more accurate approximation, we would have more confidence and like to investigate its validity at middle temperatures.

We performed the opacity calculation for four ρ-T points for a composition X/Y/Z = 0.770/ 0.212/ 0.018 using both the detailed configuration-accounting and the average populations of electrons. The results are given in Table 3.1. At high temperatures, e.g., $T>10^5$ K, where the heavy elements play a role in the opacity contribution, the detailed configuration-

accounting leads to greater opacities than those calculated by using the average populations of electrons.

Table 3.1 : Comparison of opacities $\kappa(cm^2/g)$ calculated using the detailed configuration accounting (DCA) with those calculated using electron average populations (EAP).

T (K)	$\rho(g/cm^3)$	(DCA) κ	(EAP) κ
$5*10^5$	10^{-4}	3.53	1.32
$2*10^5$	10^{-5}	14.2	13.9
$1*10^5$	10^{-5}	299.0	215.0
$3*10^4$	10^{-7}	141.0	146.7

Both continuum and line frequency-dependent opacities calculated by using the detailed configuration-accounting are plotted in Figures 3.1-3.4 respectively for the four ρ-T points. They also show the continuum Rosseland mean opacities BF(H/He) contributed by the particles excluding the atoms of the heavy elements and BF(all) contributed by all particles as well as the line Rosseland mean opacities BB(H/He) contributed by the particles excluding the atoms of the heavy elements and BB(all) contributed by all particles. These figures show that the new AA model can account for the reasonable increases of the absorption coefficients by the heavy elements in the middle temperature range.

Figure 3.4 shows, by the raising of the continuum, that the line absorption of low energy photons (E<0.2 Ry) by the heavy elements appears very broadened and thus contributes a lot to the opacity. This is due to the hydrogenic formula for the line broadening (Griem 1960) which is used for the heavy elements and causes a large line broadening for the transition to the higher electronic levels, since the broadening width is proportional to the fifth power of the principal quantum number.

3.6 Radiative opacity data

3.6.1 Computation

We constructed a computing code for the opacity calculation based on the hydrogen-like atom model and the average atom model. All ions of H and He are treated as H-like atoms.

Figure 3.1

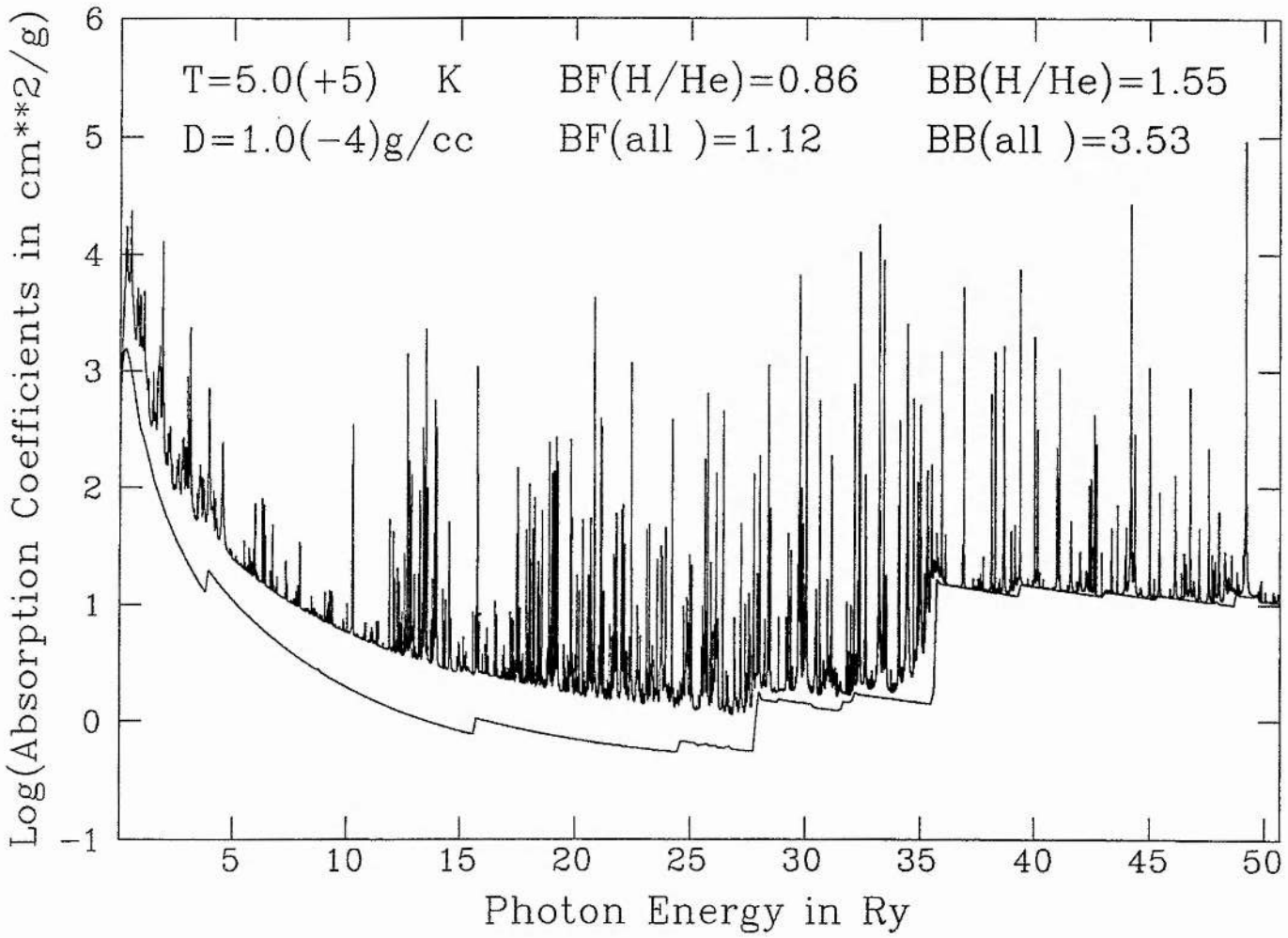
T=5.0(+5) K
D=1.0(−4)g/cc
BF(H/He)=0.86
BF(all)=1.12
BB(H/He)=1.55
BB(all)=3.53
Log(Absorption Coefficients in cm**2/g)
Photon Energy in Ry
6
5
4
3
2
1
0
−1
5
10
15
20
25
30
35
40
45
50

Figure 3.2

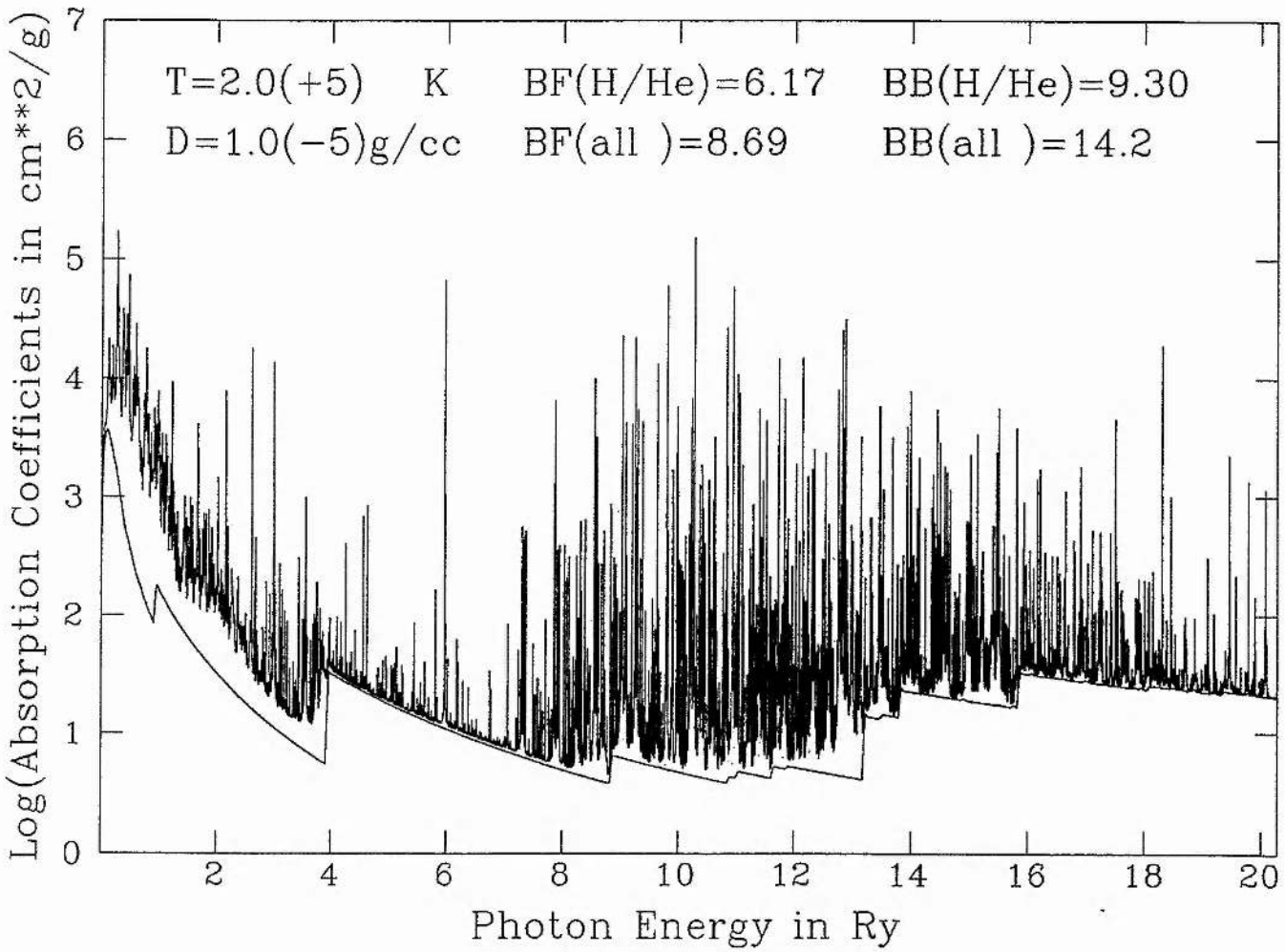
T=2.0(+5) K
D=1.0(−5)g/cc
BF(H/He)=6.17
BF(all)=8.69
BB(H/He)=9.30
BB(all)=14.2
Log(Absorption Coefficients in cm**2/g)
Photon Energy in Ry
0
1
2
3
4
5
6
7
2
4
6
8
10
12
14
16
18
20

Figure 3.3

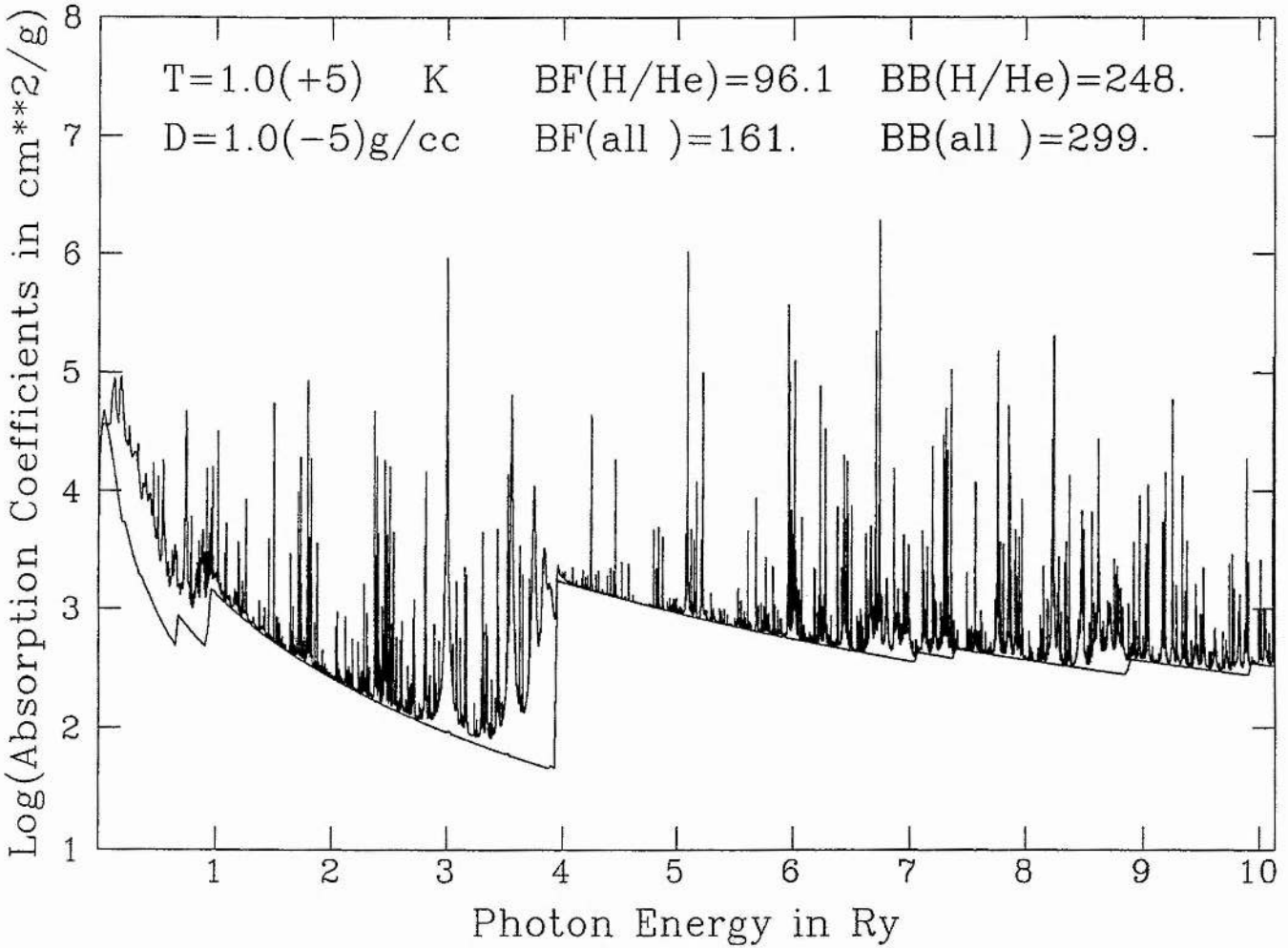
T=1.0(+5) K
D=1.0(−5)g/cc
BF(H/He)=96.1
BF(all)=161.
BB(H/He)=248.
BB(all)=299.
Log(Absorption Coefficients in cm**2/g)
Photon Energy in Ry
1
2
3
4
5
6
7
8
9
10

Figure 3.4

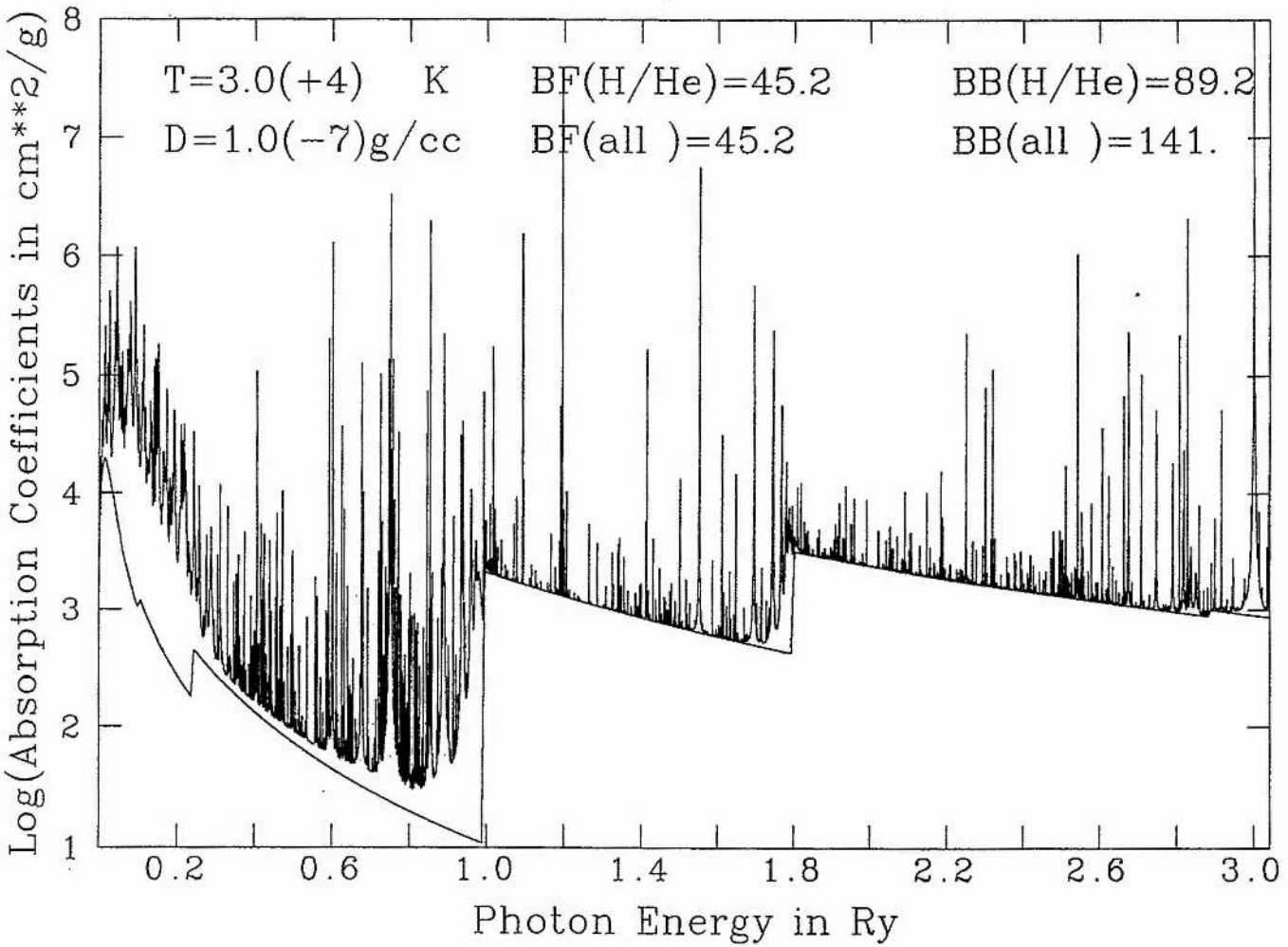
T=3.0(+4) K
D=1.0(−7)g/cc
BF(H/He)=45.2
BF(all)=45.2
BB(H/He)=89.2
BB(all)=141.
Log(Absorption Coefficients in cm**2/g)
8
7
6
5
4
3
2
1
0.2
0.6
1.0
1.4
1.8
2.2
2.6
3.0
Photon Energy in Ry

One of them, HeI, is supposed to have one electron fixed in the ground state so that the H-like atom model can be applied. All atoms of the heavy elements are dealt with by using the average atom model. Their opacity contribution is calculated by means of the average population of electrons.

The opacity calculation includes the contributions from the five processes: free electron scattering, negative hydrogen absorption, free-free, bound-free, bound-bound absorption by H, He and other heavy elements. The mass fraction of each heavy element over the heavy element abundance is listed in Table 1.1. Three compositions are employed to calculate opacity data tables for use in the study of LM stars.

The effect of pressure ionization has been taken into account in the determination of the atomic configuration probability by means of occupation probabilities. In the case of high density, the probability of the configurations with small ionization energies is very sensitive to pressure ionization which is caused by the interatomic interactions. This can affect the opacity calculation to a great extent.

3.6.2 Opacity data for three compositions

For the application in the study of LM stars, we produced opacity data tables for three compositions. They have the following mass abundances respectively for H, He and other heavy elements:

Table 3.2 : X/Y/Z=0.700/0.280/0.020;

Table 3.3 : X/Y/Z=0.710/0.289/0.001;

Table 3.4 : X/Y/Z=0.770/0.212/0.018.

The data tables cover a density range of $-14 \leq \log\rho(g/cm^3) \leq 6$ and a temperature range of $3.5 \leq \log T(K) \leq 8.0$. The opacity data are distributed in a density interval of $\Delta\log\rho=0.5$ and a temperature interval of $\Delta\log T=0.1$. So the data tables are in a rectangular distribution, which allows easy manipulation of the opacity data in computation. However,

Table 3.2 : Radiative Opacity Data for X/Y/Z=0.700/0.280/0.020

lgT\lgρ	-12.000	-11.000	-10.000	-9.000	-8.000	-7.000	-6.000	-5.000	-4.000
3.5	-4.420	-4.199	-3.730	-3.033	-2.269	-1.686	-1.343	-1.146	-1.225
3.6	-4.154	-4.123	-3.565	-2.727	-1.857	-1.022	-0.279	0.207	0.063
3.7	-2.673	-2.984	-2.877	-2.400	-1.728	-0.892	-0.045	0.698	0.865
3.8	-1.183	-1.472	-1.502	-1.214	-0.783	-0.281	0.261	0.858	1.125
3.9	-0.416	-0.231	-0.073	0.127	0.388	0.734	1.133	1.527	1.629
4.0	-0.466	-0.126	0.561	1.194	1.556	1.811	2.090	2.371	2.436
4.1	-0.486	-0.326	0.222	1.126	2.016	2.584	2.916	3.150	3.217
4.2	-0.491	-0.410	-0.076	0.681	1.703	2.717	3.428	3.795	3.932
4.3	-0.486	-0.433	-0.229	0.370	1.334	2.423	3.460	4.181	4.505
4.4	-0.486	-0.422	-0.260	0.203	1.100	2.199	3.287	4.277	4.887
4.5	-0.466	-0.407	-0.234	0.149	1.003	2.068	3.133	4.146	5.000
4.6	-0.471	-0.439	-0.265	0.184	0.992	2.080	2.959	3.946	4.880
4.7	-0.473	-0.460	-0.365	-0.005	0.749	1.745	2.648	3.534	4.511
4.8	-0.474	-0.467	-0.421	-0.206	0.407	1.340	2.227	3.078	4.044
4.9	-0.475	-0.472	-0.448	-0.322	0.079	0.877	1.768	2.675	3.691
5.0	-0.475	-0.474	-0.464	-0.386	-0.079	0.593	1.416	2.341	3.373
5.1	-0.475	-0.475	-0.471	-0.434	-0.219	0.333	1.152	2.018	3.109
5.2	-0.475	-0.475	-0.474	-0.458	-0.343	0.091	0.868	1.710	2.608
5.3	-0.476	-0.475	-0.475	-0.469	-0.418	-0.144	0.473	1.211	2.054
5.4	-0.476	-0.476	-0.475	-0.473	-0.455	-0.335	0.070	0.707	1.495
5.5	-0.476	-0.476	-0.476	-0.475	-0.469	-0.419	-0.204	0.244	0.972
5.6	-0.476	-0.476	-0.476	-0.475	-0.473	-0.453	-0.346	-0.067	0.500
5.7	-0.476	-0.476	-0.476	-0.476	-0.475	-0.464	-0.409	-0.251	0.137
5.8	-0.476	-0.476	-0.476	-0.476	-0.475	-0.472	-0.450	-0.364	-0.089
5.9	-0.476	-0.476	-0.476	-0.476	-0.476	-0.474	-0.462	-0.415	-0.239
6.0	-0.476	-0.476	-0.476	-0.476	-0.476	-0.476	-0.469	-0.445	-0.327
6.1	-0.476	-0.476	-0.476	-0.476	-0.476	-0.476	-0.474	-0.460	-0.390
6.2	-0.476	-0.476	-0.476	-0.476	-0.476	-0.476	-0.476	-0.469	-0.428
6.3	-0.477	-0.477	-0.477	-0.477	-0.477	-0.477	-0.476	-0.474	-0.453
6.4	-0.477	-0.477	-0.477	-0.477	-0.477	-0.477	-0.477	-0.473	-0.467
6.5	-0.478	-0.478	-0.478	-0.478	-0.478	-0.478	-0.478	-0.477	-0.473
6.6	-0.478	-0.478	-0.478	-0.478	-0.478	-0.478	-0.478	-0.478	-0.476
6.7	-0.479	-0.479	-0.479	-0.479	-0.479	-0.479	-0.479	-0.479	-0.478
6.8	-0.480	-0.480	-0.480	-0.480	-0.480	-0.480	-0.480	-0.480	-0.479
6.9	-0.481	-0.481	-0.481	-0.481	-0.481	-0.481	-0.481	-0.481	-0.481
7.0	-0.482	-0.482	-0.482	-0.482	-0.482	-0.482	-0.482	-0.482	-0.482
7.1	-0.484	-0.484	-0.484	-0.484	-0.484	-0.484	-0.484	-0.484	-0.484
7.2	-0.486	-0.486	-0.486	-0.486	-0.486	-0.486	-0.486	-0.486	-0.486
7.3	-0.489	-0.489	-0.489	-0.489	-0.489	-0.489	-0.489	-0.489	-0.489
7.4	-0.492	-0.492	-0.492	-0.492	-0.492	-0.492	-0.492	-0.492	-0.492
7.5	-0.497	-0.497	-0.497	-0.497	-0.497	-0.497	-0.497	-0.497	-0.497
7.6	-0.502	-0.502	-0.502	-0.502	-0.502	-0.502	-0.502	-0.502	-0.502
7.7	-0.511	-0.511	-0.511	-0.511	-0.511	-0.511	-0.511	-0.511	-0.511
7.8	-0.532	-0.532	-0.532	-0.532	-0.532	-0.532	-0.532	-0.532	-0.532
7.9	-0.574	-0.574	-0.574	-0.574	-0.574	-0.574	-0.574	-0.574	-0.574
8.0	-0.638	-0.638	-0.638	-0.638	-0.638	-0.638	-0.638	-0.638	-0.638

Table 3.2 : Continued

lgT\lgρ	-3.000	-2.000	-1.000	0.000	1.000	2.000	3.000	4.000	5.000
3.5	-1.767	-1.309	0.717	4.484	11.179	12.383	13.588	14.614	15.616
3.6	-0.592	-0.557	1.088	4.857	10.853	12.035	13.250	14.267	15.268
3.7	0.302	0.293	1.572	5.127	10.532	11.687	12.915	13.919	14.920
3.8	0.842	0.647	1.755	5.287	10.217	11.340	12.569	13.571	14.572
3.9	1.367	0.946	1.790	5.394	9.906	10.992	12.221	13.224	14.224
4.0	2.207	1.495	1.882	5.508	9.599	10.644	11.873	12.875	13.876
4.1	3.061	2.250	2.256	5.637	9.282	10.295	11.526	12.527	13.528
4.2	3.852	2.983	2.692	5.796	8.940	9.947	11.177	12.179	13.180
4.3	4.538	3.680	3.224	5.959	8.591	9.599	10.828	11.830	12.831
4.4	5.067	4.360	3.846	5.987	8.241	9.256	10.479	11.481	12.482
4.5	5.356	4.925	4.474	5.877	7.891	8.928	10.129	11.131	12.132
4.6	5.422	5.274	5.077	5.684	7.539	8.626	9.778	10.780	11.781
4.7	5.203	5.333	5.393	5.470	7.188	8.334	9.427	10.429	11.430
4.8	4.846	5.204	5.373	5.251	6.832	8.041	9.074	10.076	11.077
4.9	4.543	4.977	5.130	5.033	6.477	7.706	8.721	9.722	10.723
5.0	4.263	4.748	4.870	4.817	6.120	7.352	8.366	9.367	10.368
5.1	3.964	4.477	4.626	4.600	5.762	6.995	8.009	9.010	10.011
5.2	3.534	4.157	4.382	4.381	5.405	6.637	7.651	8.653	9.654
5.3	3.000	3.708	4.090	4.150	5.050	6.277	7.292	8.293	9.294
5.4	2.450	3.226	3.745	3.902	4.701	5.916	6.931	7.932	8.933
5.5	1.934	2.750	3.355	3.628	4.363	5.554	6.569	7.570	8.571
5.6	1.418	2.311	2.952	3.331	4.039	5.191	6.205	7.207	8.207
5.7	0.992	1.905	2.576	3.022	3.725	4.827	5.840	6.842	7.843
5.8	0.625	1.572	2.260	2.725	3.413	4.465	5.475	6.477	7.478
5.9	0.324	1.236	1.991	2.456	3.107	4.105	5.108	6.110	7.111
6.0	0.075	0.933	1.780	2.233	2.814	3.747	4.741	5.744	6.744
6.1	-0.108	0.618	1.511	2.037	2.540	3.392	4.374	5.377	6.377
6.2	-0.208	0.380	1.257	1.866	2.275	3.038	4.006	5.008	6.008
6.3	-0.336	0.119	0.973	1.645	2.021	2.689	3.639	4.641	5.641
6.4	-0.409	-0.087	0.644	1.371	1.753	2.342	3.273	4.273	5.273
6.5	-0.444	-0.248	0.346	1.043	1.481	2.001	2.907	3.906	4.906
6.6	-0.464	-0.381	0.029	0.685	1.180	1.666	2.543	3.539	4.539
6.7	-0.472	-0.432	-0.219	0.333	0.873	1.340	2.180	3.172	4.172
6.8	-0.477	-0.454	-0.337	0.055	0.584	1.024	1.822	2.807	3.806
6.9	-0.479	-0.472	-0.418	-0.169	0.295	0.729	1.472	2.442	3.440
7.0	-0.482	-0.477	-0.444	-0.319	0.055	0.463	1.139	2.080	3.076
7.1	-0.484	-0.482	-0.464	-0.398	-0.139	0.235	0.830	1.722	2.712
7.2	-0.486	-0.485	-0.478	-0.429	-0.278	0.044	0.549	1.371	2.350
7.3	-0.489	-0.489	-0.486	-0.464	-0.355	-0.108	0.300	1.035	1.990
7.4	-0.492	-0.492	-0.491	-0.481	-0.416	-0.236	0.088	0.721	1.635
7.5	-0.497	-0.497	-0.496	-0.492	-0.463	-0.332	-0.086	0.438	1.288
7.6	-0.502	-0.502	-0.502	-0.500	-0.486	-0.414	-0.224	0.193	0.956
7.7	-0.511	-0.511	-0.511	-0.510	-0.504	-0.467	-0.334	-0.016	0.639
7.8	-0.532	-0.532	-0.532	-0.531	-0.528	-0.509	-0.427	-0.199	0.341
7.9	-0.574	-0.574	-0.574	-0.574	-0.573	-0.564	-0.518	-0.364	0.064
8.0	-0.638	-0.638	-0.638	-0.638	-0.638	-0.634	-0.610	-0.512	-0.184

Table 3.3 : Radiative Opacity Data for X/Y/Z=0.710/0.289/0.001

lgT\lgρ	-12.000	-11.000	-10.000	-9.000	-8.000	-7.000	-6.000	-5.000	-4.000
3.5	-5.681	-5.417	-4.853	-4.096	-3.313	-2.634	-2.220	-2.070	-2.321
3.6	-4.518	-4.764	-4.536	-3.882	-3.015	-2.127	-1.339	-0.821	-0.931
3.7	-2.701	-3.044	-2.996	-2.614	-2.132	-1.596	-1.002	-0.376	-0.261
3.8	-1.182	-1.475	-1.507	-1.234	-0.824	-0.386	0.066	0.475	0.453
3.9	-0.409	-0.225	-0.068	0.122	0.385	0.717	1.095	1.450	1.477
4.0	-0.459	-0.120	0.568	1.202	1.555	1.807	2.075	2.337	2.382
4.1	-0.480	-0.318	0.232	1.133	2.022	2.589	2.918	3.143	3.204
4.2	-0.484	-0.403	-0.068	0.683	1.703	2.722	3.433	3.795	3.933
4.3	-0.479	-0.427	-0.221	0.364	1.327	2.421	3.465	4.186	4.510
4.4	-0.480	-0.415	-0.255	0.206	1.093	2.195	3.294	4.267	4.890
4.5	-0.459	-0.402	-0.228	0.153	0.965	2.054	3.134	4.153	5.005
4.6	-0.464	-0.432	-0.258	0.191	0.995	2.050	2.964	3.914	4.880
4.7	-0.466	-0.453	-0.357	0.003	0.753	1.738	2.652	3.515	4.488
4.8	-0.468	-0.460	-0.415	-0.198	0.407	1.326	2.217	3.063	4.026
4.9	-0.468	-0.465	-0.441	-0.315	0.084	0.878	1.757	2.660	3.672
5.0	-0.468	-0.467	-0.457	-0.378	-0.075	0.590	1.413	2.311	3.368
5.1	-0.469	-0.468	-0.464	-0.426	-0.223	0.322	1.128	2.007	3.082
5.2	-0.469	-0.468	-0.467	-0.451	-0.336	0.090	0.849	1.662	2.547
5.3	-0.469	-0.469	-0.468	-0.462	-0.412	-0.148	0.442	1.137	1.928
5.4	-0.469	-0.469	-0.468	-0.467	-0.449	-0.328	0.043	0.605	1.318
5.5	-0.469	-0.469	-0.469	-0.468	-0.462	-0.413	-0.209	0.164	0.770
5.6	-0.469	-0.469	-0.469	-0.469	-0.466	-0.447	-0.350	-0.118	0.327
5.7	-0.469	-0.469	-0.469	-0.469	-0.467	-0.458	-0.413	-0.284	0.021
5.8	-0.469	-0.469	-0.469	-0.469	-0.469	-0.466	-0.447	-0.378	-0.168
5.9	-0.469	-0.469	-0.469	-0.469	-0.469	-0.468	-0.460	-0.424	-0.312
6.0	-0.469	-0.469	-0.469	-0.469	-0.469	-0.469	-0.466	-0.451	-0.377
6.1	-0.469	-0.469	-0.469	-0.469	-0.469	-0.469	-0.468	-0.461	-0.428
6.2	-0.470	-0.470	-0.470	-0.470	-0.470	-0.470	-0.469	-0.466	-0.449
6.3	-0.470	-0.470	-0.470	-0.470	-0.470	-0.470	-0.470	-0.468	-0.460
6.4	-0.470	-0.470	-0.470	-0.470	-0.470	-0.470	-0.470	-0.470	-0.466
6.5	-0.471	-0.471	-0.471	-0.471	-0.471	-0.471	-0.471	-0.470	-0.469
6.6	-0.471	-0.471	-0.471	-0.471	-0.471	-0.471	-0.471	-0.471	-0.470
6.7	-0.472	-0.472	-0.472	-0.472	-0.472	-0.472	-0.472	-0.472	-0.472
6.8	-0.473	-0.473	-0.473	-0.473	-0.473	-0.473	-0.473	-0.473	-0.473
6.9	-0.474	-0.474	-0.474	-0.474	-0.474	-0.474	-0.474	-0.474	-0.474
7.0	-0.475	-0.475	-0.475	-0.475	-0.475	-0.475	-0.475	-0.475	-0.475
7.1	-0.477	-0.477	-0.477	-0.477	-0.477	-0.477	-0.477	-0.477	-0.477
7.2	-0.479	-0.479	-0.479	-0.479	-0.479	-0.479	-0.479	-0.479	-0.479
7.3	-0.482	-0.482	-0.482	-0.482	-0.482	-0.482	-0.482	-0.482	-0.482
7.4	-0.486	-0.486	-0.486	-0.486	-0.486	-0.486	-0.486	-0.486	-0.486
7.5	-0.490	-0.490	-0.490	-0.490	-0.490	-0.490	-0.490	-0.490	-0.490
7.6	-0.495	-0.495	-0.495	-0.495	-0.495	-0.495	-0.495	-0.495	-0.495
7.7	-0.504	-0.504	-0.504	-0.504	-0.504	-0.504	-0.504	-0.504	-0.504
7.8	-0.525	-0.525	-0.525	-0.525	-0.525	-0.525	-0.525	-0.525	-0.525
7.9	-0.567	-0.567	-0.567	-0.567	-0.567	-0.567	-0.567	-0.567	-0.567
8.0	-0.632	-0.632	-0.632	-0.632	-0.632	-0.632	-0.632	-0.632	-0.632

Table 3.3 : Continued

lgT\lgρ	-3.000	-2.000	-1.000	0.000	1.000	2.000	3.000	4.000	5.000
3.5	-3.014	-3.079	-1.334	8.781	11.366	12.441	13.595	14.595	15.595
3.6	-1.742	-2.109	-0.942	8.479	11.020	12.095	13.247	14.248	15.248
3.7	-0.819	-1.238	-0.592	8.184	10.672	11.749	12.900	13.900	14.900
3.8	-0.091	-0.747	-0.336	7.897	10.325	11.404	12.552	13.552	14.552
3.9	1.074	0.167	0.328	7.622	9.977	11.058	12.204	13.204	14.204
4.0	2.111	1.187	0.998	7.369	9.628	10.712	11.856	12.856	13.856
4.1	3.030	2.113	1.775	7.147	9.280	10.365	11.508	12.508	13.508
4.2	3.845	2.914	2.569	6.944	8.932	10.029	11.159	12.159	13.159
4.3	4.539	3.646	3.314	6.735	8.582	9.721	10.810	11.810	12.810
4.4	5.068	4.338	4.007	6.511	8.232	9.416	10.461	11.461	12.461
4.5	5.357	4.906	4.634	6.267	7.881	9.099	10.111	11.111	12.111
4.6	5.423	5.260	5.200	6.013	7.529	8.759	9.760	10.760	11.760
4.7	5.189	5.321	5.448	5.755	7.178	8.408	9.408	10.409	11.409
4.8	4.827	5.194	5.370	5.492	6.824	8.054	9.055	10.055	11.055
4.9	4.513	4.966	5.112	5.229	6.473	7.700	8.701	9.701	10.701
5.0	4.261	4.726	4.849	4.971	6.123	7.344	8.345	9.345	10.345
5.1	3.957	4.463	4.606	4.716	5.775	6.986	7.987	8.987	9.987
5.2	3.486	4.133	4.361	4.464	5.430	6.628	7.629	8.629	9.629
5.3	2.866	3.662	4.065	4.202	5.091	6.267	7.268	8.268	9.268
5.4	2.239	3.116	3.705	3.926	4.759	5.905	6.906	7.906	8.906
5.5	1.654	2.562	3.288	3.627	4.429	5.541	6.542	7.542	8.542
5.6	1.140	2.038	2.838	3.302	4.095	5.176	6.177	7.177	8.177
5.7	0.726	1.577	2.386	2.953	3.753	4.810	5.810	6.810	7.810
5.8	0.364	1.209	1.955	2.590	3.405	4.443	5.443	6.443	7.443
5.9	0.099	0.838	1.576	2.223	3.051	4.074	5.074	6.074	7.074
6.0	-0.134	0.468	1.221	1.873	2.695	3.705	4.705	5.705	6.705
6.1	-0.282	0.189	0.918	1.538	2.340	3.336	4.335	5.335	6.335
6.2	-0.358	-0.043	0.625	1.232	1.986	2.966	3.964	4.964	5.964
6.3	-0.416	-0.220	0.325	0.922	1.639	2.598	3.594	4.594	5.594
6.4	-0.443	-0.328	0.052	0.619	1.300	2.231	3.224	4.223	5.223
6.5	-0.457	-0.391	-0.137	0.330	0.975	1.867	2.854	3.853	4.853
6.6	-0.465	-0.435	-0.282	0.074	0.669	1.510	2.486	3.484	4.484
6.7	-0.469	-0.453	-0.372	-0.115	0.399	1.165	2.119	3.115	4.115
6.8	-0.472	-0.463	-0.413	-0.246	0.165	0.840	1.758	2.748	3.747
6.9	-0.473	-0.469	-0.444	-0.336	-0.031	0.546	1.404	2.382	3.380
7.0	-0.475	-0.473	-0.459	-0.394	-0.176	0.289	1.065	2.019	3.014
7.1	-0.477	-0.476	-0.469	-0.431	-0.286	0.077	0.749	1.661	2.649
7.2	-0.479	-0.479	-0.475	-0.453	-0.361	-0.093	0.466	1.312	2.287
7.3	-0.482	-0.482	-0.480	-0.468	-0.411	-0.222	0.222	0.980	1.928
7.4	-0.486	-0.485	-0.485	-0.479	-0.445	-0.317	0.020	0.672	1.574
7.5	-0.490	-0.490	-0.489	-0.486	-0.468	-0.385	-0.139	0.397	1.231
7.6	-0.495	-0.495	-0.495	-0.494	-0.483	-0.434	-0.261	0.162	0.903
7.7	-0.504	-0.504	-0.504	-0.504	-0.498	-0.470	-0.356	-0.039	0.593
7.8	-0.525	-0.525	-0.525	-0.525	-0.522	-0.506	-0.436	-0.213	0.302
7.9	-0.567	-0.567	-0.567	-0.567	-0.566	-0.558	-0.518	-0.372	0.033
8.0	-0.632	-0.632	-0.632	-0.632	-0.631	-0.627	-0.606	-0.515	-0.207

Table 3.4 : Radiative Opacity data for X/Y/Z=0.770/0.212/0.018

lgT\lgρ	-12.000	-11.000	-10.000	-9.000	-8.000	-7.000	-6.000	-5.000	-4.000
3.5	-4.455	-4.211	-3.727	-3.018	-2.252	-1.675	-1.347	-1.169	-1.294
3.6	-4.170	-4.138	-3.569	-2.723	-1.847	-1.010	-0.267	0.207	0.009
3.7	-2.655	-2.960	-2.843	-2.370	-1.711	-0.884	-0.036	0.698	0.819
3.8	-1.157	-1.439	-1.458	-1.163	-0.734	-0.241	0.301	0.869	1.098
3.9	-0.367	-0.182	-0.026	0.172	0.440	0.783	1.182	1.567	1.631
4.0	-0.417	-0.063	0.631	1.254	1.611	1.863	2.142	2.411	2.475
4.1	-0.453	-0.275	0.295	1.207	2.086	2.641	2.967	3.195	3.253
4.2	-0.461	-0.372	-0.026	0.751	1.790	2.795	3.492	3.846	3.976
4.3	-0.456	-0.401	-0.187	0.419	1.392	2.490	3.535	4.243	4.554
4.4	-0.459	-0.390	-0.214	0.252	1.148	2.258	3.359	4.339	4.940
4.5	-0.448	-0.387	-0.203	0.203	1.055	2.139	3.208	4.214	5.060
4.6	-0.453	-0.418	-0.240	0.215	1.038	2.105	3.014	3.970	4.926
4.7	-0.455	-0.441	-0.341	0.027	0.790	1.785	2.722	3.548	4.542
4.8	-0.457	-0.449	-0.400	-0.177	0.443	1.372	2.264	3.092	4.062
4.9	-0.457	-0.454	-0.422	-0.301	0.113	0.911	1.791	2.694	3.686
5.0	-0.457	-0.456	-0.447	-0.372	-0.048	0.614	1.430	2.333	3.372
5.1	-0.457	-0.457	-0.443	-0.420	-0.222	0.331	1.175	2.017	3.057
5.2	-0.457	-0.457	-0.456	-0.442	-0.339	0.084	0.842	1.672	2.550
5.3	-0.458	-0.457	-0.457	-0.452	-0.409	-0.161	0.426	1.147	1.994
5.4	-0.458	-0.458	-0.457	-0.456	-0.440	-0.335	0.042	0.664	1.440
5.5	-0.458	-0.458	-0.458	-0.457	-0.451	-0.403	-0.217	0.204	0.932
5.6	-0.458	-0.458	-0.458	-0.457	-0.455	-0.438	-0.335	-0.095	0.458
5.7	-0.458	-0.458	-0.458	-0.458	-0.457	-0.447	-0.398	-0.258	0.117
5.8	-0.458	-0.458	-0.458	-0.458	-0.458	-0.455	-0.435	-0.356	-0.090
5.9	-0.458	-0.458	-0.458	-0.458	-0.458	-0.456	-0.447	-0.403	-0.234
6.0	-0.458	-0.458	-0.458	-0.458	-0.458	-0.458	-0.453	-0.426	-0.322
6.1	-0.458	-0.458	-0.458	-0.458	-0.458	-0.458	-0.456	-0.443	-0.378
6.2	-0.458	-0.458	-0.458	-0.458	-0.458	-0.458	-0.458	-0.451	-0.411
6.3	-0.459	-0.459	-0.459	-0.459	-0.459	-0.459	-0.458	-0.456	-0.437
6.4	-0.459	-0.459	-0.459	-0.459	-0.459	-0.459	-0.459	-0.458	-0.450
6.5	-0.460	-0.460	-0.460	-0.460	-0.460	-0.460	-0.460	-0.459	-0.456
6.6	-0.460	-0.460	-0.460	-0.460	-0.460	-0.460	-0.460	-0.460	-0.458
6.7	-0.461	-0.461	-0.461	-0.461	-0.461	-0.461	-0.461	-0.461	-0.460
6.8	-0.462	-0.462	-0.462	-0.462	-0.462	-0.462	-0.462	-0.462	-0.461
6.9	-0.463	-0.463	-0.463	-0.463	-0.463	-0.463	-0.463	-0.463	-0.463
7.0	-0.464	-0.464	-0.464	-0.464	-0.464	-0.464	-0.464	-0.464	-0.464
7.1	-0.466	-0.466	-0.466	-0.466	-0.466	-0.466	-0.466	-0.466	-0.466
7.2	-0.468	-0.468	-0.468	-0.468	-0.468	-0.468	-0.468	-0.468	-0.468
7.3	-0.471	-0.471	-0.471	-0.471	-0.471	-0.471	-0.471	-0.471	-0.471
7.4	-0.474	-0.474	-0.474	-0.474	-0.474	-0.474	-0.474	-0.474	-0.474
7.5	-0.479	-0.479	-0.479	-0.479	-0.479	-0.479	-0.479	-0.479	-0.479
7.6	-0.484	-0.484	-0.484	-0.484	-0.484	-0.484	-0.484	-0.484	-0.484
7.7	-0.493	-0.493	-0.493	-0.493	-0.493	-0.493	-0.493	-0.493	-0.493
7.8	-0.514	-0.514	-0.514	-0.514	-0.514	-0.514	-0.514	-0.514	-0.514
7.9	-0.556	-0.556	-0.556	-0.556	-0.556	-0.556	-0.556	-0.556	-0.556
8.0	-0.621	-0.621	-0.621	-0.621	-0.621	-0.621	-0.621	-0.621	-0.621

Table 3.4 : Continued

lgT\lgρ	-3.000	-2.000	-1.000	0.000	1.000	2.000	3.000	4.000	5.000
3.5	-1.809	-1.362	0.637	8.924	11.423	12.489	13.629	14.631	15.632
3.6	-0.648	-0.579	1.219	8.617	11.091	12.144	13.281	14.283	15.284
3.7	0.292	0.267	1.528	8.318	10.756	11.798	12.934	13.935	14.936
3.8	0.836	0.607	1.724	8.028	10.411	11.453	12.586	13.588	14.589
3.9	1.375	0.885	1.800	7.750	10.064	11.109	12.238	13.240	14.241
4.0	2.243	1.445	2.159	7.494	9.716	10.765	11.890	12.892	13.893
4.1	3.093	2.191	2.574	7.260	9.367	10.421	11.542	12.544	13.544
4.2	3.887	2.936	3.043	7.030	9.019	10.079	11.194	12.195	13.196
4.3	4.575	3.643	3.598	6.799	8.670	9.763	10.845	11.846	12.847
4.4	5.105	4.328	4.213	6.557	8.320	9.450	10.495	11.497	12.498
4.5	5.399	4.891	4.815	6.309	7.970	9.129	10.145	11.147	12.147
4.6	5.458	5.238	5.278	6.055	7.618	8.781	9.794	10.795	11.796
4.7	5.221	5.316	5.540	5.797	7.267	8.431	9.443	10.444	11.445
4.8	4.851	5.199	5.386	5.535	6.912	8.077	9.089	10.091	11.091
4.9	4.535	4.960	5.115	5.271	6.559	7.722	8.735	9.736	10.737
5.0	4.244	4.710	4.839	5.006	6.207	7.366	8.379	9.381	10.382
5.1	3.915	4.429	4.577	4.742	5.855	7.009	8.022	9.023	10.024
5.2	3.464	4.080	4.316	4.477	5.507	6.650	7.664	8.665	9.666
5.3	2.924	3.639	4.017	4.205	5.161	6.290	7.303	8.304	9.305
5.4	2.380	3.166	3.670	3.923	4.822	5.928	6.941	7.943	8.943
5.5	1.887	2.691	3.284	3.623	4.484	5.565	6.578	7.580	8.581
5.6	1.377	2.267	2.887	3.308	4.144	5.201	6.214	7.216	8.216
5.7	0.973	1.865	2.519	2.990	3.802	4.836	5.848	6.851	7.851
5.8	0.582	1.534	2.211	2.691	3.463	4.473	5.482	6.485	7.485
5.9	0.308	1.215	1.950	2.423	3.134	4.112	5.115	6.117	7.117
6.0	0.058	0.879	1.736	2.201	2.825	3.753	4.747	5.750	6.750
6.1	-0.106	0.596	1.481	2.006	2.539	3.395	4.379	5.382	6.382
6.2	-0.202	0.361	1.232	1.835	2.264	3.040	4.011	5.013	6.013
6.3	-0.327	0.116	0.947	1.616	2.002	2.688	3.644	4.646	5.646
6.4	-0.395	-0.089	0.621	1.344	1.734	2.339	3.277	4.278	5.278
6.5	-0.427	-0.238	0.352	1.018	1.458	1.996	2.911	3.910	4.910
6.6	-0.447	-0.368	0.021	0.672	1.158	1.659	2.547	3.544	4.544
6.7	-0.455	-0.417	-0.215	0.321	0.851	1.331	2.184	3.177	4.176
6.8	-0.459	-0.438	-0.326	0.047	0.567	1.013	1.826	2.812	3.811
6.9	-0.461	-0.454	-0.401	-0.165	0.288	0.721	1.477	2.448	3.446
7.0	-0.464	-0.459	-0.427	-0.308	0.054	0.458	1.144	2.086	3.081
7.1	-0.466	-0.464	-0.447	-0.383	-0.134	0.235	0.836	1.728	2.718
7.2	-0.468	-0.467	-0.461	-0.412	-0.267	0.049	0.555	1.378	2.356
7.3	-0.471	-0.471	-0.468	-0.446	-0.341	-0.099	0.308	1.043	1.997
7.4	-0.474	-0.474	-0.473	-0.464	-0.397	-0.225	0.098	0.730	1.643
7.5	-0.479	-0.479	-0.478	-0.474	-0.445	-0.315	-0.074	0.449	1.297
7.6	-0.484	-0.484	-0.484	-0.482	-0.469	-0.397	-0.210	0.206	0.966
7.7	-0.493	-0.493	-0.493	-0.492	-0.486	-0.449	-0.319	-0.003	0.650
7.8	-0.514	-0.514	-0.514	-0.513	-0.510	-0.492	-0.411	-0.184	0.352
7.9	-0.556	-0.556	-0.556	-0.556	-0.555	-0.546	-0.501	-0.348	0.077
8.0	-0.621	-0.621	-0.621	-0.620	-0.620	-0.616	-0.592	-0.495	-0.169

it should be mentioned that the opacity data may not be reliable in the corner with extremely high densities and low temperatures in spite of our careful treatments. This is because this region is concerned with many complicated physical processes of dense gases.

We present our opacity data in Table 3.2, 3.3 and 3.4 respectively for the three compositions. For clarity of presentation, they only cover a temperature-density plane of $3.5 \leq \log T \leq 8.0$ and $-12 \leq \log\rho \leq 5$ with the interval of $\Delta\log T=1.0$ and $\Delta\log\rho=0.1$.

3.7 Investigation of opacity model

To examine the opacity model established, we present the following investigation of how much each process of absorption and scattering contributes to the opacity, as well as how much the heavy elements contribute. The composition for the present calculation is X/Y/Z=0.770/0.212/0.018.

3.7.1 Numerical calculation

In our opacity calculation, the frequency-dependent opacities in a frequency-grid are calculated by adding the contribution from each process one by one. The five processes are included by a sequence: free electron scattering, negative hydrogen (H^-) absorption, atomic free-free absorption (by all atoms of H,He and heavy elements), atomic bound-free absorption, and bound-bound absorption. So we are allowed to calculate the Rosseland mean opacities (RMOs) from several sequential processes. They are the RMO from the free electron scattering, denoted by ES, the RMO from free electron scattering and H^- absorption, denoted by ES+NH, the RMO from ES+NH and atomic free-free absorption (ES+NH+FF), the RMO from ES+NH+FF and atomic bound-free absorption (ES+NH+FF+BF), and the RMO form ES+NH+FF+BF and atomic bound-bound absorption (ES+NH+FF+ BF+BB).

We performed calculations for the above RMOs for four densities in a temperature range $3.5 \leq \log T \leq 8.0$. The results are plotted in Figure 3.5-3.8, each of which is for one density.

3.7.2 Free electron scattering

First, let us see the contribution from the free electron scattering to the RMO, which is revealed by the RMOs of ES. Its dominant range is at high temperatures and extends to lower temperatures as the density decreases. The figures shows that the free electron scattering starts to dominate the opacity at the temperature logT=5.2 for the density 10^{-9} g/cm^3, at logT=5.8 for 10^{-6} g/cm^3, at logT=6.5 for 10^{-3} g/cm^3, and at logT=7.0 for 1.0 g/cm^3.

3.7.3 Negative hydrogen absorption

The comparison of the RMOs of NH with those of other contributions shows the importance of H^- in the opacity calculation. The figures indicates that it has its most important contribution at the temperature below 10^4 K, and can even dominate the opacity at lower temperatures. However, it loses its dominant position at high densities owing to its pressure ionization.

3.7.4 Atomic free-free absorption

Although the process of atomic free-free absorption by the atoms does increase the opacity from that of ES+NH in the middle temperature range. However, it becomes an important source of the opacity in the case of extremely high density for the temperature below 10^6 K. the reason is that a great number of free electrons are produced due to pressure ionization at high densities, which therefore contribute to the opacity by means of free-free absorption. Also the cross-section of free-free absorption is inversely proportional to the photon frequency and thus to the temperature. This increases the contribution to the opacity from the free-free absorption at low temperatures.

3.7.5 Atomic bound-free absorption

The bound-free absorption is an important source of opacity in the range of middle

temperatures. The figures show that it dominates the opacity determination from the low end of the temperature range of around 10^4 K to high temperatures which rises as the density is raised. Beyond its high temperature end, the free electron scattering takes its place. At extremely high densities, e.g., $\rho \leq 1.0$ g/cm^3, its dominant range is only between 10^6 K to 10^7 K. In such a case, the opacity is mostly contributed by the ions of heavy elements with their inner electrons as main absorbers.

3.7.6 Atomic bound-bound absorption

The bound-bound absorption, or line absorption, makes its most important contribution to the opacity at middle temperatures as well as at middle densities. In the case of low density, e.g. for $\rho=10^{-9}$ g/cm^3, the broadening of lines is not strong enough to play a role, while at high densities, see for $\rho=1.0$ g/cm^3, the probability of the atomic configurations is reduced by pressure ionization. So it increases the RMOs at temperatures between 10^4 K and 10^5 K in Figure 3.6 for the density $\rho=10^{-6}$ g/cm^3 and in Figure 3.7 for $\rho=10^{-3}$ g/cm^3.

A detailed examination of the contribution from the line absorption is presented in Figure 3.9. It plots in a three-dimensional form the ratio of the total opacity to the continuous opacity, i.e. the ratios of the RMO of ES+NH+FF+BF+BB to that of ES+NH+FF+BF. It reveals that line absorption plays its maximum role at the density around 10^{-4} g/cm^3. At high densities, i.e. $\rho>0.1$ g/cm^3, its contribution is reduced dramatically by pressure ionization. Its dominant temperatures range from 10^4 K to 10^6 K, and it raises the opacity considerably for temperatures below 10^5 K.

3.7.7 Contribution from heavy elements

It is interesting to see how much the heavy elements can contribute to the opacity and in what region they play a role. We performed the calculation of the RMOs by excluding the atomic absorption processes by heavy elements, which gives the RMOs only for H, He absorption and electron scattering. The ratios of the total RMOs are plotted in Figure 3.10

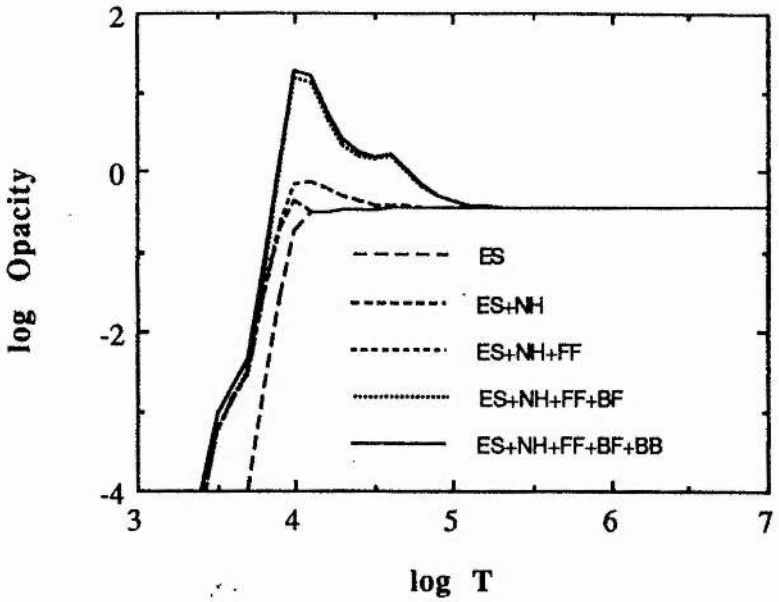

Figure 3.5 : The Rosseland mean opacities from the five sequential processes for the density 10^{-9} g/cm^3. See Section 3.7.1.

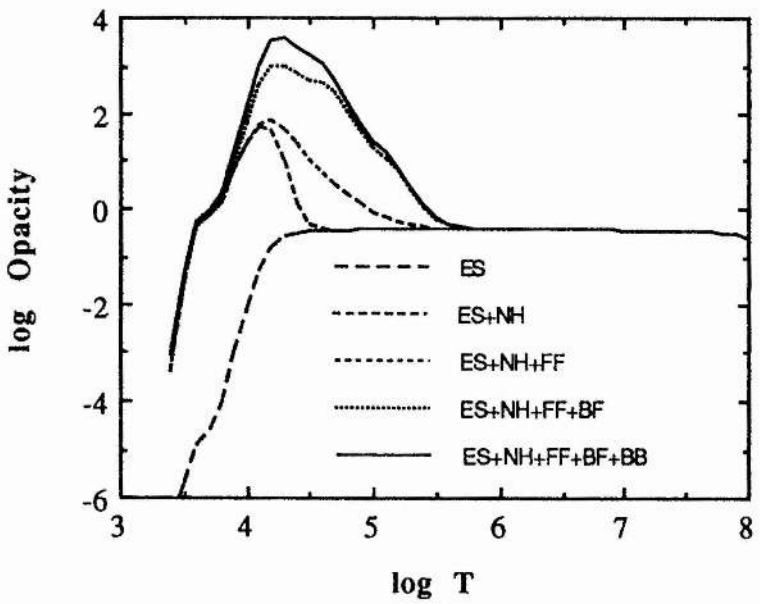

Figure 3.6 : The same as in Figure 3.5 but for the density 10^{-6} g/cm^3.

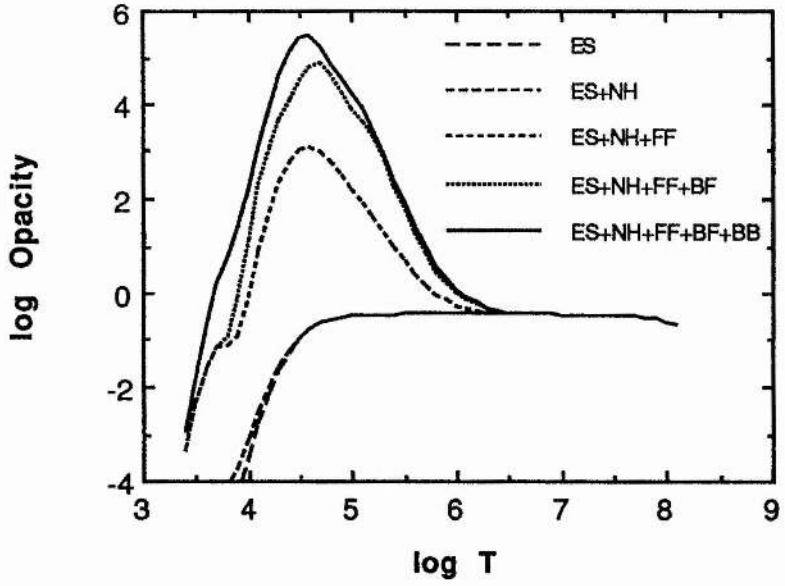

Figure 3.7 : The same as in Figure 3.5 but for the density 10^{-3} g/cm^3.

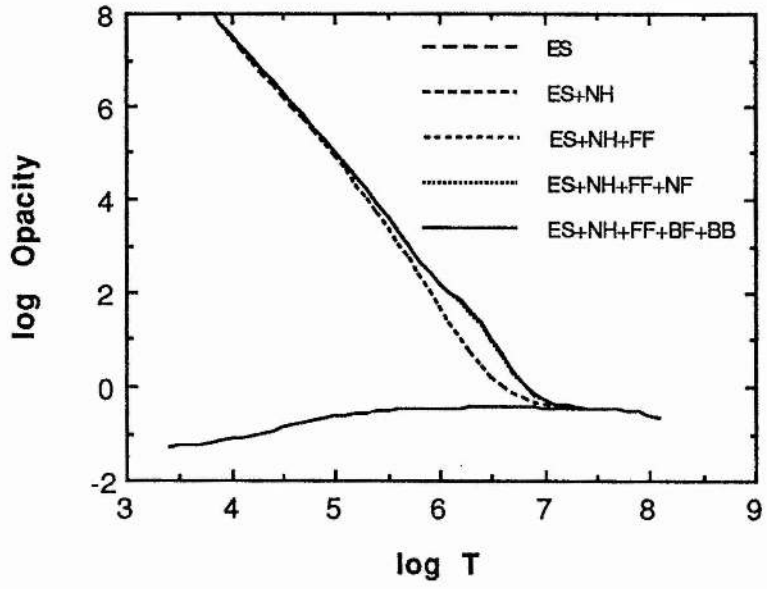

Figure 3.8 : The same as in Figure 3.5 but for the density 1.0 g/cm^3.

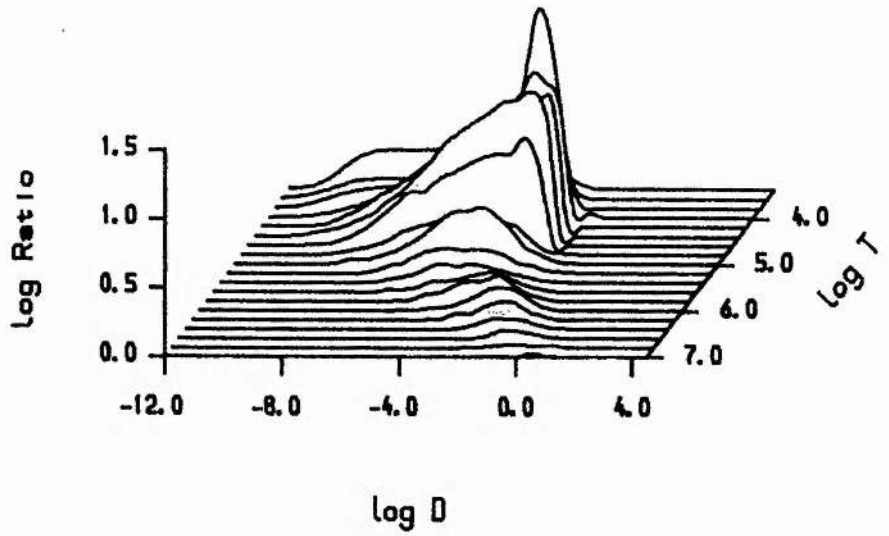

Figure 3.9 : The ratio of the total opacity to the continuous opacity on the temperature (T in K) and density (D in g/cm^3) plane.

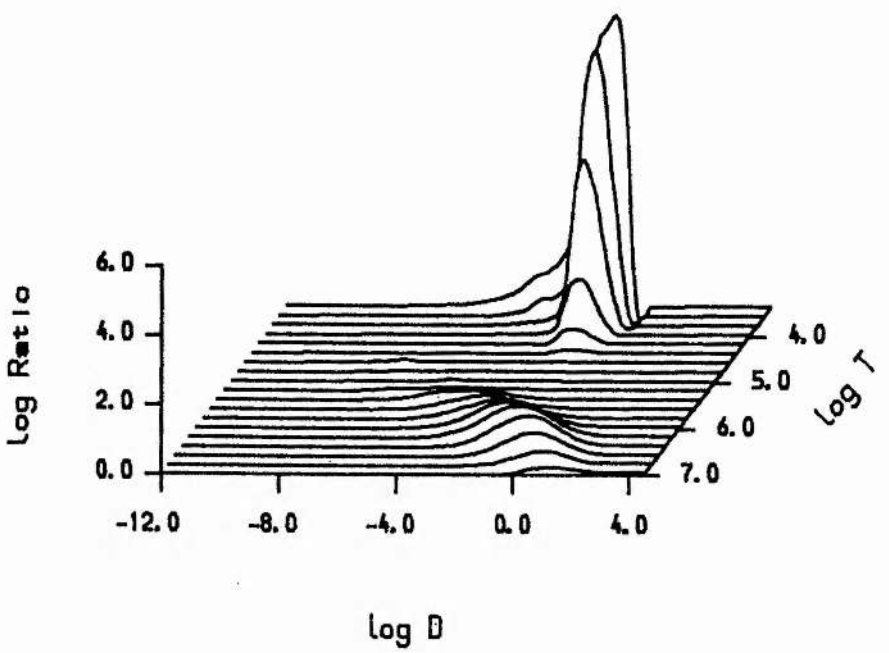

Figure 3.10 : The ratios of the total opacity to the opacity without the contribution from the absorption by the heavy elements, for a temperature range from $10^{3.4}$ K to 10^7 K.

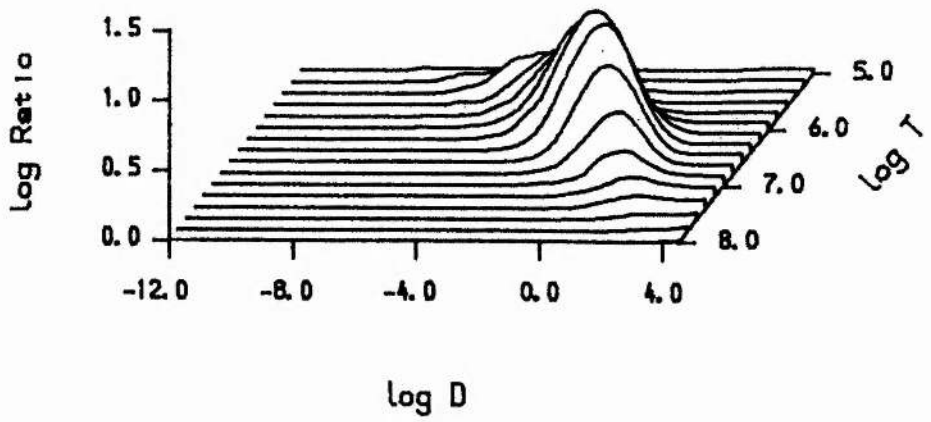

Figure 3.11 : The same as in Figure 3.10 but for a temperature range from 10^5 K to 10^8 K.

and 3.11 respectively for two temperature ranges.

Figure 3.10 covers a temperature range of $3.6 \leq \log T \leq 7.0$. It shows a remarkable increase of the opacity by the heavy elements at the density around 0.1 g/cm^3 for the temperature below 10^4 K. This is contributed by the free electrons released by heavy elements from their low ionization energy levels due to pressure ionization. Figure 3.11 shows the ratios over a range of $5.0 \leq \log T \leq 8.0$. The heavy elements are found to increase the opacity at temperatures above $10^{5.4}$ K = $2.5*10^5$ K. The maximum ratio reaches a factor of about 7 at the temperature $10^{6.2}=1.6*10^6$ K and a density of 0.1 g/cm^3.

3.8 Comparison with recent opacity data

As a check on our opacity data , we make comparison with a recent set of opacity data calculated by Iglesias and Rogers (1991). Their calculation is based a sophisticated atomic model. Unlike other opacity calculations, they take into account the complex of energy levels due to multi-electron interactions in the atoms of heavy elements, which is found to increase the opacities considerably at temperatures around $5*10^5$ K.

We plot the logarithm ratio of their opacities K(ir) to our opacities K(gl) in Figures 3.12 and 3.13, respectively, for Population I and Population II compositions. We see that for Population I their opacities can be several times ours in the temperature range $5.4<\lg T<6.2$. This corresponds to an increase of opacity by the inclusion of the complex of multi-electron interactions. For Population II, the difference between the two sets of opacities is much smaller, since the heavy elements cannot play a significant role.

Figure 3.12 : lgK(ir)–lgK(gl) for Pop I

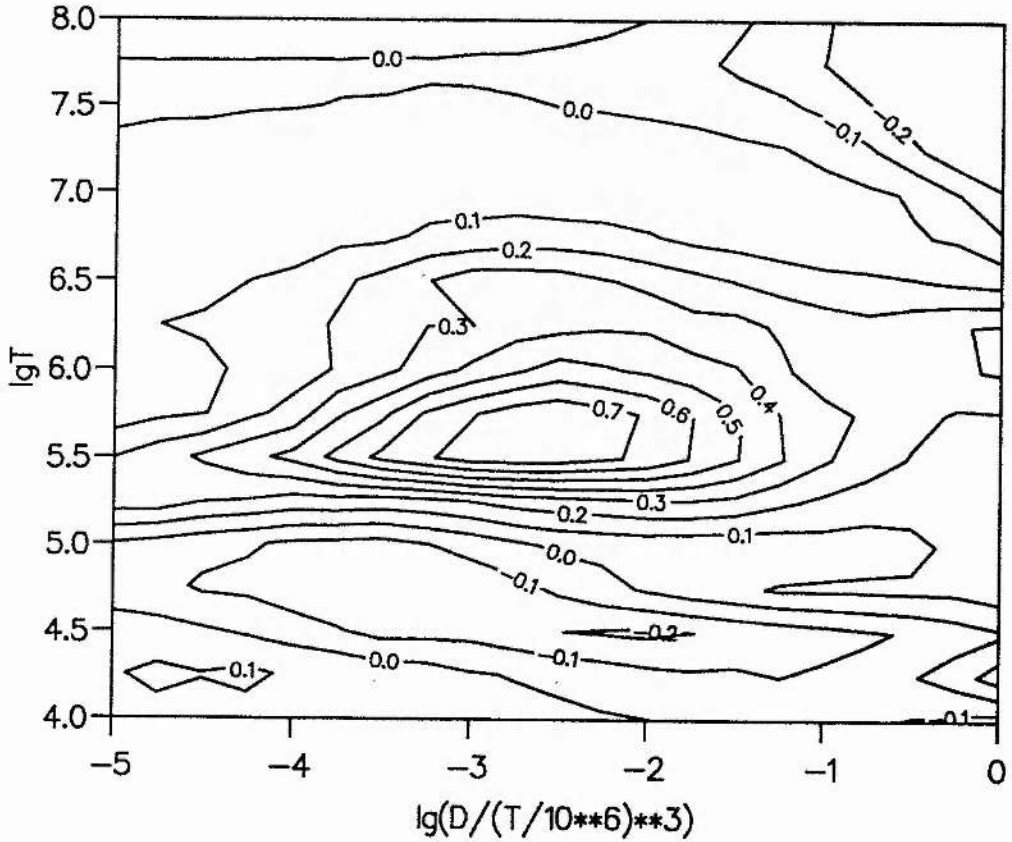

Figure 3.13 : lgK(ir)–lgK(gl) for Pop II

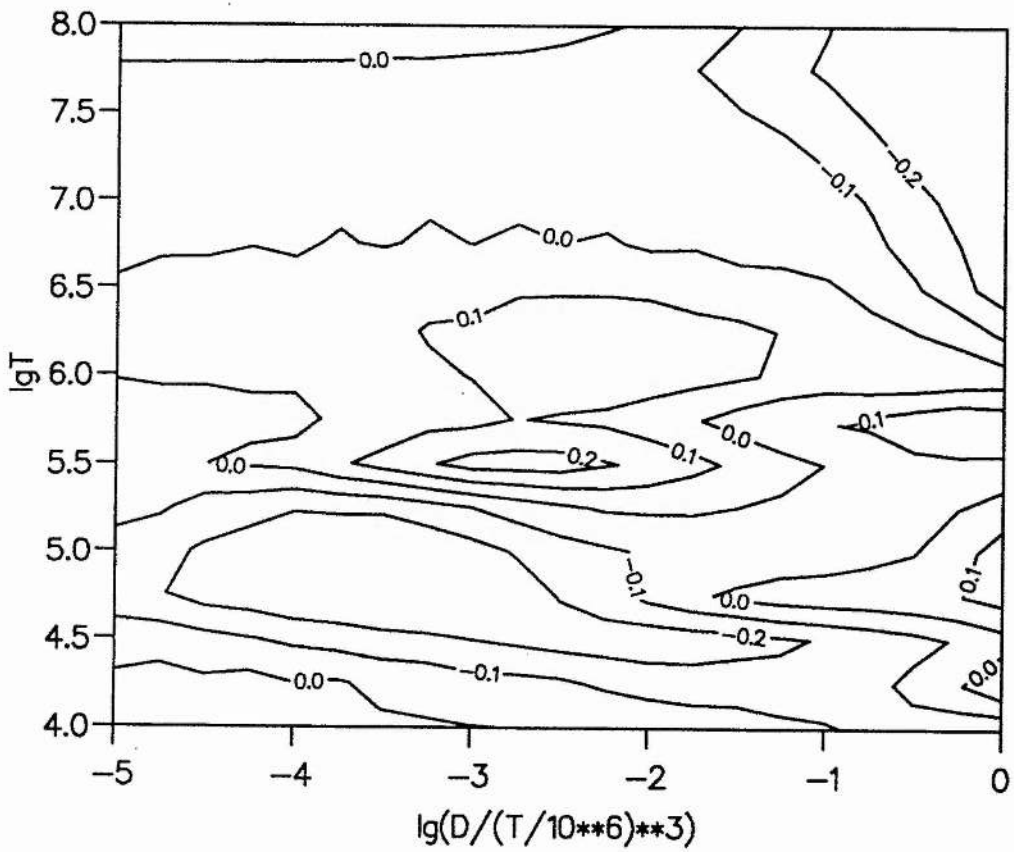

Chapter IV Other Elements of Input Physics

Introduction

In addition to the equation of state and the radiative opacities of stellar gases, the input physics of a stellar model includes the energy generation rates from thermo-nuclear reactions and the conductive opacities (see Section 4.1 and 4.3). In thermo-nuclear reactions, electron screening in nuclear reaction is found to play a role in the case of high densities, so it has to be taken into account in the study of LM stars whose central region is in the state of relatively high density and low temperature (see Section 4.2). In addition, opacity data including molecular absorption are needed to supplement the opacity data calculated by our opacity model (see Section 4.4), since the surface conditions in the LM stars can allow the formation of hydrogen molecules and other molecules. The molecule formation can always contribute significantly to the opacity as well as to the equation of state at low temperatures .

4.1 Energy generation by thermo-nuclear reactions

4.1.1 Thermo-nuclear reaction in stars

Thermo-nuclear reactions have two functions in the stars. One is to provide the main energy source of stars with nuclear binding energy released from the fusion reactions. The other function is to change the element abundances in the process of fusion reactions. This causes a star to change its state progressively during its the evolution. During most of a star's life the fusion reaction of hydrogen into helium maintains the star on the main sequence. In massive stars, the fusion process may proceed to its endpoint and the burning of many elements may be involved until the formation of Fe group nuclei.

Although the thermo-nuclear reactions may lead to the burning of many elements, the nuclear burning stages beginning with hydrogen (the most common fuel) involve a

relatively slow build-up of nuclear species. Therefore, the most important reactions supplying stellar energy are from the light elements, i.e. H,He,C,N,O, etc. Hydrogen burning dominates the life of stars. There are two major reaction chains in H burning: the proton-proton chain (pp) and the carbon-nitrogen-oxygen cycle (CNO). After hydrogen exhaustion in the stellar interior the resulting helium rich material can be ignited if the star is massive enough to obtain a core temperature higher than 10^8 K from its gravitational contraction. The helium burning reaction is known as the triple-alpha process. At temperatures greater than about $6*10^8$ K, carbon burning can takes place. Then other elements left successively become contributors to the energy generation.

4.1.2 Thermo-nuclear energy generation rates

The important aspects of thermo-nuclear reactions as an energy source in stars are the amount of energy released and the rates of the reactions. The energy released by each of the nuclear reactions depends on the physics of the nuclei involved. The rate at which the energy is released depends on the relative velocity of the reacting nuclei, their average separation, nuclear charge, and possibly on the nature of other particles. These factors in turn depend on the temperature T, density ρ and composition $\mathbf{C}=(X, Y, Z)$ of the gas, which are the ultimate parameters that determine the energy generation rate ε, i.e. $\varepsilon = \varepsilon(\rho,T,\mathbf{C})$.

At present, the theory of nuclear reactions does not enable us to calculate all reaction cross sections accurately. So the knowledge of reaction cross-sections is still limited by the availability of experimental data.

In the following subsections, we briefly summarize the formulation of thermo-nuclear energy generation rates from the work of Fowler, et al. (1967,1975) and Harris et al. (1983).

4.1.3 Formulation of the energy generation rates

The energy generation rates due to the thermo-nuclear reactions are formulated in terms of the parameters for the temperature T, the mass density ρ, the mass abundances X, Y, Z, and the molecular weights A_H, A_{He}, A_Z, respectively for hydrogen, helium and heavy elements. All quantities employed are defined in c.g.s. units. The parameter T_9 is defined by $T_9=T/(10^9\ K)$. Avogadro's number is taken as $N_A=6.022*10^{23}$ per given mole. The formulation is restricted to p-p, CNO and 3α chains.

4.1.3.1 p-p chain

The energy generation rate for the p-p reaction is

$$\varepsilon_{pp} = N_A(X/A_H)^2\rho\ Q_{pp}\ F_{pp}(T,\rho)/2!\ \ \text{erg/sec/g.}$$

The energy released per p-p reaction for the entire p-p chain is

$$Q_{pp} = 13.81\ \text{MeV} = 2.213*10^{-5}\ \text{erg.}$$

The reaction rate function is given by

$$F_{pp}(T,\rho) = 3.82*10^{-15}\ T_9^{-2/3}\ \exp(-3.38/T_9^{1/3})$$
$$(1+0.123T_9^{1/3}+1.09T_9^{2/3}+0.938T_9)\ \ \text{sec}^{-1}\ (\text{mole/cm}^3)^{-1}\ .$$

4.1.3.2 CNO chain

The energy generation rate is

$$\varepsilon_{CNO} = N_A\left(\frac{X\ Z}{A_H\ A_Z}\right)\rho\ Q_{CNO}\ F_{CNO}(T,\rho)\ \ \text{erg/sec/g}\ .$$

The energy released per reaction is

$$Q_{CNO} = 24.97\ \text{MeV} = 4.001*10^{-5}\ \text{erg}\ .$$

The reaction rate function is

$$F_{CNO} = 5.08*10^7\, T_9^{-2/3}\ \exp\left[-15.228/T_9^{1/3}-(T_9/3.090)^2\right]$$

$$*\left[1+0.027T_9^{1/3}-0.778T_9^{2/3}-0.149T_9+0.261T_9^{4/3}+0.127\ T_9^{5/3}\ \right]$$

$$+2.29*10^3\, T_9^{3/2}\exp(-3.001/T_9) +1.65*10^4/T_9^{1/3}\exp(-12.007/T_9)\ .$$

4.1.3.3 Triple-alpha chain

The energy generation rate is

$$\varepsilon_{3\alpha} = N_A\left(\frac{Y}{A_{He}}\right)^3 \rho^2\, Q_{3\alpha}\, F_{3\alpha}(T,\rho) \quad \text{erg/sec/g}\ .$$

The released energy per reaction is

$$Q_{3\alpha} = 14.436\ \text{MeV} = 2.313*10^{-5}\ \ \text{erg}\ .$$

The reaction rate function is

$$F_{3\alpha} = 2.79*10^{-8}\, T_9^3\ \exp(-4.4027/T_9) +1.35*10^{-7}\, T_9^{3/2}\exp(-24.811/T_9)\ .$$

4.2 Electron screening effect in thermo-nuclear reactions

4.2.1 Astrophysical application

High density plasmas are found in the cores of red grains, in hot white dwarfs, and in the central regions of other highly evolved stars. In such plasmas, the thermo-nuclear reactions are affected by the electron screening of nuclei, which cause the enhancement of nuclear reactions. In the study of the LM stars, the relatively high densities and low temperatures may also be found in stellar central parts . Therefore, it is necessary to introduce the study of the electron screening in nuclear reactions for the purpose of our application.

4.2.2 Theory of electron screening

In a high density plasma, the electron gas tends to screen the ion charges and therefore reduces the effective Coulomb barrier. The theory of nuclear reactions shows that the enhancement of the thermo-nuclear reaction rates is approximated to be

$$f_{enh} = \langle \sigma v \rangle_s / \langle \sigma v \rangle = \exp[-U_s(0)/kT] ,$$

where $U_s(0)$ is the screening correction to the potential at the nuclei.

In the case of weak screening, the screening correction may be given by the Debye-Hückel model, i.e.

$$U_s(0) = Z_1 Z_2 \, e^2 / \lambda_D ,$$

with the Debye length of the plasma

$$\lambda_D = \left(\frac{kT}{4\pi \, n_e \, e^2} \right)^{1/2} .$$

So the enhancement factor f_{enh} is written as

$$\log_e f_{enh} = Z_1 Z_2 \, (4\pi \, n_e)^{1/2} \, (e^2/kT)^{3/2} .$$

The condition of weak screening requires

$$e^2/\lambda_D << kT .$$

In the case of strong screening, the ion-sphere model may be employed to obtain the screening correction to the potential, i.e.

$$U_s(0) = Z_1 Z_2 \, e^2 / a ,$$

with the Wigner-Seitz radius

$$a = (4\pi \, n_n/3)^{-1/3} ,$$

and the nuclei number density n_n. Therefore, the enhancement factor f_{enh} is given by

$$\log_e f_{enh} = Z_1 Z_2 e^2 (4\pi n_n/3)^{1/3} / kT.$$

The formulae obtained above are only suitable for the limiting cases. For general conditions, a detailed study for astrophysical application has been presented by Salpeter (1969). In our study of the LM stars we employ the results of the study by Ichimara (1984) to formulate the enhancement factor for the thermo-nuclear reactions of hydrogen.

4.2.3 Formulation of enhancement factor

The resulting enhancement factor for the thermo-nuclear reaction rate is defined by

$$f_{enh} = \exp[\, H(0) \,] .$$

The parameterized expression for H(0) is given by

$$H(0) = \Gamma^{3/2} \frac{1.732+0.7174\beta + (1.644-0.1039\beta)\, \Gamma^{1/2}}{1 + (1.096-0.5286\beta)\, \Gamma^{1/2} + (1.416-0.3238\beta)\, \Gamma} .$$

The Coulomb coupling constant of the ion system with the electric charge Ze and the Wigner-Seitz radius $a = (4\pi n_n/3)^{-1/3}$ is $\Gamma = (Ze)^2/a\,kT$. The parameter β is defined in terms of the electron Fermi energy E_F at T=0 by $\beta = \exp[-E_F/5kT]$.

In the weak coupling limit ($\Gamma<<1$) with $\beta\rightarrow 1$, H(0) approaches $\sqrt{6}\Gamma^{3/2}$, the Debye-Huckel value. In the strong coupling limit ($\Gamma>>1$) with $\beta\rightarrow 0$, H(0) approaches 1.161Γ.

Figure 4.1 shows the contours of the enhancement factor in the temperature-density plane for a plasma with X=0.71. For a plasma with logT=6.5 and logρ=3.0, which is near the condition of the central region of the LM stars, the enhancement factor is found to be about f_{enh}=2. This implies that the electron screening effect can change the thermo-nuclear reactions under the condition found in LM stars. However, it is hard to predict how much the electron screening can affect the structure of a LM star since the stellar structure is a

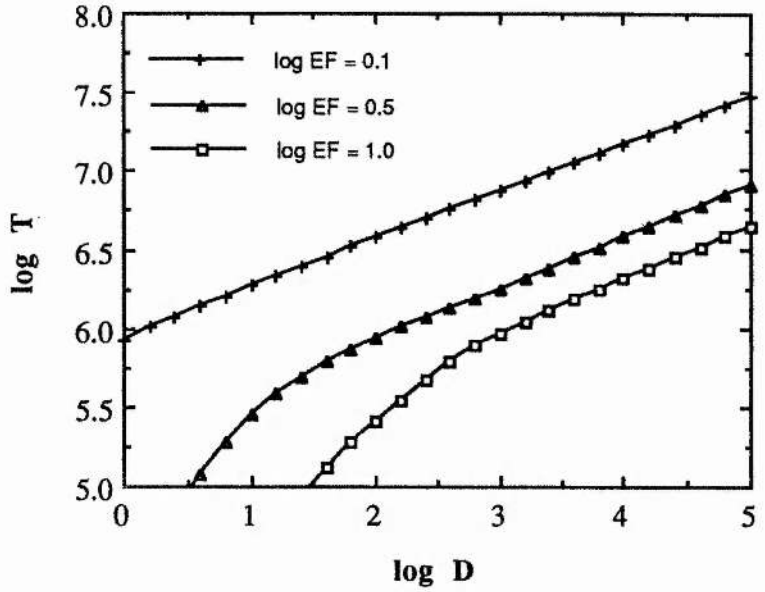

Figure 4.1 : Contours of the enhancement factor (EF) on the temperature (T in K) and density (D in g/cm^3) plane. The data are plotted for a p-p chain in a plasma with the hydrogen mass fraction X=0.71.

complicated system in which many physical factors are involved. The calculation of the LM star models must be carried out in order to check the effect of the electron screening on the stellar structure. This will be seen in Chapter VI.

4.3 Conductive opacities

4.3.1 Energy transfer by electron conduction

In a highly degenerate plasma the mean free path of electrons is long and thus the energy can be carried by the motion of electrons. The condition of high degeneracy may exist in the interior of some stars with high densities and low temperatures, such as white dwarfs, LM stars, etc. In these stars the electron conduction is always an important way to transport stellar energy.

Stellar energy can be transported mainly by three methods: radiation, electron conduction, and convection. Which one is dominant depends on the local condition of stellar gases. By introducing the Rosseland mean radiative opacity κ_r and the electron conduction opacity κ_c, a combined opacity κ, given by

$$\frac{1}{\kappa}=\frac{1}{\kappa_r}+\frac{1}{\kappa_c},$$

is used to incorporate energy transfer by both electron conduction and radiation into the radiative transfer equation.

4.3.2 Theory of electron conduction

In astrophysical applications, the conductive opacity κ_c is introduced by defining

$$\kappa_c=\frac{4acT^3}{3\rho\lambda_c},$$

so that the conductive energy flow can be described by the same form as in the radiative transfer equation, i.e.

$$F_{cond} = -\frac{4ac}{3\kappa_c \rho} T^3 \frac{dT}{dr}.$$

The thermal conductivity λ_c is defined by the equation

$$F_{cond} = -\lambda_c \frac{dT}{dr}$$

and is the quantity which determines the conductive opacity.

By introducing an electron mean free path l_c, the energy flux is given by

$$F_{cond} = -n_e v l_c \frac{\partial \varepsilon}{\partial r},$$

with the electron flux $n_e v$ and the electron energy ε. So the thermal conductivity is found to be

$$\lambda_c = n_e v l_c \frac{\partial \varepsilon}{\partial r}.$$

Taking into account the dependence on electron energy, the thermal conductivity must be calculated by averaging over the energy distribution function of electrons $f(\varepsilon)$, i.e.

$$\lambda_c = n_e \int d\varepsilon\, f(\varepsilon)\, v(\varepsilon)\, l_c(\varepsilon) \frac{\partial \varepsilon}{\partial T}.$$

Since $f(\varepsilon)$, $v(\varepsilon)$, $\varepsilon(T)$ are all known functions of the temperature and density, the problem reduces to the determination of the electron mean free path $l_c(\varepsilon)$.

The mean free path of electrons is determined by their collisions with other particles and themselves. The quantum theory can be employed to calculate the cross section of the electron due to collisions, and therefore to determine the mean free path.

The standard theory of the electron conduction has been developed by Marshak (1941),

and refined by Mestel (1950) and Lee (1950) based on the Lorentz gas approximation. The later study by Hubbard and Lampe (1969) and Lampe (1968a,1968b) shows the importance of the inclusion of various particle interactions and correlations in the calculation of the conductive opacities. Hubbard (1969) presented the data tables of conductive opacities which incorporate the advances in the study of electron conduction.

4.3.3 Conductive opacity data

In our study of the LM stars, we include the conductive opacity data given by Hubbard and Lampe (1969) in the radiative opacity data for the calculation of stellar models. The table presented by Hubbard and Lampe is over a range of density $-5.75 \leq \log \rho\ (g/cm^2) \leq 6$ and a range of temperature $3 \leq \log T\ (K) \leq 9$. The ranges where their theory breaks down are excluded. We find that the excluded ranges are mostly in the ρ-T region of pressure ionization. This region, however, is important for the study of the LM stars so that it is necessary to extend their conductive opacity data. Since the variation of the conductive opacity with density is approximately linear over a limited range, we are allowed to simply use extrapolation to obtain the data in the excluded ranges.

Figure 4.2 plots the electron conductive opacities for five temperatures in a density range $-8 \leq \log\rho \leq 6$ after extrapolation to the excluded ranges. The importance of electron conduction in energy transfer compared with radiation is shown in Figure 4.3. The ratios of the radiative opacity to the conductive opacity are plotted as contours on the temperature-density plane. The radiative opacity data are calculated from the opacity model presented in Chapter III.

4.4 Low temperature opacity

4.4.1 Molecular opacity

The spectra of late-type stars with effective temperatures less that 5000 K are dominated by molecular bands. This indicates the possible importance of molecular band absorption in

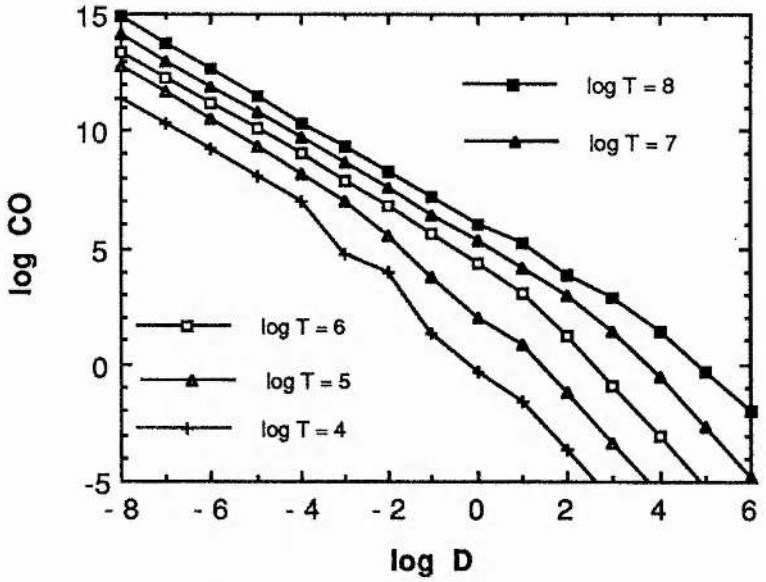

Figure 4.2 : The conductive opacities (CO in cm^2/g) from the data given by Hubbard and Lampe (1969) for five temperatures.

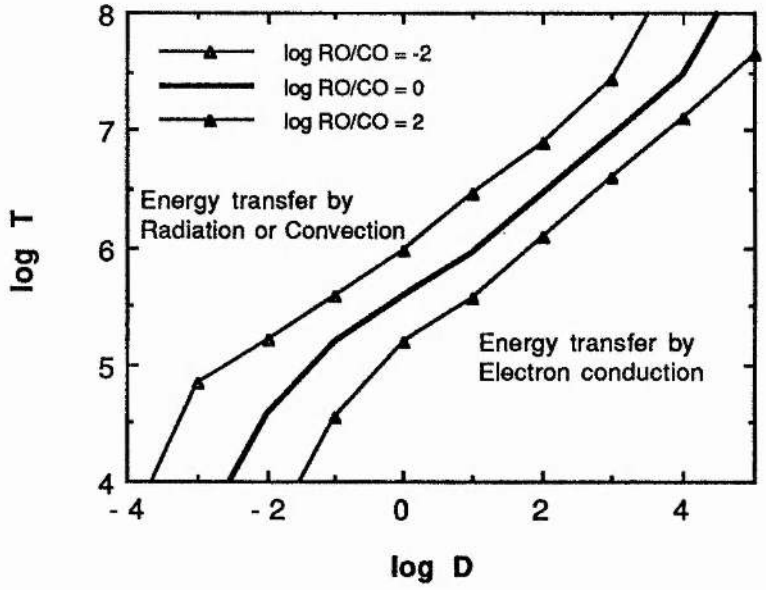

Figure 4.3 : Contours of the ratio of the radiative opacity to the conductive opacity on the temperature (T in K) and density (D in g/cm^3) plane.

the radiative transfer in the atmosphere of these stars. Indeed, a number of calculations which include some low temperature absorbers, such as those presented by Gaustad (1963), Tsuji (1971) and Alexander (1975), indicate the dramatic effect of molecular absorption on the Rosseland mean opacity for temperatures below 4000 K,

The importance of the molecular contribution to the opacity is its effect on the thermal and mechanical structure of stellar atmospheres and envelopes. The increased radiative absorption by molecular bands leads to steeper temperature gradients and therefore causes the mass-luminosity relation of the late-type stars to be much different from that for stars without molecules. Furthermore, the presence of molecules affects the equation of state considerably, which is also an important factor in changing the states of these stars.

In the calculation of the opacity data commonly used in astrophysics, such as that presented by Cox (1970a,b, 1976), the molecular absorption was ignored or treated only by some simple sampling methods. In our calculation of radiative opacity data, no molecular absorbers are considered. Fortunately, there are some recent calculations which include the contribution from molecular band absorption and give complete opacity data at low temperatures. We will incorporate these opacity data into our calculated opacity in the low temperature range in order to make reliable calculations of the LM star models.

4.4.2 Alexander opacity and Carson and Sharp opacity

Alexander (1975) computed detailed low temperature opacities, and refined his calculation in 1983 (see Alexander et al. 1983). In their calculations, the molecular effects are computed wherever possible with the opacity sampling method which has been developed by Peytremann (1974), Smeden et al. (1976). The condensation to form grains was also included for iron and magnesium. They tabulated the Rosseland mean opacity data for a solar composition over the range from 700 K to 10000 K. The effects of molecules and grains were found to be dominant at temperatures below 4000 K.

Unlike Alexander et al. (1983) who use the sampling method, Carson and Sharp (1991) compute the monochromatic absorption spectrum, both continuum and lines by performing line by line calculations for the diatomic and tri-atomic bands, and obtain the Rosseland mean opacities. It is found in their study that averaging and smearing of the absorption coefficients within frequency intervals are completely unreliable, except in special circumstances, in the calculation of mean opacities. They give Rosseland mean opacity tables in the range $3.3 \leq \log T \leq 4.0$ and $-13.0 \leq \log \rho \leq -2.0$ for four compositions with up to 20 elements, 50 diatomic molecules and 5 tri-atomic molecules. At the low temperatures considered, the band absorption by the tri-atomic molecules H_2O and CO_2 is found to increase the opacity over that due to diatomic bands by a factor of up to 100.

In addition, we also use the Christy formula to calculate the low temperature opacities for $T<10^4$ K. It is adopted from one code of Carson for a simple calculation of approximate opacity data, and found to be very sensitive to the free electron number density. We perform its calculation based on the EOS established in Chapter II, which deals with the free electron number obtained from heavy elements at low temperatures.

In our study of the LM stars, three sets of opacity data given by Alexander (1983), Carson and Sharp(1991) and the Christy formula are all employed in the structure calculation, in order to investigate the effects they have on the LM star models. So we need to check the differences of the three sets of opacity data at first. Figure 4.4 shows the comparison of the Carson and Sharp opacities with the Alexander opacities for the solar composition. They basically agree with each other but at temperatures below $\log T = 3.5$ the Alexander opacities can be greater than the Carson opacities by a factor up to 5. This difference may be made by the sampling method employed by Alexander and the line-by-line calculation by Carson and Sharp. The comparison of the Carson opacities with the Christy formula opacities is given in Figure 4.5. It shows that they differ from each other at temperatures below about 5000 K, where the Christy formula opacities can be a factor of about 4 or 5

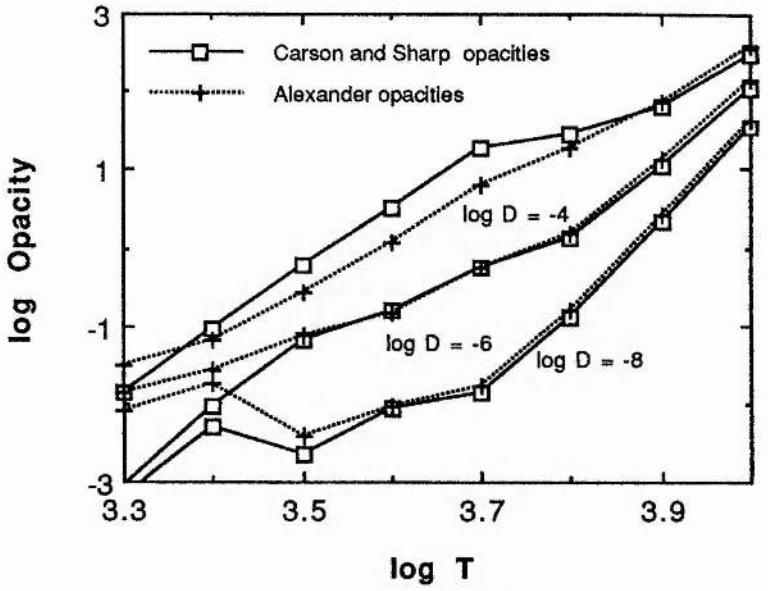

Figure 4.4 : Comparison of the Carson and Sharp opacities (in cm^2/g) and the Alexander opacities (in cm^2/g) in the low temperature range (T in K) for three densities (D in g/cm^3).

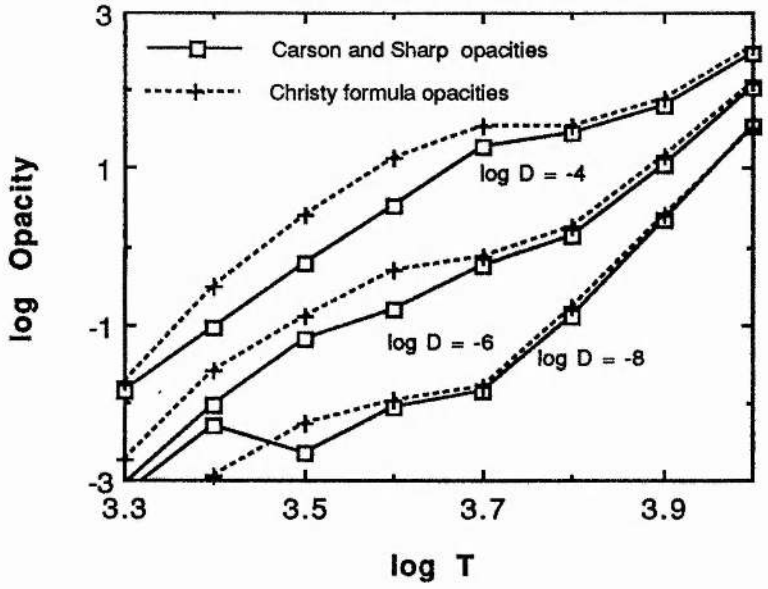

Figure 4.5 : Comparison of the Carson and Sharp opacities with the Christy formula opacities, otherwise as in Figure 4.4.

greater than the Carson opacities. All of these differences affect the LM star models considerably, which will be seen in Chapter VI.

4.4.3 Combination of low temperature opacities and calculated opacities

In order to utilize the low temperature opacities κ_{low} given by Alexander (1983), and Carson and Sharp (1991) as well as the Christy formula in the study of LM star models, we must perform the combination of our calculated opacities κ_{cal} with theirs. In our study of LM stars, a linear combination is performed in the temperature range $3.7 \leq \log T \leq 4.1$ in terms of

$$\kappa = \beta\, \kappa_{cal} + (1-\beta)\, \kappa_{low} ,$$

with

$$\beta = (\log T - 3.7) /(4.1 - 3.7) ,$$

$$\beta = \min (1, \beta) ,$$

$$\beta = \max (0, \beta).$$

The agreement of the tabulated low temperature opacities with the calculated opacities in the region of overlap is important to the data combination, so that we have to check whether they fit each other in the combination range.

Figure 4.6 shows the comparison of the Alexander opacities of the solar composition with the calculated opacities. Figure 4.7 gives the combined opacities from them. Figure 4.8 and 4.9 give the comparison and combination of the Carson opacities of the solar composition with the calculated opacities. The comparison and combination of Carson opacities of the composition of Population II (Z=0.001) are given in Figure 4.10 and 4.11. For the Christy formula opacities, their comparison and combination with the calculated opacities are presented in Figure 4.12 and 4.13. All of these figures indicate that good combinations of the low temperature opacities and our calculated opacities are achieved.

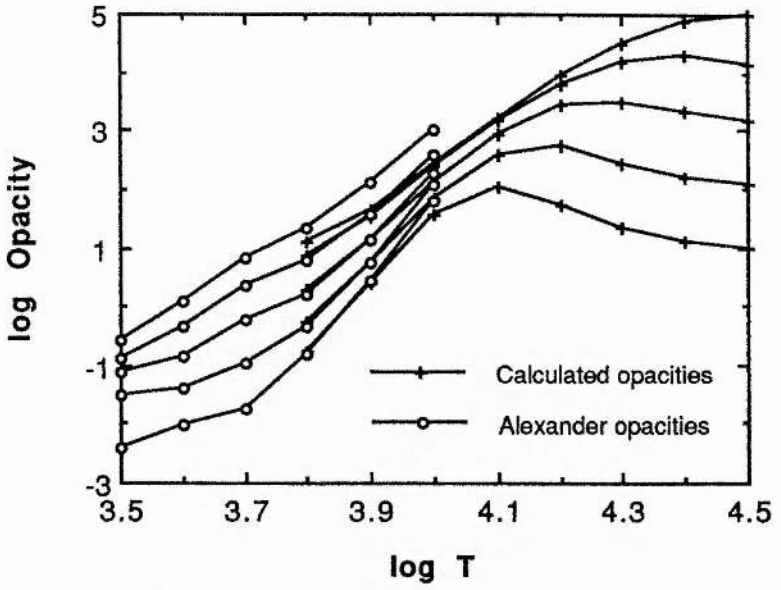

Figure 4.6 : Comparison of the Alexander opacities with the calculated opacities for a Population I composition for five densities indicated in Figure 4.7.

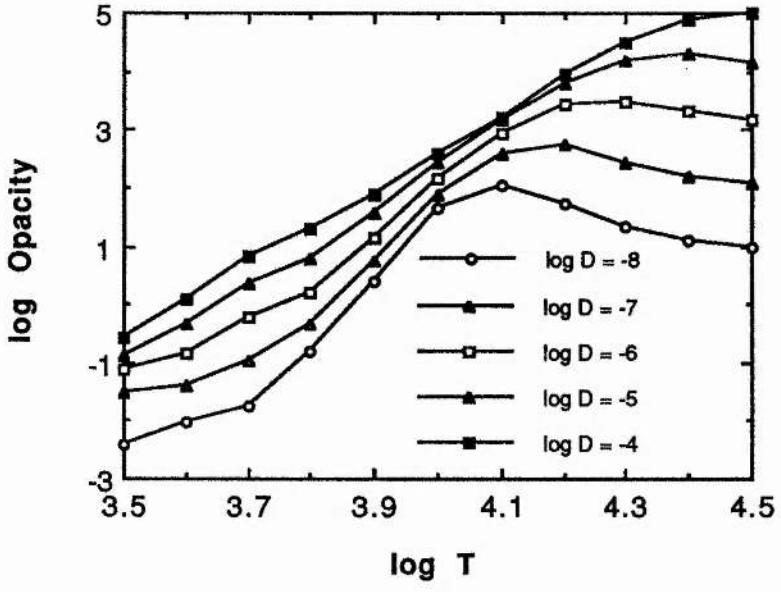

Figure 4.7 : The combined opacities from the Alexander opacities and the calculated opacities for five densities (D in g/cm^3), which are also plotted in Figure 4.6.

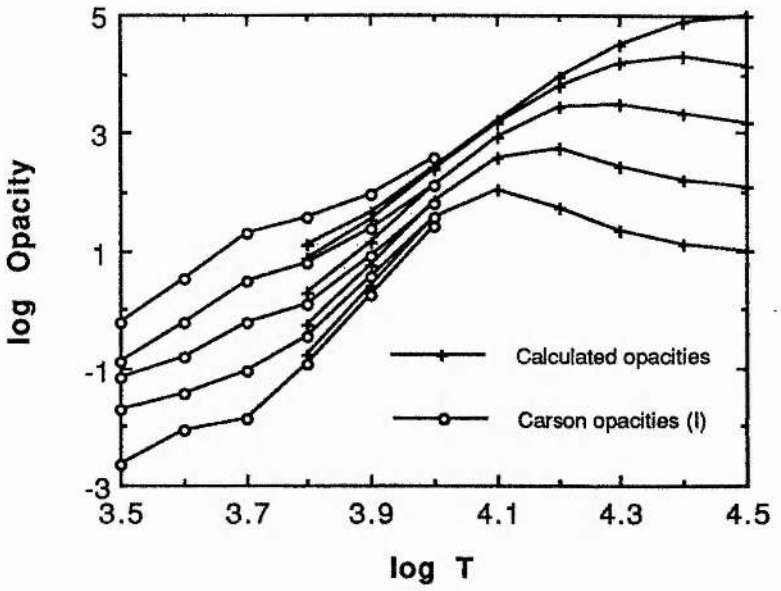

Figure 4.8 : Comparison of the Carson and Sharp opacities with the calculated opacities for a Population I composition for five densities indicated in Figure 4.9.

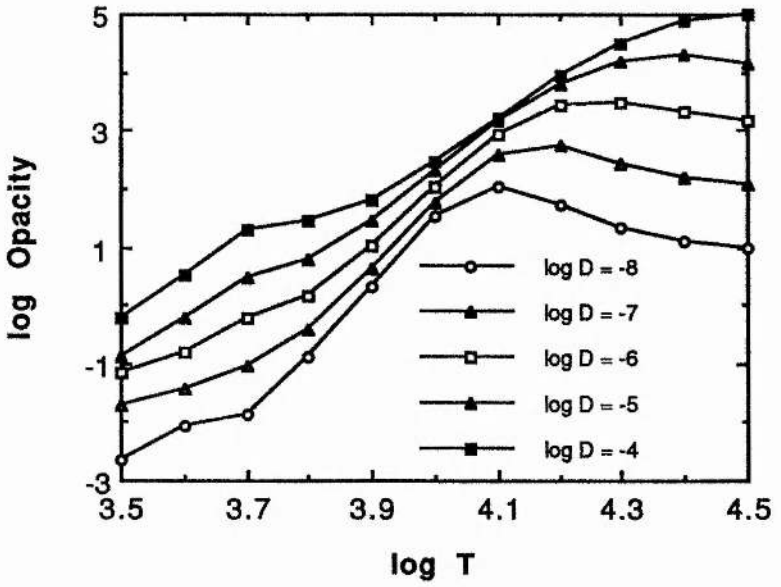

Figure 4.9 : The combined opacities from the Carson and Sharp opacities and the calculated opacities for five densities (D in g/cm^3), which are also plotted in Figure 4.8.

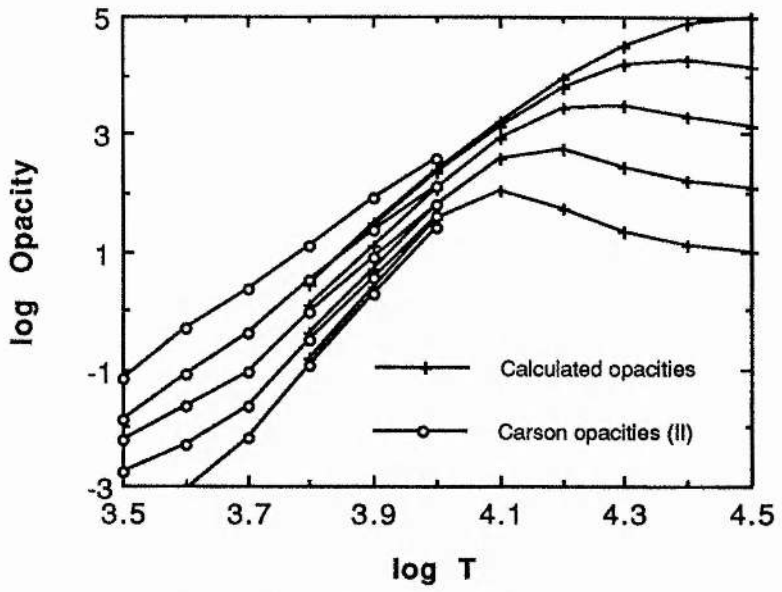

Figure 4.10 : Comparison of the Carson and Sharp opacities with the calculated opacities for a Population II composition for five densities indicated in Figure 4.11.

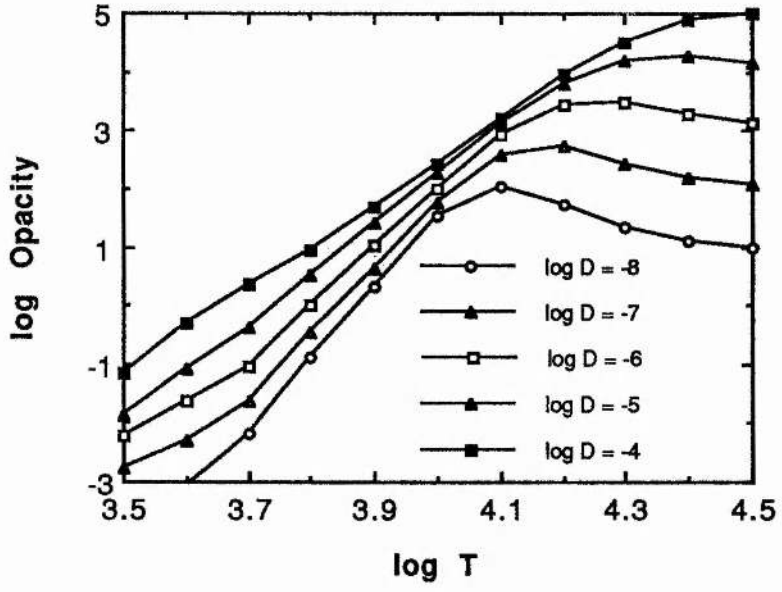

Figure 4.11 : The combined opacities from the Carson and Sharp opacities and the calculated opacities for five densities (D in g/cm^3), which are also plotted in Figure 4.10.

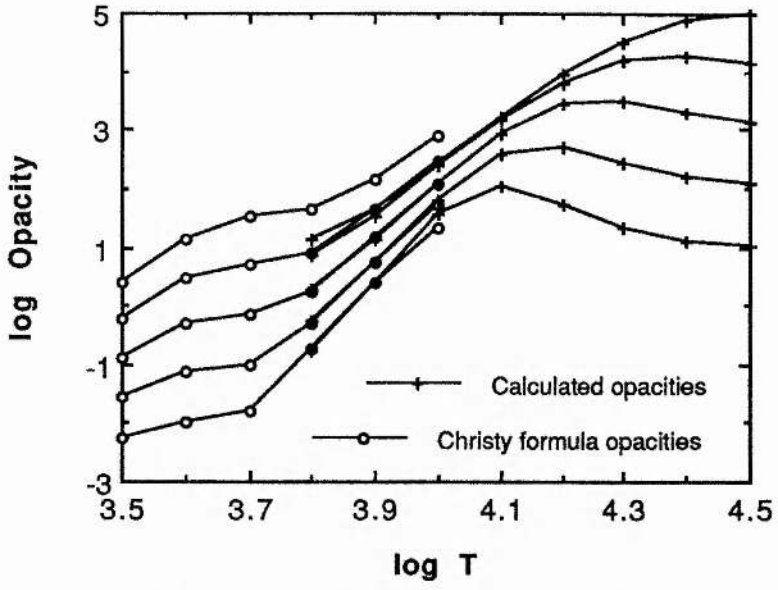

Figure 4.12 : Comparison of the Christy formula opacities with the calculated opacities, for a Population I composition for five densities indicated in Figure 4.13.

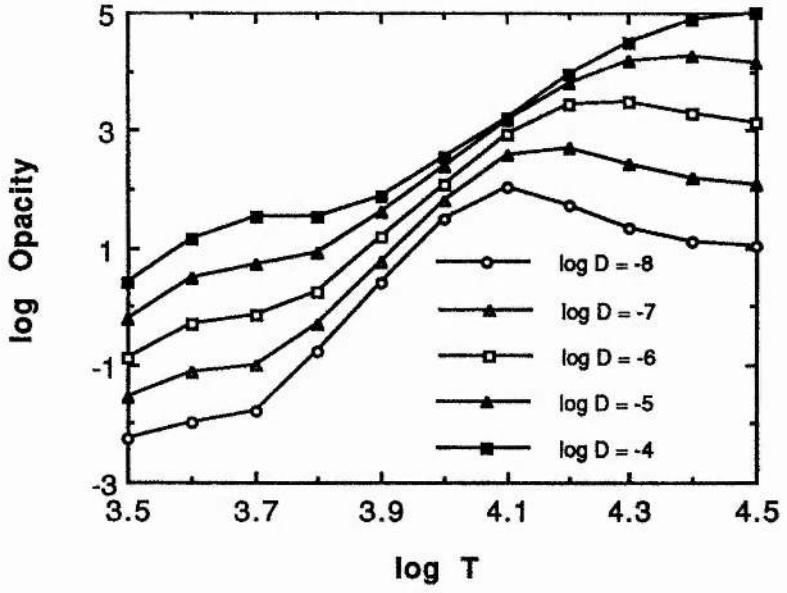

Figure 4.13 : The combined opacities from the Christy formula opacities and the calculated opacities for five densities (D in g/cm^3), which are also plotted in Figure 4.13.

Chapter V Theory and Computation of Stellar Structure and Evolution

Introduction

The present study of LM stars is carried out using a stellar model code. The code was written by Carson according to the theory of stellar structure and evolution using the Henyey method. In the computation of stellar models, most of the physical quantities as input physics are provided by the form of data tables.

5.1 Physics in stars

In the stellar interior and envelope there are many physical processes which determine the state of a star and govern its structure and evolution. However, some assumptions have to be made in order to make the problem solvable. Firstly, the excluding of magnetic and tidal forces and rotation make possible the assumption of spherical symmetry for the stars. Consequently, the problem of determining the stellar structure is reduced to a one-dimensional problem. In addition, the stars in most evolution stages, after reaching the main sequence, can be assumed to be in a hydrostatic state. Based on these two assumptions, the theory of stellar structure and evolution has been developed (see Chandrasekher 1939) to include important physical processes in the star and establish a mathematical model for the quantitative study. In this section we briefly review the physical processes involved in the study of stellar structure and evolution.

5.1.1 Structure equations

There are four basic differential equations which govern stellar structure, all of which are the results of physical principles. Since the mass is usually defined for a given stellar model, the independent variable of the differential equations should be chosen to be the mass within a sphere of radius r around the centre M_r. Another independent variable is time

t which incorporates the evolutionary terms into the structure equations. The dependent variables for stellar structure consist of the local pressure P, temperature T, luminosity L_r, radius r, and composition of elements **C**=(X,Y,Z). The other physical quantities include the mass density ρ, the internal energy density u, the energy generation rate ε, and the temperature gradient ∇. They are found as be functions of the dependent variables P, T, L_r, r, **C** and the independent variables M_r and t. The four structure equations are

1) Equation of mass continuity

$$\frac{\partial r}{\partial M_r} = \frac{1}{4\pi r^2 \rho} ,$$

2) Equation of hydrostatic equilibrium

$$\frac{\partial P}{\partial M_r} = - \frac{G M_r}{4\pi r^4} ,$$

3) Equation of energy conservation

$$\frac{\partial L_r}{\partial M_r} = \varepsilon - \frac{\partial u}{\partial t} + \frac{P}{\rho^2} \frac{\partial \rho}{\partial t} ,$$

4) Equation of energy transport

$$\frac{\partial T}{\partial M_r} = - \frac{G M_r T}{4\pi r^4 P} \nabla$$

with the gravitational constant G.

5.1.2 Input Physics

The input physics defines the dependent relations between the physical quantities ρ, u, ε,∇, and the variables r, L_r, P, T, M_r and t.

1) The equation of state defines the density ρ and internal energy density u, i.e.

$$\rho = \rho(T, P, \mathbf{C}) ,$$

$$u = u(T, P, \mathbf{C}) .$$

2) The thermonuclear reaction rates define the energy generation rate, i.e.

$$\varepsilon = \varepsilon (T, P, \mathbf{C})$$

$$= \varepsilon_{pp} + \varepsilon_{CNO} + \varepsilon_{3\alpha} .$$

3) The radiative, conductive and convective transport of energy defines the temperature gradient ∇, i.e.

$$\nabla = \nabla_{rad+cond} \qquad \text{if } \nabla_{rad+cond} < \nabla_{ad}$$

$$= \nabla_{con} \qquad \text{if } \nabla_{rad+cond} > \nabla_{ad} .$$

The radiative and conductive temperature gradient $\nabla_{rad+cond}$ is defined in terms of

$$\nabla_{rad+cond} = \frac{3}{16\pi acG} \frac{\kappa L_r P}{M_r T^4} ,$$

with the radiative and conductive opacity $\kappa = \kappa(T, P, \mathbf{C})$. The adiabatic temperature gradient ∇_{ad} is defined by the equation of state in terms of

$$\nabla_{ad} = - \frac{P}{C_p T \rho} \left(\frac{\partial \ln \rho}{\partial \ln T} \right)_P ,$$

with

$$C_p = \left(\frac{\partial u}{\partial T} \right)_P - \frac{P}{\rho^2} \left(\frac{\partial u}{\partial T} \right)_P ,$$

and is therefore a function of T, P, and **C**, i.e.

$$\nabla_{ad} = \nabla_{ad}(T,P,\mathbf{C}) .$$

The convective temperature gradient ∇_{conv} must be calculated in terms of the convection

theory. The mixing length theory of Böhm-Vitense (1958) is used to obtain the solution of ∇_{conv} (see Hofmeister et al., 1964; Baker, 1963). The value of ∇_{conv} can also be obtained from the formulation of the mixing length theory given by Baker and Temesvary (1966), which has been used by Eggleton (1971) to study the evolution of the LM stars. From the mixing length theory it is found that ∇_{conv} depends on the local variables of stellar structure M_r, r, L_r, T and P, i.e.

$$\nabla_{conv} = \nabla_{conv} (M_r, r, L_r, T, P) .$$

In the mixing length theory, a major source of uncertainty for ∇_{conv} is a free parameter for the path length of a turbulent element before it is destroyed or loses its identity, i.e. the mixing length λ. This parameter is mostly chosen proportional to the pressure scale height H_P, so that the ratio $\alpha=\lambda/H_P$ is a freely chosen parameter of order unity.

5.1.3 Change of element abundances

The nuclear burning due to thermonuclear reactions changes the element abundances. For a given element, the change of the mass fraction X_i depends on the reactions j destroying it and reactions k producing it. This yields

$$\frac{\partial X_i}{\partial t} = \sum_k \frac{\varepsilon_{ki}}{Q_{ki}} - \sum_j \frac{\varepsilon_{ij}}{Q_{ij}} ,$$

where ε_{ij} and ε_{ki} are the energy generation rates, Q_{ij} and Q_{ki} are the energy released per unit mass.

In a convection region where instantaneous mixing takes place, the change of mass fraction should given by

$$\frac{\partial X_i}{\partial t} = \frac{\int_{conv} dM_r \left(\sum_k \frac{\varepsilon_{ki}}{Q_{ki}} - \sum_j \frac{\varepsilon_{ij}}{Q_{ij}} \right)}{\int_{conv} dM_r}$$

with an integration over the whole convective region.

5.1.4 Boundary conditions

The four differential equations of stellar structure need four boundary conditions. Of them, two are found to be at the centre of the star while the other two are at the surface. Two types of surface boundary conditions will be discussed.

5.1.4.1 Boundary condition at the centre

The radius r and the luminosity L_r at the centre of a star must vanish, i.e.

$$r = L_r = 0 \quad \text{for } M_r = 0.$$

These conditions are certainly satisfied if there is no non-physical condition there.

5.1.4.2 Atmospheric boundary conditions at the surface

If the stellar atmosphere beyond the photosphere is considered, the Eddington approximation for radiative transport may be used to obtain the relation between the effective temperature T_{eff} and the temperatures in the atmosphere, i.e.

$$T^4 = T_{eff}^4 \frac{3}{4} (\tau + 2/3)$$

with the optical depth τ. With the equation of hydrostatic equilibrium and a given optical depth $\tau = \tau_0$, it defines the surface boundary conditions as in the form

$$T = T(R,L,\tau_0)$$

$$P = P(R,L,\tau_0) ,$$

where T, P, R, L are all variables evaluated at the surface. For example, τ_0=2/3 defines a photosphere with the temperature equal to the effective temperature.

5.1.4.3 Photospheric boundary condition at the surface

In the atmosphere with the low temperatures and high densities, the integration for the atmospheric boundary condition may fail in computations because of its sensitivity to the surface opacity. In such a case, the surface boundary condition can be obtained by supposing that the opacities beyond the photosphere are constant and only depend on the conditions of the photosphere. If the photosphere is defined at $\tau=2/3$ where the temperature is equal to the effective temperature, the atmospheric boundary condition is reduced to

$$T^4 = \frac{L}{4\pi R^2 \sigma} ,$$

$$P = \frac{2}{3}\frac{GM}{R^2\,\kappa(T,P)} ,$$

where $\kappa(T, P)$ is the opacity at the photosphere and is determined by the photospheric conditions of temperature and density (or pressure).

5.1.5 Initial Condition

Since an evolutionary problem is concerned, some initial conditions are required for the structure equations which incorporate the time-dependent terms. One of the initial conditions is the stellar mass. It is assumed to remain constant in time in many phases of the evolution for most stars. Exceptional examples cover the massive stars with stellar winds and the binary stars with mass exchange. For the LM stars of our interest, the assumption of constant mass is correct because of their slow evolution.

Another initial condition is the physical state throughout the whole star, i.e., an initial model. For a massive star with fast evolution, its physical state depends considerately on the pre-main sequence status. For a slowly evolving star, however, the contraction evolution in the pre-main sequence does not affect its states on the main sequence. Therefore, the initial state at zero age can be simply defined by the equilibrium solution of

the structure equations with the neglect of the time-dependent terms and with uniform chemical composition. The distribution of element abundances in the star is also one of the initial conditions. It is also hard to define the zero age of the main sequence for the massive stars because their nuclear burning has started and has changed the element abundances before they stop gravitational contraction. In contrast, the slowly evolving stars do not change their element abundances in the gravitational contraction phase. Therefore, a low mass star can be supposed to be homogeneous in the element abundances at its zero age on the main sequence.

We conclude that for the LM stars, their initial states can be regarded to be a hydrostatic structure with homogeneous distribution of element abundances, while the initial state of a massive star depends on its pre-main sequence evolution.

5.2 Computational method of stellar structure

5.2.1 Two point boundary value problem

The four differential equations of stellar structure with their boundary conditions at the centre and the surface constitute a two point boundary value problem. Theoretically, such a problem can be solved by two methods: the shooting method and the relaxation method. In the computation of stellar structure, however, the relaxation method is preferred owing to the delicate boundary conditions and complicated algebraical relations involved.

According to the relaxation method, the differential equations and their boundary conditions are converted into a number of difference equations. Then the Newton-Raphson method is used to obtain the solution from a guessed or trial solution.

5.2.2 Henyey method

In the study of stellar structure and evolution, the relaxation method was first developed by Henyey et al. (1959,1964) to calculate accurate models. The features of the Henyey method

can be summarized briefly. First, the steps both in time and in mass are limited to be sufficiently small in order to keep the maximum differences of physical quantities between two zones in structure and between two evolutionary models within bearable limits. Second, the integration strategy of the outer layers is employed to overcome the convergence difficulty due to the delicate outer boundary condition.

5.2.3 Carson's code

The code constructed by Carson for stellar structure and evolution is utilized in our study of the LM stars. It is based on the method described by Kippenhahn et al. (1967). One feature of this code is that the input physics is incorporated into the main Henyey code by means of interchangeable subroutines. This enables us to manipulate the elements of the input physics independently according to application. Furthermore, this method of including physical quantities allows us to use data tables for the input physics as an alternative to inline subroutines. The inclusion of derivatives in both methods required by the Newton-Raphson method is assured.

In addition, most parameters used in the stellar model can be changed in Carson's code. One of them is the ratio of the mixing length to pressure scale height. The other one is to control the boundary condition at the surface. The simplified photosphere model and the atmospheric model are both used to produce the surface boundary conditions in the code. Changing these parameters in the calculation can allow us to investigate their effects on the LM star models.

In the code, the calculation of the initial model for any mass can be started from an approximate solution of a standard solar model. The initial model is defined to be homogeneous in element abundances.

5.3 Utilization of data tables

5.3.1 Data table of input physics

Since the equation of state and the radiative opacities that we employ are calculated from the sophisticated physical models we established, it is impossible to incorporate them by functional subroutines into the calculation of the LM star models. Therefore, we utilize data tables to interpolate for most of the input physics, thus dramatically speeding the computation.

The physical quantities tabulated in the data tables include the total pressure, the internal energy density, the free electron number density, the specific entropy, the opacity, as well as their derivatives with respect to the independent variables, namely, the temperature and mass density. The opacity data tabulated incorporate the radiative opacity and the conductive opacity. The data tables range from 10^3 K to 10^9 K in the temperature, and from 10^{-14} g/cm^3 to 10^6 g/cm^3 in the mass density. The wide ranges guarantee that the interpolation of physical quantities in the computation can never go beyond the table. A grid square in the table is defined by a temperature interval of $\Delta \log T=0.1$ and a mass density interval of $\Delta \log \rho=0.5$.

5.3.2 Interpolation of data tables

Two methods of two-dimensional interpolation are used to calculate physical quantities from the data tables. One is the bilinear interpolation which is simpler and faster, and can ensure the continuity of interpolated quantities but not their gradients. The other one is bicubic interpolation which can preserve the continuity of both interpolated quantities and their gradients, but slower in computation since a number of coefficients need to be calculated. The use of the two methods of interpolation has been studied in detail by Press et al. (1986).

In the computation by using Carson's code, both methods are found to be usable.

5.3.3 Treatment of composition change

A problem in the utilization of data tables for the input physics is the change of element abundances in stellar evolution. Generally, several data tables with different compositions have to be used to interpolate for the data of a desired composition. In the case of the LM stars, however, the composition changes very slowly because of their slow evolution. Even if there are small changes of composition in the central parts, they can be treated by some approximate methods in order to obtain the required data. In the central region of a star, there are three quantities, among those tabulated, which can be affected considerably by the composition change. They are the total pressure, the internal energy density, and the opacity. Because the composition change due to nuclear fusion only changes the number density of nuclei, the correction to the tabular data for chemical abundances can be made according to their contribution to the energy generation. The nuclei can always be treated as ideal gases, therefore the total pressure P and the internal energy density U are calculated from the tabular data P^* and U^* by means of

$$P = P^* - kT\rho N_A [(X-X^*)+(Y-Y^*)/4+(Z-Z^*)/14] ,$$

$$U = U^* - kT\rho N_A [(X-X^*)+(Y-Y^*)/4+(Z-Z^*)/14]*2/3 ,$$

where X, Y and Z are the element abundances for the required data while X^*, Y^* and Z^* are the element abundances of the tabular data. The density ρ and the temperature T are required in the above formula as well as the Boltzmann constant k and Avogadro number N_A.

Similarly, the opacity data for the required composition are calculated from the tabular data κ^* in terms of

$$\kappa = \kappa^* - 0.2 (X-X^*).$$

This is based on the condition of complete ionization, with the opacity contributed solely by the electron scattering in the region of composition change.

Chapter VI Zero Age Main Sequence of Low Mass Stars

Introduction

The theoretical study of low mass (LM) star models may now be made after we have established all of the input physics. In this chapter, we will calculate zero-age main sequence models of the LM stars and investigate a number of uncertainties in the input physics as well as some model parameters and element abundances. In addition, detailed comparisons of the calculation results are made with the observed data and other theoretical results.

6.1 Zero age main sequence models of LM stars

The calculation of zero age main sequence models is performed for two compositions, or populations. The mass fractions of hydrogen, helium and other heavy elements are taken to be X/Y/Z=0.700/0.280/0.020 for Population I, and X/Y/Z=0.710/0.289/0.001 for Population II. First of all, we need to look into problems met with in the numerical computation.

6.1.1 Computation

In the calculation of the zero age model for a star of given mass, an approximate solution is required as initial input. This can be a previous model with a similar mass, or can be obtained from an approximate method, such as the polytropic method. The convergence of the calculation is easy to achieve if a good model is used as initial input. In the calculation of the zero age main sequence, however, we found that when a previous solution is used as initial input for a successive calculation of a model of the same mass, the next solution is somewhat different from the previous one.

We performed calculations for a series of zero age models of the same mass, just by using each previous solution as initial input of the next one. The successive solutions for zero-

age model of a solar mass are given in Table 6.1. We see from Table 6.1 that the successive solutions converge to one although the first few have different results. There is a difference of effective temperature of about 400 K and luminosity of 2.6 percent between the first one and the convergent one.

Two factors may be responsible for this problem. One is the use of data in table form for the input physics. In our calculation, all physical quantities, except nuclear generation rates which are provided with a functional routine, are tabulated. Although the bicubic interpolation employed can keep the continuity of physical quantities and their first derivatives, the problem still remains. The other factor is that in the code the second derivatives of physical quantities are ignored in the iteration by the Newton-Raphson method. This can reduce the consistency of the convergence of the solution. In such a situation, we take the solution obtained from the successive convergent calculations.

An unfortunate case appeared in the calculation of the model with mass near or below 0.1 M_{sun}. In this case, we could never obtain a convergence to one solution, in spite of the fact that the calculation of every model is able to reach a convergence. Table 6.2 lists the successive solutions for the 0.1 M_{sun} model. It shows that the solutions of successive models keep oscillating within a range. In this case, we can only take an average solution from the last two models as our calculation results.

It should be mentioned that the above calculations were performed by using the standard physics input, obtaining which we call a "standard model", which will be defined in the next section. The interesting result was found that the problem of oscillating solutions was removed when a modified EOS is used in the input physics. This will be discussed in Section 6.2.9.

Table 6.1 : The successive models of a zero age star (with mass 1.0 M_{sun}) of the Standard Pop I by using the standard EOS.

Succession	log L	log R	log T_e	log T_c	log ρ_c	log P_c
1	-0.1544	0.0284	3.7104	7.1170	1.9186	17.1680
2	-0.1452	0.0161	3.7189	7.1201	1.9201	17.1725
3	-0.1440	0.0005	3.7270	7.1205	1.9203	17.1730
4	-0.1438	-0.0151	3.7349	7.1205	1.9203	17.1730
5	-0.1436	-0.0247	3.7397	7.1205	1.9203	17.1731
6	-0.1433	-0.0307	3.7428	7.1206	1.9203	17.1732
7	-0.1433	-0.0318	3.7433	7.1206	1.9203	17.1732
8	-0.1433	-0.0317	3.7433	7.1206	1.9203	17.1732

Table 6.2 : The successive models of a zero age star (with mass 0.1 M_{sun}) of the Standard Pop I by using the standard EOS.

Succession	log L	log R	log T_e	log T_c	log ρ_c	log P_c
1	-3.3331	-0.8529	3.3564	6.5929	2.4969	17.3489
2	-3.3088	-0.8566	3.3644	6.5950	2.5070	17.3632
3	-3.0448	-0.9035	3.4538	6.6106	2.6400	17.5505
4	-3.1146	-0.8897	3.4295	6.6077	2.5977	17.4922
5	-2.9919	-0.9168	3.4737	6.6124	2.6755	17.5988
6	-3.0735	-0.8983	3.4440	6.6098	2.6209	17.5244
7	-2.9731	-0.9219	3.4809	6.6129	2.6895	17.6177
8	-3.0768	-0.8977	3.4429	6.6097	2.6187	17.5215

6.1.2 Standard Pop I and Standard Pop II

We define the Standard Pop I and the Standard Pop II models as those calculated from the standard input physics and standard model parameters, respectively, for the compositions of Population I and Population II. The standard input physics include :

1> the thermodynamic quantities calculated from the equation of state established in Section 2.4 of Chapter II;

2> the radiative opacities calculated form the radiative opacity model established in Chapter III;

3> the molecular opacities for temperatures below 10^4 K from the calculation by Carson and Sharp;

4> the electron conductive opacities given in Chapter IV;

5> the nuclear generation rates given in Chapter IV;

6> the enhancement factor due to the electron screening effect on nuclear reactions, which is given in Chapter IV.

The standard model parameters in the code for the standard model are

1> the ratio of mixing length to pressure scale-height equal to 1.5;

2> the simple photosphere model for the surface boundary condition.

The reason why we did not use the atmosphere model as the surface boundary condition is that it fails to work for the models with masses below 0.7 M_{sun}. In order to have a unified comparison of all models with different masses, the same surface condition should be used.

The calculated results for zero-age main-sequence models of LM stars are given in Table 6.3 for Standard Pop I, and in Table 6.4 for Standard Pop II. The minimum mass for the model with stable solution is just below 0.1 M_{sun}. We will see in Section 6.2.9 that the use of a modified EOS makes the minimum mass for hydrogen burning reach as low as 8 percent of the solar mass.

Table 6.3 : The zero age models of the lower main sequence for the Standard Pop I.

Mass	log L	log R	log T_e	log T_c	log ρ_c	log P_c
1.00	-0.143	-0.032	3.743	7.121	1.920	17.173
0.80	-0.629	-0.131	3.672	7.041	1.888	17.064
0.60	-1.227	-0.234	3.574	6.949	1.852	16.937
0.50	-1.501	-0.329	3.553	6.909	1.838	16.885
0.40	-1.728	-0.421	3.542	6.880	1.833	16.853
0.30	-1.942	-0.511	3.533	6.846	1.942	16.932
0.25	-2.077	-0.568	3.528	6.818	2.036	17.006
0.20	-2.249	-0.641	3.521	6.781	2.156	17.105
0.15	-2.495	-0.744	3.511	6.727	2.338	17.262
0.12	-2.721	-0.830	3.498	6.676	2.507	17.417
0.10	-3.022	-0.910	3.462	6.611	2.656	17.572
0.09	-3.346	-0.985	3.419	6.538	2.828	17.771

Table 6.4 : The zero age models of the lower main sequence for the Standard Pop II .

Mass	log L	log R	log T_e	log T_c	log ρ_c	log P_c
1.00	0.203	-0.051	3.840	7.176	2.009	17.324
0.80	-0.252	-0.138	3.769	7.099	1.986	17.226
0.60	-0.850	-0.270	3.686	7.004	1.956	17.102
0.50	-1.223	-0.333	3.624	6.946	1.938	17.030
0.40	-1.565	-0.434	3.589	6.896	1.924	16.968
0.30	-1.810	-0.530	3.575	6.857	2.000	17.010
0.20	-2.141	-0.658	3.555	6.786	2.208	17.175
0.15	-2.401	-0.761	3.542	6.729	2.393	17.334
0.10	-3.000	-0.950	3.489	6.592	2.776	17.735

6.1.3 Observation data from binary systems

There exist a great number of observational data for M dwarfs, most of them based on infrared photometry, such as those presented by Veeder (1974) and those by Upgren and Weis (1975). The most reliable data so far are from the results of eclipsing binary analysis. So we compare our theoretical determinations with the observed properties of the LM stars in binary systems given by Popper (1980). Table 6.5 lists the observed data for the binary stars with luminosities lower than one solar luminosity. The data errors are also listed so as to make reliable comparisons.

In addition to the data from binary stars, a recent study of M dwarfs by Berriman and Reid (1987) summarized the data for stars in the solar neighbourhood with effective temperatures below 4000 K. This study indicates that the previously determined effective temperatures of some stars should be adjusted to lower values. The shift to cooler temperatures tends to increase discrepancies with the results from most theoretical studies. This problem is very much of concern in our study and will be discussed in Section 6.3.

Table 6.5 : Observed properties from the binary stars with the error data . The mass, the luminosity L and the radius R are in solar units, the effective temperature T_e in K.

Object	Mass	Error	log L	Error	log R	Error	log T_e	Error
L726-8 B	0.110	0.020	-2.980	0.150	-0.820	0.080	3.425	0.015
L726-8 A	0.110	0.020	-2.830	0.070	-0.790	0.040	3.443	0.007
o Eri BC B	0.160	0.030	-2.250	0.200	-0.660	0.140	3.520	0.025
Kr 60 B	0.160	0.020	-2.300	0.150	-0.640	0.190	3.503	0.015
Kr 60 A	0.280	0.030	-1.860	0.070	-0.460	0.040	3.518	0.005
FU 46 A	0.300	0.070	-1.710	0.070	-0.430	0.040	3.546	0.025
FU 46 B	0.300	0.070	-1.730	0.100	-0.410	0.060	3.528	0.010
Wolf 630	0.420	0.100	-1.620	0.150	-0.370	0.100	3.538	0.015
HR 6426 B	0.540	0.100	-0.980	0.200	-0.220	0.120	3.622	0.025
η Gas B	0.560	0.100	-1.130	0.060	-0.230	0.120	3.590	0.020
70 Oph B	0.610	0.100	-0.840	0.050	-0.170	0.080	3.631	0.030
ξ Boo B	0.720	0.150	-0.960	0.060	-0.260	0.070	3.645	0.020
HR 6426 A	0.780	0.200	-0.770	0.085	-0.240	0.060	3.685	0.015
70 Oph A	0.840	0.150	-0.350	0.040	-0.100	0.030	3.721	0.010
ξ Boo A	0.900	0.200	-0.270	0.060	-0.115	0.030	3.745	0.005
η Gas A	0.910	0.050	0.060	0.060	-0.010	0.030	3.777	0.005
α Cen B	0.930	0.040	-0.280	0.015	-0.025	0.200	3.700	0.010

6.1.4 Comparison with observed data

The comparisons of the calculated data with the observed data for binary stars are given in Figure 6.1-6.4, respectively for the mass-luminosity relation, mass-effective temperature relation, mass-radius relation and H-R diagram. Figure 6.1-6.3 reveal that considerable uncertainties in stellar mass reduces the reliability of comparisons. The H-R diagram in Figure 6.4 shows relatively small error boxes, so as to give a reliable comparison. It shows that there is good agreement of the calculated results with the observed data for the models with effective temperature above 3200 K $\approx 10^{3.5}$ K. In spite of this, a discrepancy at cooler effective temperatures can be seen for the models of masses below 0.1 M_{sun}. This result can also be seen from the comparison with other sources of observational data, e.g. that given by Berriman and Reid (1987). Other theoretical studies by VandenBerg et al. (1983) and that by Dorman et al. (1990) also show the same result.

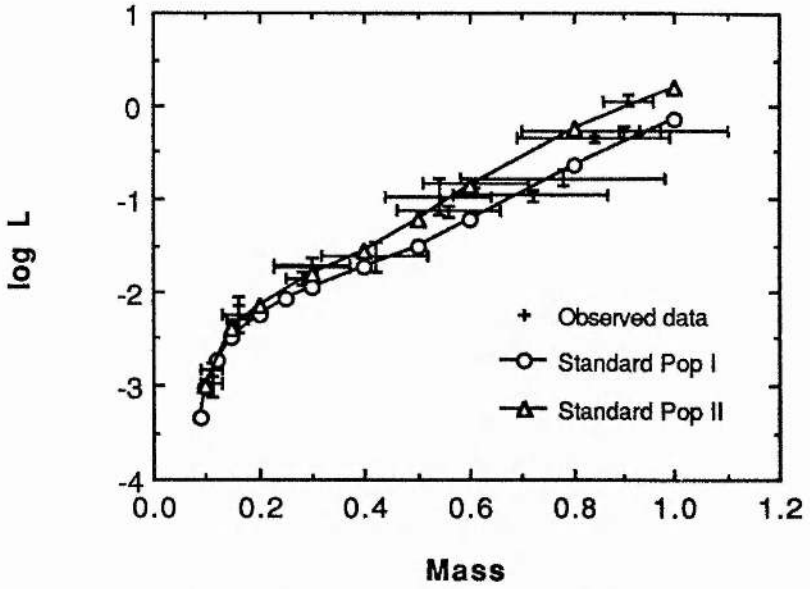

Figure 6.1 : Comparison of the calculated data of the zero age models of LM stars with the observed data of binary stars, for the mass (in M_{sun}) and luminosity (L in L_{sun}) relations for two compositions (Pop I and II).

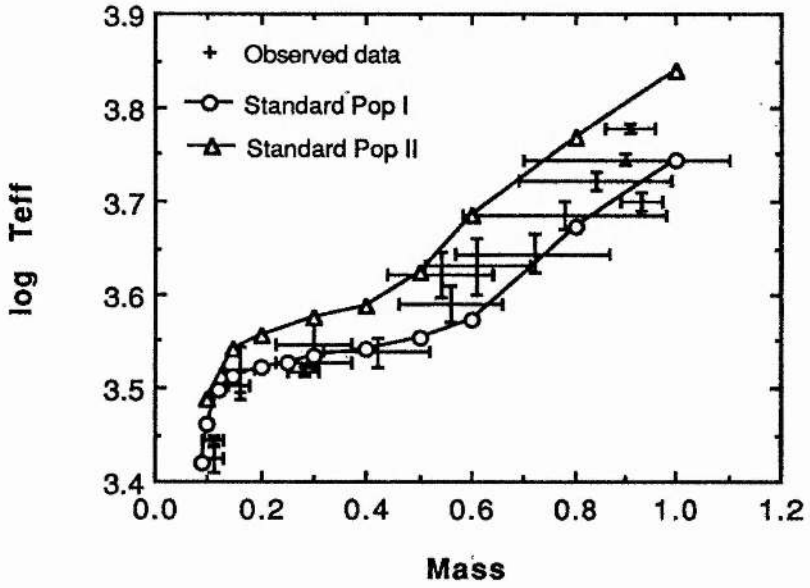

Figure 6.2 : The same as in Figure 6.1 but for the mass and effective temperature (T_{eff} in K) relations.

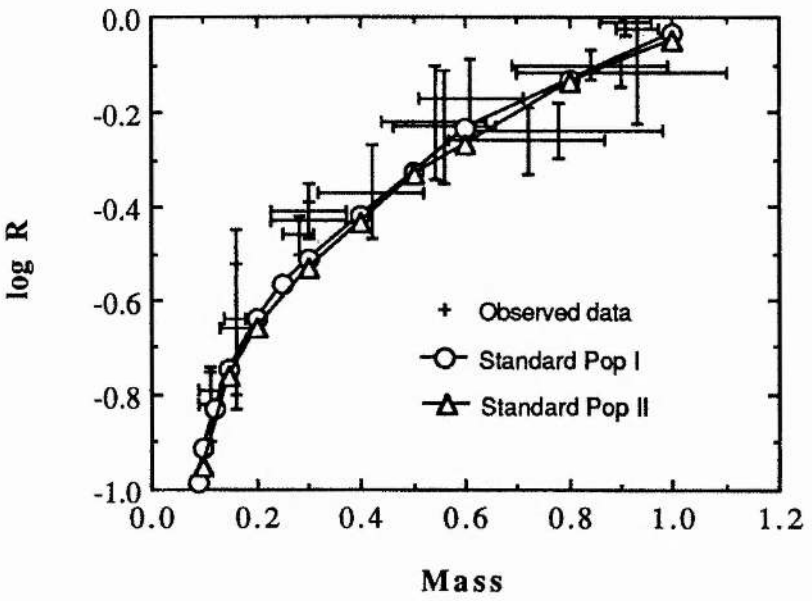

Figure 6.3 : The same as in Figure 6.1 but for the mass and radius (R in R_{sun}) relations.

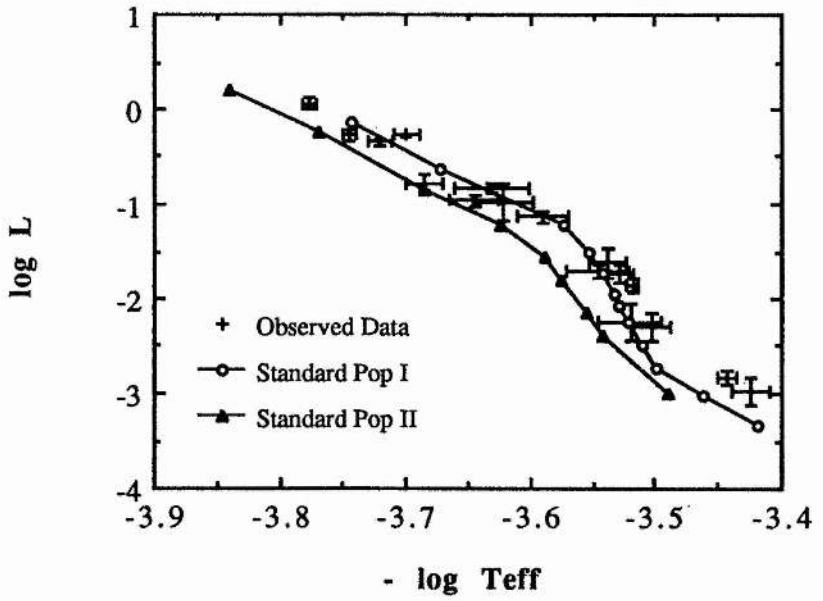

Figure 6.4 : The same as in Figure 6.1 but for the H-R diagram with the effective temperature Teff in K and the Luminosity L in L_{sun}.

So we now come to the question of what theoretical factors can be responsible for the discrepancy. Cox et al. (1981) have suggested that the magnetic field in most low mass stars might inhibit convection, but the importance of the correction is not unknown. From the study by Dorman et al. (1990) we see that two determinations of the EOS leads to different results for LM star models. This could hint at the importance of the EOS in the study of LM stars. Especially the nonideal effect on the EOS has been a continuing uncertainty. So this will be a substantial point of our study.

6.2 Investigation of Uncertainties

In this section we investigate uncertainties in most elements of the input physics for the calculation of the LM star models. Based on the standard model defined in Section 6.1.2, we check the importance of each element of input physics by excluding it or replacing it with an alternative one in the model calculations. The model parameters, such as element abundances, the ratio of mixing length, and the surface boundary condition, will also be examined by being changed. The investigations will highlight uncertainties in the input physics and the model parameters.

The Standard Pop I models are compared with the alternative models.The calculations for the investigation of uncertainties will cover the zero age main sequence of stars with masses from one solar mass down to 10 percent of the solar mass, or below it if it is easy to obtain convergence of the calculation.

6.2.1 Mixing length ratio

The ratio of mixing length to pressure scale-height α is a free parameter in the determination of convective transport. In most cases, the ratio α is supposed to be between 1 and 2 for reasonable calculations of stellar models. However, the study of the LM stars by Cox et al. (1981) pointed out that acceptable models for a LM star of mass $M = 0.3$ M_{sun} needs $\alpha = 0.1$. This unusual result was explained as due to strong surface magnetic

fields which suppress convection in the outer envelopes. Despite the fact that the later studies, e.g. that by Neece (1984), have solved the problem by introducing the use of molecular opacities, we would like to check the effect of changing the mixing length ratio in the LM star models. Based on the Standard Pop I with the mixing length ratio α=1.5, the calculation of alternative zero age models of the LM stars is performed by using α=0.5.

Table 6.6 lists the properties of the models of zero age main sequence LM stars with α=0.5. Comparisons with the Standard Pop I are shown in Figures 6.5-6.7. The comparison of mass-luminosity relations in Figure 6.5 indicates no significant difference of luminosity for all models of masses from 0.1 M_{sun} to M_{sun}. Nevertheless, Figures 6.6 and 6.7 show that effective temperatures are lower in the alternative models with α=0.5 than in the Standard Pop I models. Furthermore, they show that the more massive stars have greater shifts of the effective temperatures to cooler values. The effective temperature is reduced by 8 percent for a solar mass model while there is almost no shift for the model of mass 0.1 M_{sun}. It is concluded that the uncertainty due to the mixing length ratio α affects only the effective temperatures for the models of relatively massive stars but not their luminosities and does not affect models of smaller mass.

Table 6.6 : The zero age models of the lower main sequence for the Standard Pop I but with a mixing length ratio equal to 0.5.

Mass	log L	log R	log T_e	log T_c	log ρ_c	log P_c
1.00	-0.144	0.041	3.707	7.120	1.920	17.173
0.80	-0.645	-0.046	3.625	7.039	1.887	17.060
0.60	-1.267	-0.192	3.543	6.943	1.849	16.929
0.50	-1.556	-0.308	3.528	6.901	1.835	16.874
0.40	-1.793	-0.410	3.520	6.869	1.828	16.837
0.30	-2.004	-0.504	3.514	6.839	1.918	16.902
0.25	-2.134	-0.561	3.510	6.812	2.016	16.978
0.20	-2.300	-0.635	3.506	6.776	2.137	17.079
0.15	-2.536	-0.738	3.498	6.723	2.321	17.239
0.12	-2.758	-0.825	3.486	6.673	2.492	17.396
0.10	-3.026	-0.909	3.461	6.612	2.651	17.566

6.2.2 Surface boundary condition

As mentioned in Section 5.1.4, the atmospheric model is probably better for the surface condition than the simple photospheric condition. The reason is that the former takes into account the physical condition of the stellar atmosphere while the later ignores it and defines the surface condition at the photosphere.

Unfortunately, the calculation of the LM star models failed for the mass below 0.8 M_{sun} when the atmospheric model was used as the surface condition. So we used the simple photosphere model as surface condition to carry through the calculation for the Standard Pop I and II models, making it easier to obtain convergent solutions. In order to check the difference between using two types of surface condition, we present the calculation results of the models of mass 1.0 and 0.8 M_{sun} in Table 6.7, for which the solutions can be obtained by using the atmospheric model as surface condition.

In the comparison with the Standard Pop I models in Figures 6.5-6.7, we hardly see any difference. So it implies that the calculation of zero age models of the LM stars is insensitive to the surface boundary condition. However, this conclusion is only valid for the zero age main sequence. In the next chapter, we will see how the surface boundary condition affects the evolution of the solar model.

Table 6.7 : The zero age models of the lower main sequence for the Standard Pop I but with the atmospheric model as surface condition.

Mass	log L	log R	log T_e	log T_c	log ρ_c	log P_c
1.00	-0.143	-0.042	3.748	7.121	1.920	17.173
0.80	-0.627	-0.135	3.671	7.042	1.888	17.064

6.2.3 Element abundances

In Section 6.1, the LM star models of the Standard Pop I and Pop II are calculated. The difference between them is in the abundances of the heavy elements. In this section, we present the calculated results for a composition of X/Y/Z=0.770/0.212/0.018, which is

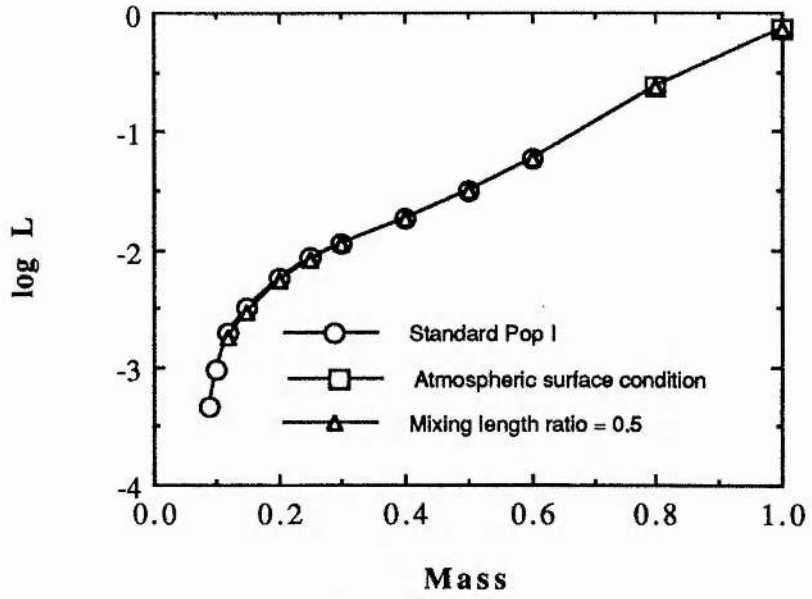

Figure 6.5 : Comparison of the mass-luminosity relations with the standard models with variations of the mixing length ratio and the surface boundary condition.

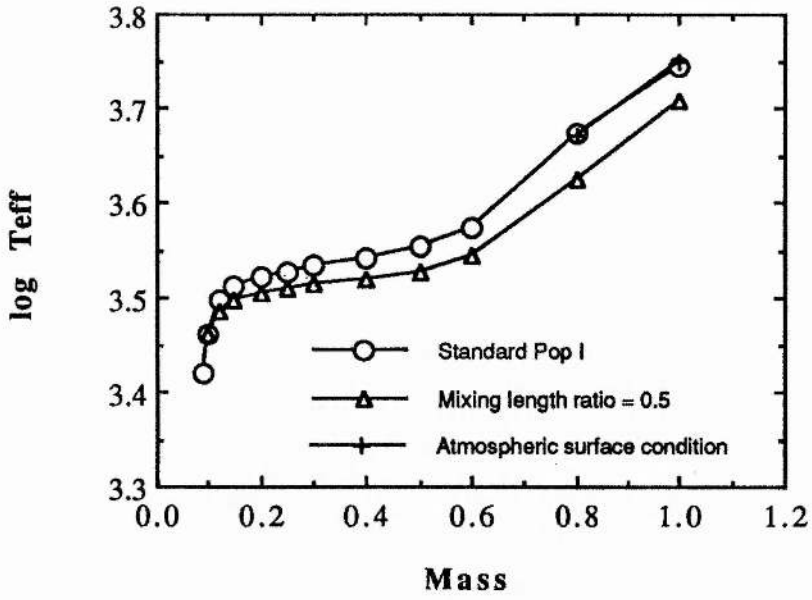

Figure 6.6 : Comparison of the mass-effective temperature relations for the same conditions as in Figure 6.5.

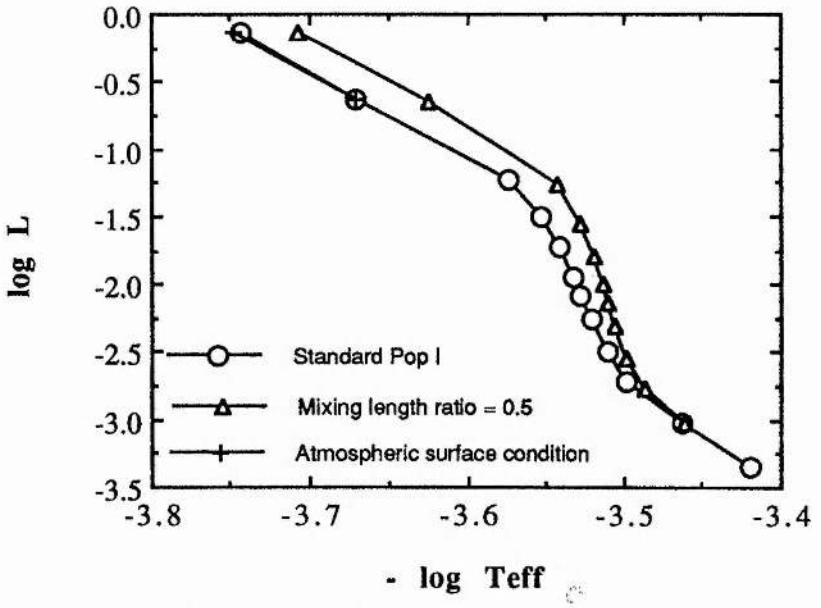

Figure 6.7: The comparison of the H-R diagrams for the same conditions as in Figure 6.5.

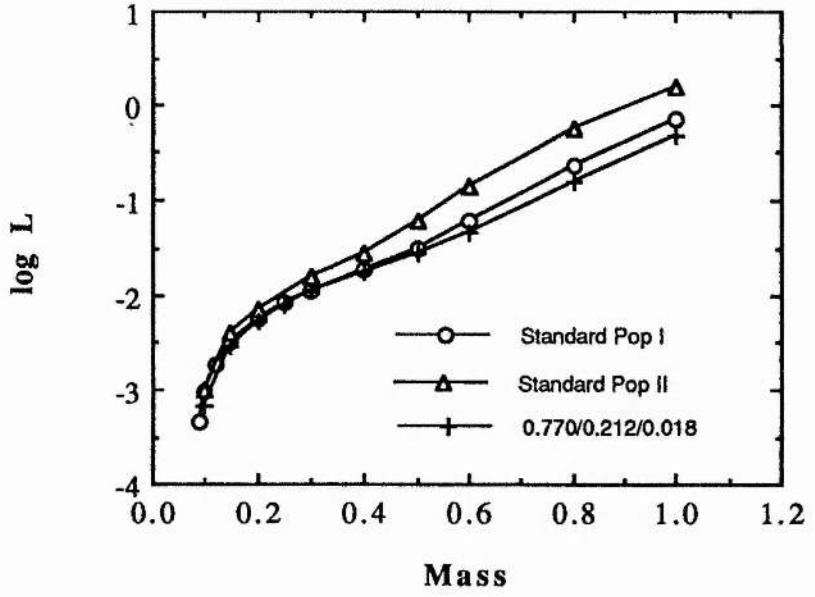

Figure 6.8 : Comparison of the mass-luminosity relations with the standard models with variation of the element abundances.

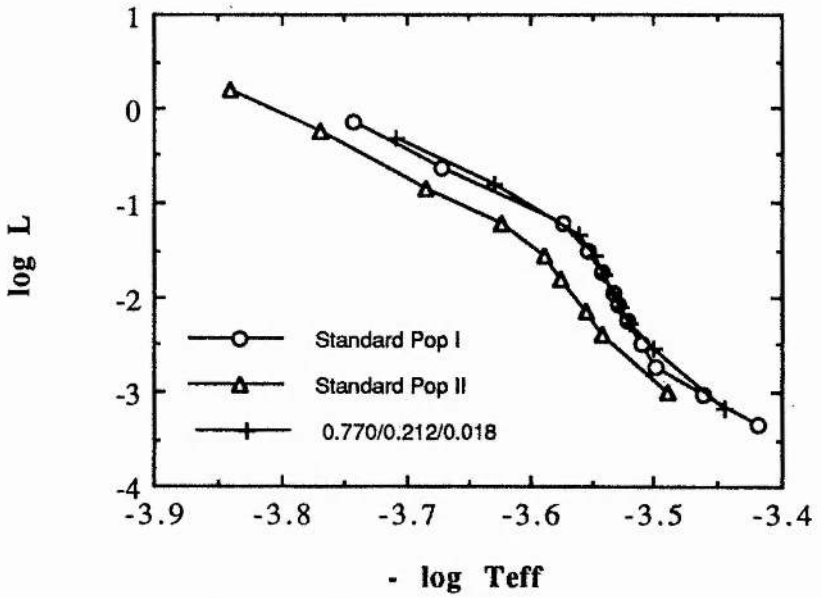

Figure 6.9 : Comparison of the H-R diagrams for the same conditions as in Figure 6.8.

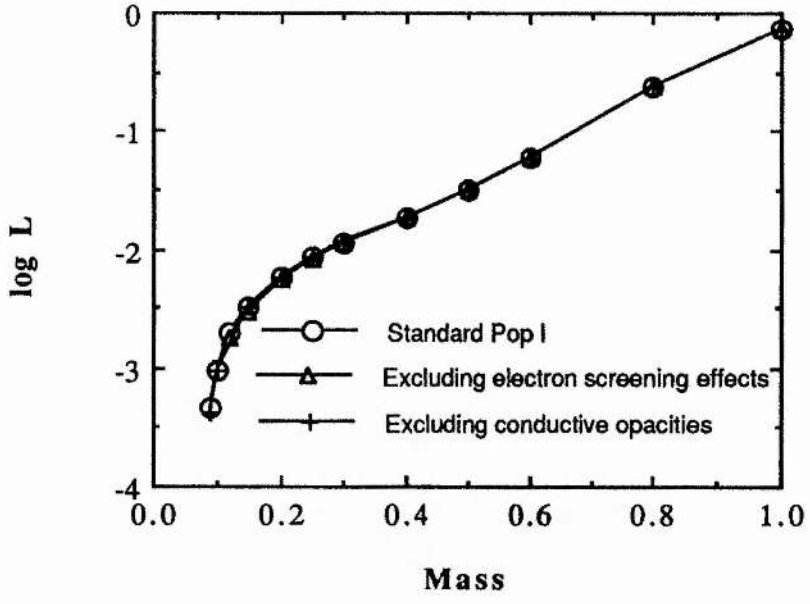

Figure 6.10 : Comparison of the mass-luminosity relations with the standard models with variations of the electron screening effects on thermonuclear reactions and the conductive opacities.

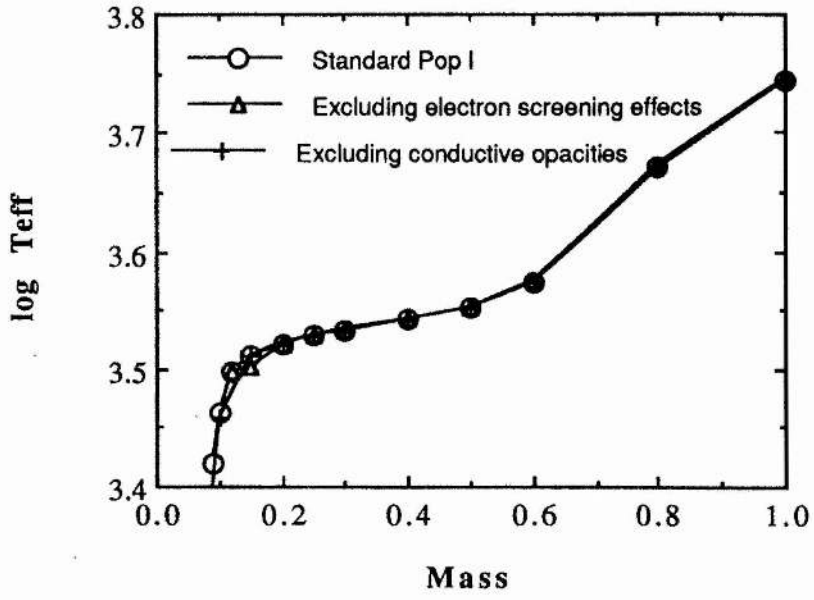

Figure 6.11 : Comparison of the mass-effective temperature relations for the same conditions as in Figure 6.10.

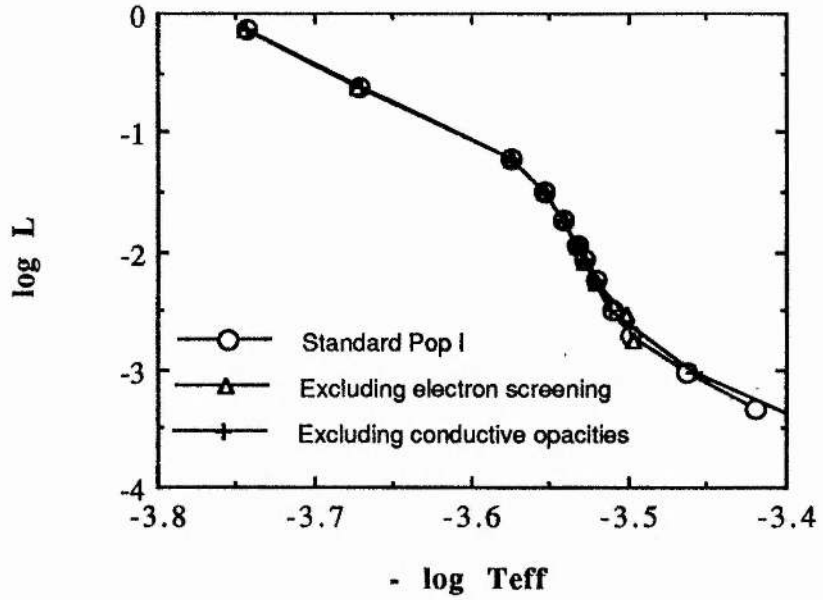

Figure 6.12 : Comparison of the H-R diagrams for the same conditions as in Figure 6.10.

more hydrogen rich than the previous two compositions. So comparisons of the models for three compositions will reveal the effects of each element abundance on the LM star models.

Table 6.8 gives the calculated results for the composition specified above. The properties of zero age models for the LM stars are compared in Figures 6.8 and 6.9. The comparisons of the mass-luminosity relations and the H-R diagrams show the sensitivity of both luminosity and effective temperature to the abundance of the elements for the relatively massive star models. The H-R diagram indicates that the increase of heavy element abundance shifts the effective temperatures to cooler values, even for very low mass star models.

Table 6.8 : The zero age models of the lower main sequence for the Standard Pop I but with a composition X/Y/Z = 0.770/0.212/0.018.

Mass	log L	log R	log T_e	log T_c	log ρ_c	log P_c
1.00	-0.313	-0.050	3.710	7.077	1.861	17.095
0.80	-0.795	-0.132	3.630	7.000	1.832	16.990
0.60	-1.334	-0.262	3.560	6.919	1.802	16.881
0.50	-1.558	-0.348	3.548	6.888	1.793	16.843
0.40	-1.748	-0.426	3.539	6.869	1.808	16.840
0.30	-1.958	-0.516	3.532	6.825	1.957	16.952
0.25	-2.093	-0.574	3.527	6.797	2.053	17.028
0.20	-2.270	-0.648	3.519	6.758	2.176	17.132
0.15	-2.545	-0.750	3.501	6.699	2.360	17.291
0.10	-3.175	-0.950	3.444	6.554	2.767	17.722

6.2.4 Electron screening effects on nuclear reactions

The electron screening effect on nuclear reactions begins to play a role in conditions of high density. So most studies of the LM stars have taken into account such a physical effect. How important it is for the LM star models will be examined in this section.

In the Standard Pop I model, the electron screening effect has been incorporated into the calculation of nuclear energy generation rates. By excluding it the calculation of zero age

models of the LM star models produces the results in Table 6.9. Comparisons in Figures 6.10-6.12 do not indicate any appreciable difference. A detailed comparison of Table 6.9 with Table 6.3 shows that the difference in both luminosities and effective temperatures is below one percent for all model masses. We conclude that the electron screening effect in nuclear energy generation does not play a significant role under the conditions in the LM stars.

Table 6.9 : The zero age models of the lower main sequence for the Standard Pop I but excluding electron screening effects on nuclear reactions

Mass	log L	log R	log T_e	log T_c	log ρ_c	log P_c
1.00	-0.140	-0.033	3.745	7.124	1.929	17.185
0.80	-0.625	-0.132	3.673	7.045	1.899	17.078
0.60	-1.225	-0.235	3.575	6.953	1.865	16.954
0.50	-1.503	-0.331	3.553	6.912	1.852	16.903
0.40	-1.734	-0.424	3.542	6.883	1.848	16.871
0.30	-1.951	-0.516	3.533	6.851	1.956	16.951
0.25	-2.088	-0.574	3.528	6.823	2.052	17.028
0.20	-2.264	-0.648	3.521	6.787	2.177	17.133
0.15	-2.545	-0.749	3.501	6.731	2.356	17.286
0.12	-2.754	-0.844	3.497	6.684	2.546	17.473

6.2.5 Conductive opacity of electrons

Electron conduction may be an important means of energy transfer under conditions of high density. So the conductive opacity cannot be ignored in the study of the LM stars which are concerned with relatively high density. Similarly, by excluding the conductive opacities from the Standard Pop I model, the calculation results are listed in Table 6.10 for the zero age models. No difference is found in the comparison with the Standard Pop I model in Figures 6.10-6.12. This implies there is little effect due to conductive opacities in the condition of the LM stars.

Table 6.10 : The zero age models of the lower main sequence for the Standard Pop I but excluding electron conductive opacities.

Mass	log L	log R	log T_e	log T_c	log ρ_c	log P_c
1.00	-0.144	-0.032	3.743	7.121	1.920	17.173
0.80	-0.630	-0.129	3.670	7.041	1.888	17.063
0.60	-1.227	-0.236	3.574	6.949	1.851	16.937
0.50	-1.501	-0.330	3.553	6.909	1.837	16.884
0.40	-1.727	-0.421	3.542	6.881	1.832	16.852
0.30	-1.941	-0.511	3.534	6.846	1.942	16.933
0.25	-2.076	-0.568	3.528	6.818	2.036	17.006
0.20	-2.249	-0.641	3.522	6.781	2.156	17.105
0.15	-2.494	-0.744	3.512	6.727	2.338	17.262
0.10	-3.034	-0.907	3.458	6.610	2.649	17.564

6.2.6 Alexander opacity

Molecular formation has an important influence on the radiative opacity for temperatures below 4000 K. So all studies of the very low mass stars have to incorporate molecular opacity. This can be seen from the studies by Sienkiewicz (1982), VandenBerg et al. (1983), Neece (1984), Dorman (1990), etc.

In the Standard Pop I and Pop II models, we have applied the molecular opacities of Population I and II which are calculated by Carson and Sharp. In this section, the calculation of the LM star models by using the molecular opacities given by Alexander et al. (1983), instead of Carson and Sharp opacities, is performed for Population I. Their opacities are incorporated into the opacity data for temperatures below 10^4 K.

The calculation results are given in Table 6.11. The comparisons with Standard Pop I models given in Figures 6.13-6.15 show there is no considerable difference between using the two sets of opacity data. However, when using the Alexander opacities the calculations only succeed for models with masses above 0.15 M_{sun}.

Table 6.11 : The zero age models of the lower main sequence for the Standard Pop I but using Alexander opacity for $T < 10^4$ K

Mass	log L	log R	log T_e	log T_c	log ρ_c	log P_c
1.00	-0.143	-0.032	3.743	7.121	1.920	17.173
0.80	-0.629	-0.131	3.672	7.041	1.888	17.064
0.60	-1.228	-0.233	3.573	6.949	1.851	16.937
0.50	-1.504	-0.328	3.551	6.908	1.837	16.884
0.40	-1.731	-0.420	3.541	6.880	1.833	16.852
0.30	-1.945	-0.509	3.530	6.845	1.938	16.928
0.20	-2.251	-0.641	3.521	6.781	2.156	17.104
0.15	-2.495	-0.743	3.511	6.727	2.338	17.262

6.2.7 Christy formula opacities

The Christy formula is an approximate method of calculating radiative opacities. In the case of temperatures below 5000 K, the opacity data produced by the formula depend very much on the free electron number density n_e. By using the EOS established in Chapter II which provides n_e, the opacities calculated by the Christy formula are about 3 to 4 times greater than the Carson and Sharp opacities. The comparison has been shown in Chapter IV. This illustrates the invalidity of the Christy formula outside the region where it was fitted.

In spite of the approximation of the Christy formula, we use the opacity data it produces, in place of the Carson and Sharp opacities, to calculate alternative zero age models of the LM stars. The calculation results show the effect of the increase of low temperature opacities on the LM star models.

Table 6.12 lists the calculated results from the use of the Christy formula. The comparison of the mass- luminosity relation with the Standard Pop I models in Figure 6.13 shows that the luminosity of the models with masses below 0.4 M_{sun} is decreased but not considerably. However, the effective temperatures of these models are shifted markedly to cooler values, as is revealed in Figure 6.14. The H-R diagram in Figure 6.15 indicates the

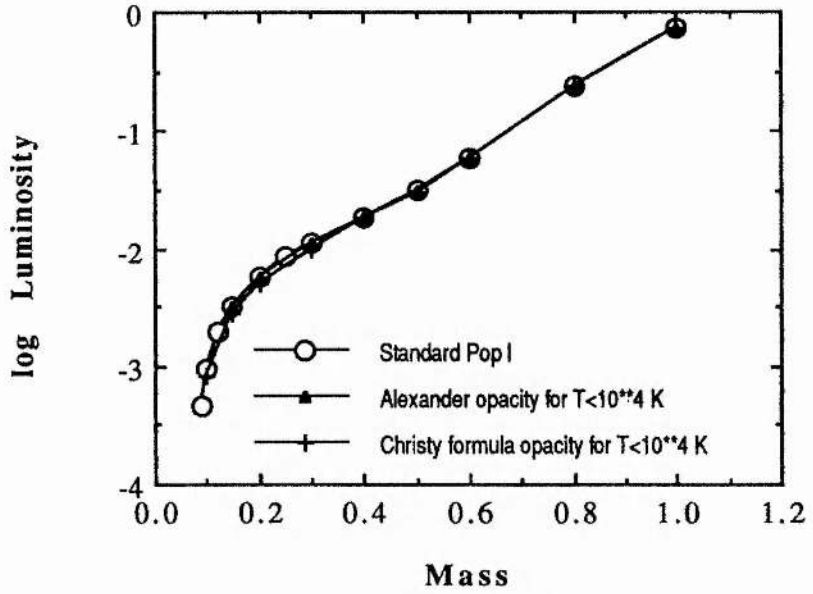

Figure 6.13 : Comparison of the mass-luminosity relations with the standard models with variations of the low temperature opacities (for $T<10^4$ K), mainly from molecular opacities.

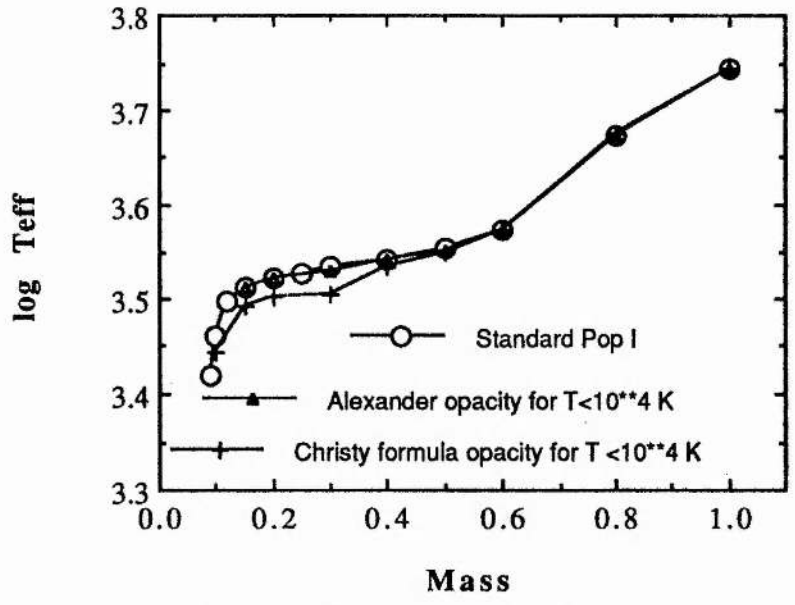

Figure 6.14 : Comparison of the mass-effective temperature relations for the same conditions as in Figure 6.13.

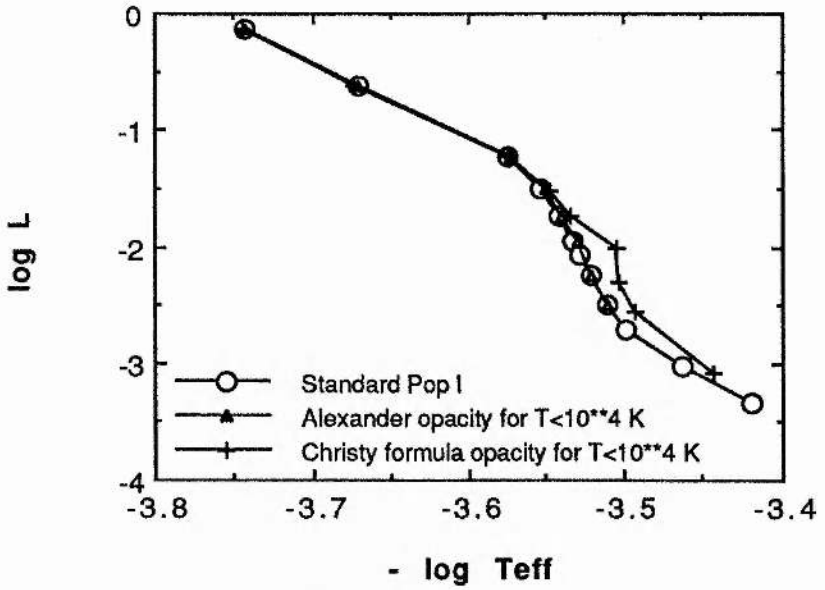

Figure 6.15 : Comparison of the H-R diagrams for the same conditions as in Figure 6.13.

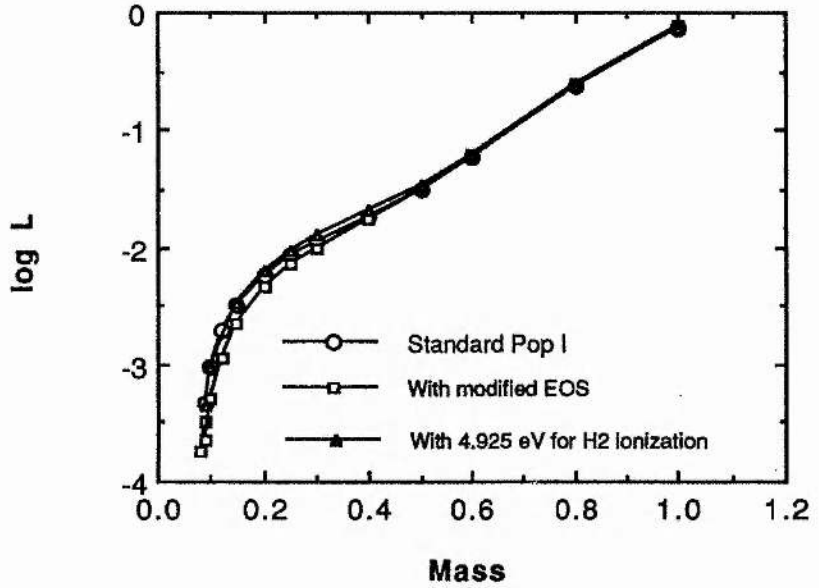

Figure 6.16 : Comparison of the mass-luminosity relations with the standard models with variations of the H_2 dissociation energy and the pressure ionization in the EOS.

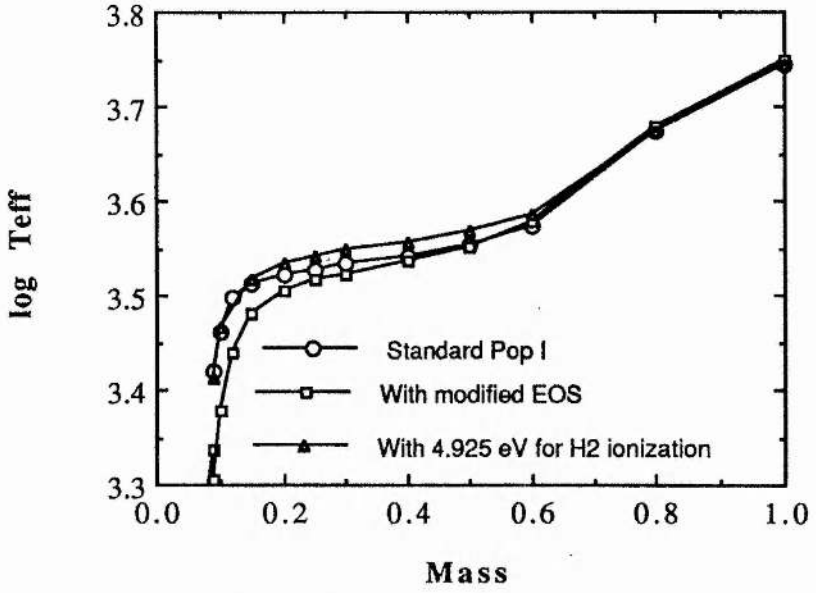

Figure 6.17 : Comparison of the mass-effective temperature relations for the same conditions as in Figure 6.16.

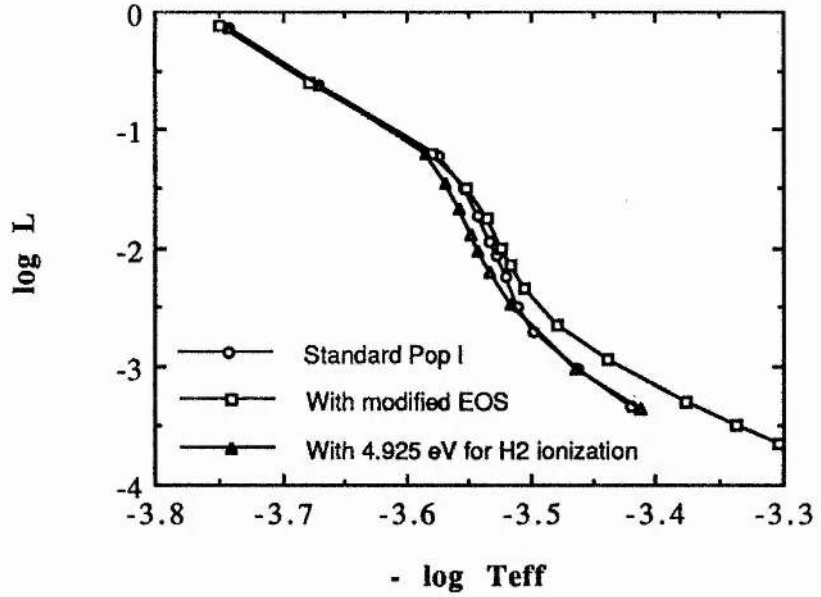

Figure 6.18 : Comparison of the H-R diagrams for the same conditions as in Figure 6.16.

shift of the zero age main sequence of the models with effective temperatures below 4000 K. These comparisons show that the increase of low temperature opacities reduces the effective temperatures of the LM star models.

Table 6.12 : The zero age models of the lower main sequence for the Standard Pop I but using Christy formula opacities for $T<10^4$ K

Mass	log L	log R	log T_e	log T_c	log ρ_c	log P_c
1.00	-0.143	-0.034	3.745	7.121	1.920	17.173
0.80	-0.627	-0.136	3.675	7.042	1.888	17.064
0.60	-1.226	-0.235	3.574	6.949	1.852	16.938
0.50	-1.513	-0.325	3.548	6.907	1.837	16.882
0.40	-1.746	-0.416	3.534	6.877	1.832	16.848
0.30	-2.007	-0.498	3.505	6.835	1.909	16.892
0.20	-2.305	-0.633	3.503	6.775	2.134	17.076
0.15	-2.555	-0.735	3.492	6.721	2.313	17.229
0.10	-3.075	-0.898	3.443	6.610	2.621	17.524

6.2.8 Dissociation of hydrogen molecules

The hydrogen molecule H_2 appears in the envelope of M dwarfs in which the temperature reaches as low as 4000 K. Consequently, its formation can affect the LM star models by its contribution to the equation of state as well as to the radiative opacity.

The dissociation of H_2 for temperatures below 4000 K is very dependent on the dissociation energy. In the formula presented by Vardya 1960 for the dissociation equilibrium constants for H_2, the dissociation energy was assumed to be 4.477 eV. In order to investigate the effect of H_2 dissociation on the main sequence models of LM stars, we artificially changed the H_2 dissociation energy to be 4.925 eV and performed the model calculation. We found this difference of 10 percent in dissociation energy leads to a marked change in the calculated results. We list the calculated results by using 4.925 eV as the dissociation energy for H_2 in Table 6.13. Comparisons with the Standard Pop I models in Figures 6.16-6.18 indicate no distinct difference in luminosities. But the effective temperatures are increased for the models with masses below 0.6 M_{sun}. The H-R diagram

shows that the zero age main sequence is shifted to hotter temperatures for the models with effective temperatures between $10^{3.58} \approx 3800$ K to $10^{3.52} \approx 3300$ K. This temperature range is just where the dissociation of H_2 occurs. So we conclude that a decrease of H_2 dissociation energy shifts effective temperatures to cooler values.

Table 6.13 : The zero age models of the lower main sequence for the Standard Pop I but using 4.925 eV for H_2 dissociation.

Mass	log L	log R	log T_e	log T_c	log ρ_c	log P_c
1.00	-0.143	-0.032	3.743	7.121	1.920	17.173
0.80	-0.629	-0.131	3.672	7.041	1.888	17.064
0.60	-1.207	-0.249	3.586	6.952	1.853	16.941
0.50	-1.463	-0.342	3.568	6.915	1.840	16.892
0.40	-1.680	-0.428	3.557	6.889	1.839	16.866
0.30	-1.895	-0.517	3.548	6.852	1.959	16.955
0.25	-2.033	-0.573	3.542	6.823	2.051	17.027
0.20	-2.213	-0.646	3.533	6.785	2.170	17.123
0.15	-2.478	-0.746	3.517	6.728	2.344	17.271
0.10	-3.015	-0.911	3.465	6.612	2.659	17.576
0.09	-3.347	-0.971	3.412	6.546	2.784	17.713

6.2.9 The modified EOS

Nonideal effects due to interatomic interactions have been for long an uncertainty in the equation of state involved in the study of the LM stars. The importance of the effects has been expected under conditions of LM stars because of the relatively high density and low temperature involved. Therefore, it is necessary to check how the nonideal effects in the EOS affect the LM star models.

In Section 2.5, the equation of state was modified by depressing pressure ionization due to interatomic interactions. How a lessening of pressure ionization affects the LM star models is investigated in this section. Based on the Standard Pop I model but using the modified EOS, the calculation of zero age models of the LM stars gives the results listed in Table 6.14. We found that the calculation can go down to a model of 0.08 M_{sun}, in contrast to

the limiting mass of 0.09 M_{sun} of the Standard Pop I models. The comparisons of stellar properties with the Standard Pop I model are given in Figures 6.16-6.18. We see that the luminosities are decreased a little for the models of mass below 0.4 M_{sun} while the effective temperatures are shifted significantly to cooler values. The H-R diagram shows the the zero age main sequence is shifted to cooler temperatures for the models with effective temperatures below $10^{3.55} \simeq 3500$ K. The comparisons indeed indicate the importance of pressure ionization in the calculation of LM star models.

Table 6.14 : The zero age models of the lower main sequence for the Standard Pop I but using the modified EOS.

Mass	log L	log R	log T_e	log T_c	log ρ_c	log P_c
1.00	-0.121	-0.033	3.749	7.124	1.920	17.178
0.80	-0.602	-0.132	3.679	7.045	1.888	17.069
0.60	-1.201	-0.231	3.579	6.952	1.851	16.942
0.50	-1.499	-0.327	3.552	6.908	1.835	16.884
0.40	-1.760	-0.426	3.536	6.873	1.826	16.841
0.30	-2.003	-0.522	3.523	6.838	1.906	16.892
0.25	-2.154	-0.583	3.516	6.808	2.001	16.965
0.20	-2.351	-0.659	3.505	6.768	2.123	17.059
0.15	-2.644	-0.755	3.480	6.712	2.286	17.184
0.12	-2.950	-0.824	3.438	6.659	2.397	17.262
0.10	-3.292	-0.874	3.377	6.607	2.468	17.297
0.09	-3.499	-0.897	3.337	6.583	2.474	17.282
0.085	-3.657	-0.909	3.304	6.561	2.482	17.276
0.08	-3.752	-0.931	3.291	6.544	2.515	17.305

The use of the modified EOS has another effect in that the problem of oscillating solutions of the successive models of the mass near or below 0.1 M_{sun} is removed. Table 6.15 lists the solutions of the successive models of the mass 0.1 M_{sun}, which shows that the successive models converge to one solution. So we conclude that the determination of the EOS is responsible for the oscillating solutions of very low mass models. Furthermore, the factor mainly responsible seems to be the behaviour of pressure ionization.

Table 6.15 : The successive models of a zero age star (with mass 0.1 M_{sun}) of the Standard Pop I but using the modified EOS.

Succession	log L	log R	log T_e	log T_c	log ρ_c	log P_c
1	-3.3011	-0.8730	3.3745	6.6067	2.4638	17.2921
2	-3.3064	-0.8728	3.3730	6.6057	2.4634	17.2909
3	-3.2954	-0.8739	3.3763	6.6068	2.4675	17.2962
4	-3.2916	-0.8742	3.3775	6.6072	2.4688	17.2979
5	-3.2918	-0.8742	3.3774	6.6072	2.4686	17.2977
6	-3.2923	-0.8741	3.3772	6.6071	2.4684	17.2975
7	-3.2924	-0.8741	3.3772	6.6071	2.4684	17.2975

6.3 Comparison with other theoretical studies

6.3.1 Uncertainty due to nonideal effects in EOS

It has been realized that the molecular contribution to radiative opacity plays an important role in the envelopes of the LM stars with effective temperatures below 4000 K. This has also been examined in our study in Section 6.2.6 and 6.2.7. In this section, we mainly survey the nonideal effects in the EOS on the models of the LM stars.

In Section 6.2.8, the dissociation of molecular hydrogen was found to be one of the sensitive factors in the LM star models. An increase of dissociation energy of 0.45 eV for H_2 causes a distinct change of the calculated results. But this effect is appreciable only for the surface temperatures between 3800 K and 3300 K, which corresponds to the dissociation of hydrogen molecules. For lower temperatures, the nonideal effects in the EOS become a substantially sensitive factor in the LM star models. This has been examined in Section 6.2.9 by the calculation using a modified EOS. The depression of the pressure ionization is found to shift theoretical effective temperatures to cooler values. These investigations indicate the importance of nonideal effects in the EOS in the study of the LM stars.

In a recent study by Dorman et al. (1990), two determinations of the EOS (i.e. that of

Fontaine et al. (1977) and that of Magni and Mazzitelli (1979)) are used to calculate the zero age model of the LM stars. The comparison of their theoretical results with the observed data shows a considerable difference between using the two determinations of the EOS.

6.3.2 Comparison

In order to see how the nonideal effects in the EOS affect the LM star models, we compare the theoretical results from different sources with the observed data. Because there are great errors in the observed data for stellar masses, the H-R diagram is more effective for comparisons. The theoretical results are from the calculations using the four determinations of the EOS. Two of them are those presented by Dorman et al.(1990) who used the EOS given by Fontaine, Graboske and Van Horn (FGVH) and that by Magni and Mazzitelli (MM). The other two are from our calculations by using the Standard Pop I model and the modified EOS. The results are plotted in a H-R diagram in Figure 6.19 in a range of effective temperature $3.4 \leq \log T_{eff} \leq 3.6$, together with the observed data of binary systems which have been listed in Table 6.5.

In the detailed comparison in Figure 6.19, we see that the theoretical calculation results using different determinations of the EOS differ for the models with $T_{eff} < 10^{3.54} = 3600$ K. The differences between the theoretical results are comparable to that of the observed data, and shows that the use of the modified EOS gives better results.

Although we only use limited data from observation, there are other data sources, such as those given by Reid and Gilmore (1984), which indicate shifts to cooler temperatures for M dwarfs compared with theoretical results. So further attention to the nonideal effects in the EOS is worthwhile in future studies of the LM stars.

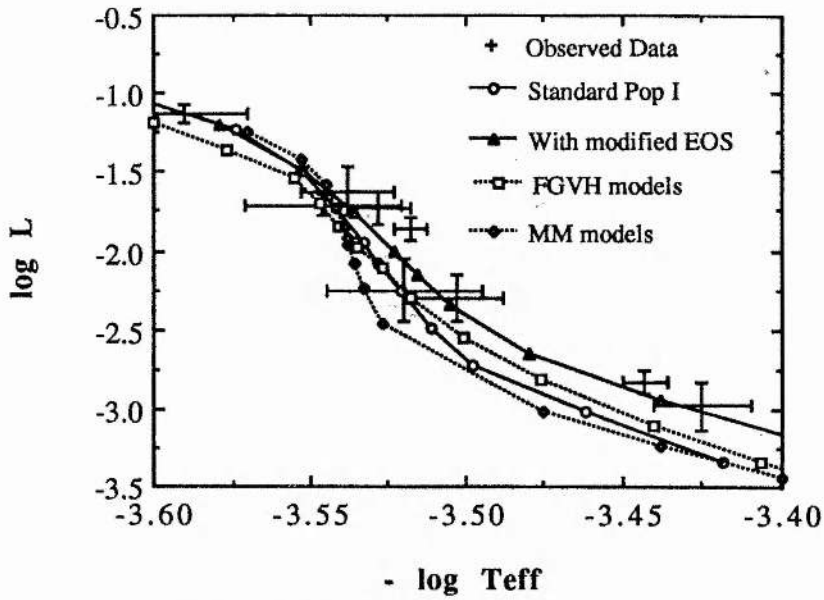

Figure 6.19: Comparison of the theoretical results in the H-R diagram from the calculations of the zero age main sequence of the LM star models using four determinations of the EOS.

Chapter VII Evolutionary Sequences for Low Mass Stars

Introduction

In this chapter we present the calculations of evolutionary models of the LM stars. The solar model is examined for different model parameters, as a check on our calculations. In spite of the very slow evolution of the LM stars, we calculate their evolutionary sequences and investigate the oscillating solutions.

7.1 Evolutionary models of the sun

A calculation of a solar model can check the validity of the mathematical model of stellar structure and evolution as well as the input physics incorporated. In the calculation of zero age models in Chapter VI, some uncertainties are found to affect the solar model substantially. They are the element abundances, and the mixing length ratio and the surface boundary condition, which will be examined in the calculation of a solar evolutionary sequence.

7.1.1 Computation

We need to state some points about the computation of evolutionary models. The first point concerns the zero age model from which an evolutionary sequence starts. As mentioned in Chapter VI, a stable solution for a zero age model is obtained after a series of successive calculations for a model of given mass. We found that a successful calculation must start from a stable zero age model, otherwise the convergence of the calculation of stellar evolutionary models cannot be achieved. So all of the zero age models used for the starting of evolution calculations are from the stable time-independent solutions.

The other point concerns the time steps in the evolution calculation. The computing code determines them automatically except the first time step which is one of the input parameters. We found that the time steps cannot be smaller than $5*10^8$ years for a model

with mass of 0.1 M_{sun} otherwise the time steps determined automatically will become smaller and smaller, and thus evolution calculation fails to carry on. For a solar model, however, the time step can be as low as $5*10^6$ years which still allows a successful calculation.

In addition, the calculated results are obtained for irregular time steps for the evolution sequence because of the automatic determination of time steps. In order to have a clear presentation of the evolutionary properties, a cubic interpolation is used to place them on regular time steps. Since the age of our universe is of the order of 10^{10} years, we perform all evolution calculations up to an age of 10^{10} years and present the results at a regular time step of 10^9 years from the zero age.

7.1.2 Standard model of the sun

As in Chapter VI, we define a standard solar model so that the uncertainties can be examined by a comparison with it. The standard solar model employed here is defined from the input physics and model parameters for the Standard Pop I (in Section 6.1.2) except that the the surface boundary condition is formulated from the atmospheric model rather than the photospheric model. This is because the atmospheric surface condition is more exact in the calculation of a solar model. A composition of X/Y/Z=0.70/0.28/0.02 is adopted for the standard solar model.

Table 7.1 lists the evolutionary properties of the standard solar model. It includes the luminosity, the radius, the effective temperature, the central temperature and density, and the central hydrogen abundances in the evolution. It shows a good agreement to the present state of the sun at an age between $4.0*10^9$ and $5*10^9$ years. The hydrogen abundance at the centre decreases from 0.7 at the zero age to about 0.4 at the present age. The central hydrogen is completely depleted before an age of $9*10^9$ years.

Table 7.1 : The evolutionary sequence for the standard solar model. The age is in 10^9 years, the luminosity L and the radius R in solar units, the effective temperature T_{eff} and the central temperature T_c in K, the central density ρ in g/cm^3, and the mass fraction of hydrogen at the solar centre X_c.

Age	L/L_{sun}	R/R_{sun}	log T_e	log T_c	log ρ_c	X_c
0.0	0.719	0.920	3.745	7.121	1.920	0.700
1.0	0.764	0.924	3.751	7.131	1.959	0.642
2.0	0.821	0.943	3.754	7.143	2.008	0.574
3.0	0.888	0.965	3.758	7.157	2.061	0.504
4.0	0.955	0.987	3.761	7.171	2.112	0.442
5.0	1.033	1.011	3.764	7.187	2.167	0.376
6.0	1.135	1.045	3.767	7.211	2.235	0.295
7.0	1.238	1.087	3.768	7.241	2.310	0.227
8.0	1.330	1.137	3.766	7.270	2.366	0.155
9.0	1.577	1.218	3.770	7.256	2.671	0.000
10.0	1.830	1.332	3.767	7.263	2.818	0.000

7.1.3 Solar mass model with X/Y/Z=0.770/0.212/0.018

The element abundances are found to be one of the important uncertainties in the study of the zero age main sequence of the LM stars. For the solar model, the mass fractions of hydrogen and helium are not well determined although the mass abundance of the heavy elements is commonly regarded to be about 2 percent. It can be seen from a great number of studies of stellar models that the solar composition has a range of hydrogen mass abundance from 68 percent to 78 percent. So it is worthwhile to investigate how much the uncertainty in composition can affect on the solar evolutionary model.

In our standard model, the solar composition is defined by the mass fractions X/Y/Z=0.70/0.28/0.02. However, a detailed study of the solar composition by Cameron (1971) found a solar composition of X/Y/Z=0.770/0.212/0.018. Using this composition,

we perform a calculation of evolution model of 1 M_{sun}, and present the results in Table 7.2.

In Figure 7.1, we see that the luminosity is 0.23 L_{sun} less than that of the standard model at the zero age, and about 0.43 L_{sun} less at $5*10^9$ years. The difference of luminosity between using the two compositions increases with age. The comparison of effective temperature with the standard solar model is shown in Figure 7.2. It shows that a difference of about 500 K persists from the zero age until the age of 10^{10} years.

Table 7.2 : The evolutionary models of 1 M_{sun} with a composition of X/Y/Z= 0.770/ 0.212/ 0.018.

Age	L/L_{sun}	R/R_{sun}	log T_e	log T_c	log ρ_c	X_c
0.0	0.487	0.884	3.711	7.077	1.861	0.770
1.0	0.506	0.888	3.714	7.084	1.886	0.729
2.0	0.525	0.898	3.716	7.090	1.912	0.689
3.0	0.552	0.911	3.719	7.099	1.947	0.637
4.0	0.578	0.922	3.721	7.107	1.978	0.594
5.0	0.599	0.931	3.723	7.113	2.005	0.559
6.0	0.640	0.948	3.726	7.125	2.050	0.500
7.0	0.669	0.959	3.728	7.133	2.081	0.465
8.0	0.705	0.974	3.731	7.142	2.119	0.421
9.0	0.762	0.998	3.734	7.158	2.174	0.366
10.0	0.800	1.014	3.736	7.168	2.209	0.332

7.1.4 Solar mass model with a unit of mixing length ratio

In the standard solar model, the ratio of mixing length to pressure scale height is defined to be α=1.5. In this section , we present the calculated results of the solar evolutionary sequence by using a ratio of unity, i.e. α=1.0, so that the uncertainty due to the mixing length ratio can be examined.

The evolutionary properties for α=1.0 are listed in Table 7.3, and are compared with the standard solar model in Figures 7.1-7.4. Figure 7.1 shows there is not any significant

difference in luminosity throughout all of the evolutionary phases covered. However, a difference of about 200 K in effective temperature remains during the whole evolution, which is indicated by Figure 7.2.

Table 7.3 : The evolutionary models of 1 M_{sun} with a mixing length ratio of unity.

Age	L/L_{sun}	R/R_{sun}	log T_e	log T_c	log ρ_c	X_c
0.0	0.718	1.002	3.727	7.120	1.920	0.700
1.0	0.762	0.992	3.735	7.131	1.959	0.642
2.0	0.817	1.011	3.739	7.143	2.006	0.577
3.0	0.885	1.034	3.743	7.157	2.060	0.506
4.0	0.959	1.058	3.746	7.172	2.115	0.437
5.0	1.032	1.082	3.749	7.187	2.167	0.376
6.0	1.128	1.116	3.752	7.209	2.232	0.300
7.0	1.231	1.162	3.753	7.238	2.297	0.227
8.0	1.332	1.224	3.750	7.272	2.373	0.138
9.0	1.558	1.311	3.752	7.261	2.638	0.000
10.0	1.822	1.434	3.750	7.267	2.798	0.000

7.1.5 Solar mass model with the photospheric model as surface condition

The surface boundary condition based on the atmosphere model is used in the standard solar model. In this section, we use the simple boundary condition formulated from the photosphere model to calculate the solar evolution sequence. The properties of the solar evolution models from the calculation are listed in Table 7.4. No appreciable difference in luminosity can be seen in the comparison with the standard model in Figure 7.2, while the effective temperature has a small difference of about 50 K over the whole evolution covered (see Figure 7.2).

Table 7.4 : The evolutionary models of 1 M_{sun} with the photospheric model as surface condition.

Age	L/L_{sun}	R/R_{sun}	log T_e	log T_c	log ρ_c	X_c
0.0	0.719	0.945	3.740	7.121	1.920	0.700
1.0	0.764	0.946	3.746	7.131	1.960	0.640
2.0	0.823	0.966	3.750	7.144	2.010	0.571
3.0	0.886	0.988	3.753	7.157	2.060	0.504
4.0	0.949	1.009	3.756	7.170	2.108	0.446
5.0	1.034	1.037	3.759	7.187	2.168	0.375
6.0	1.139	1.074	3.762	7.212	2.237	0.288
7.0	1.237	1.115	3.763	7.240	2.311	0.234
8.0	1.330	1.169	3.760	7.271	2.369	0.149
9.0	1.579	1.257	3.763	7.265	2.659	0.001
10.0	1.835	1.373	3.760	7.266	2.811	0.000

7.1.6 Discussions

A detailed comparison of the four models for solar evolution is presented in an H-R diagram in Figure 7.4. The difference of evolutionary tracks among the four models is obviously comparable to the solar evolution over 10^{10} years. In the comparisons with the standard solar model, the model with an alternative composition X/Y/Z = 0.770/0.212/0.018, rather than X/Y/Z = 0.70/0.28/0.02 in the standard model, has the biggest difference in both the luminosity and the effective temperature. The second biggest difference is made by the model with a mixing length ratio α=1.0, instead of α=1.5 as in the standard solar model, but only in the effective temperature. The model with a simple surface boundary condition has only a small difference in the effective temperature, relative to the standard model. So we conclude that the greatest uncertainty is due to the element abundances, while the mixing length ratio and the surface boundary condition lead to much smaller uncertainties in the solar evolutionary model.

In the H-R diagram in Figure 7.4, the state of the sun at its present age is also marked by the present solar luminosity L_{sun} and effective temperature of 5800 K. The standard solar

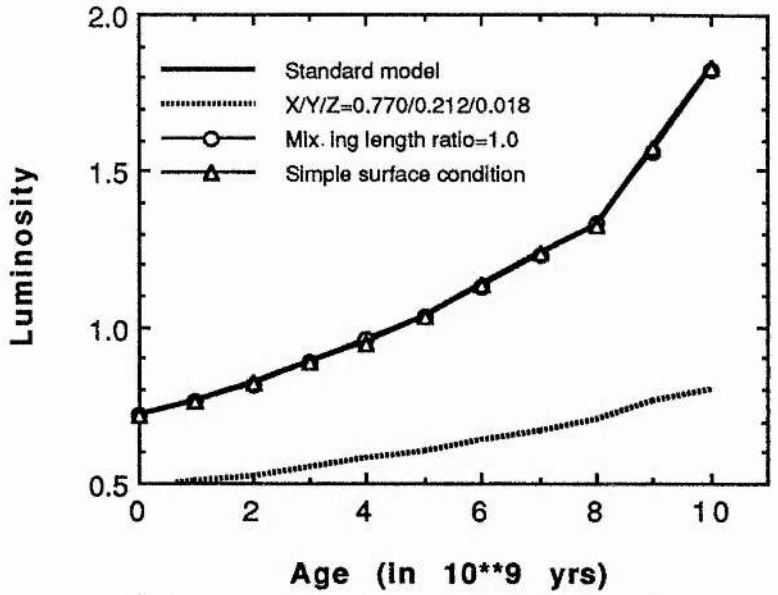

Figure 7.1 : Comparison between the standard solar evolutionary models and the models with variation of the mixing length ratio, the surface boundary condition and the element abundances, for the luminosities (in L_{sun}).

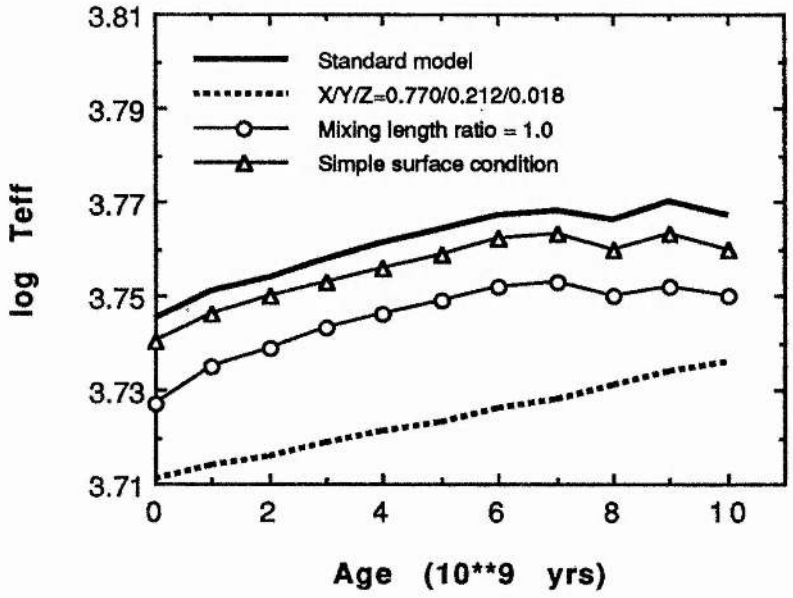

Figure 7.2 : The same as in Figure 7.1, but for the effective temperatures T_{eff} (in K).

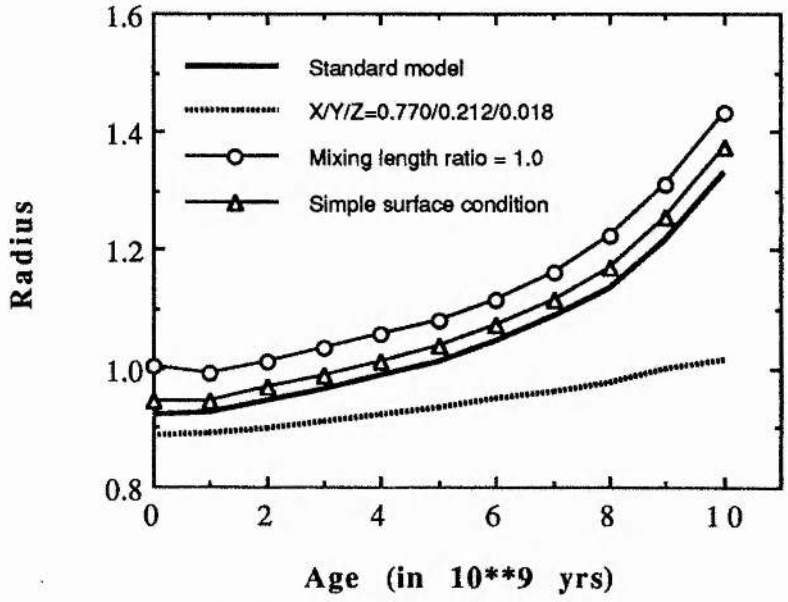

Figure 7.3: The same as in Figure 7.1, but for the radii (in R_{sun}).

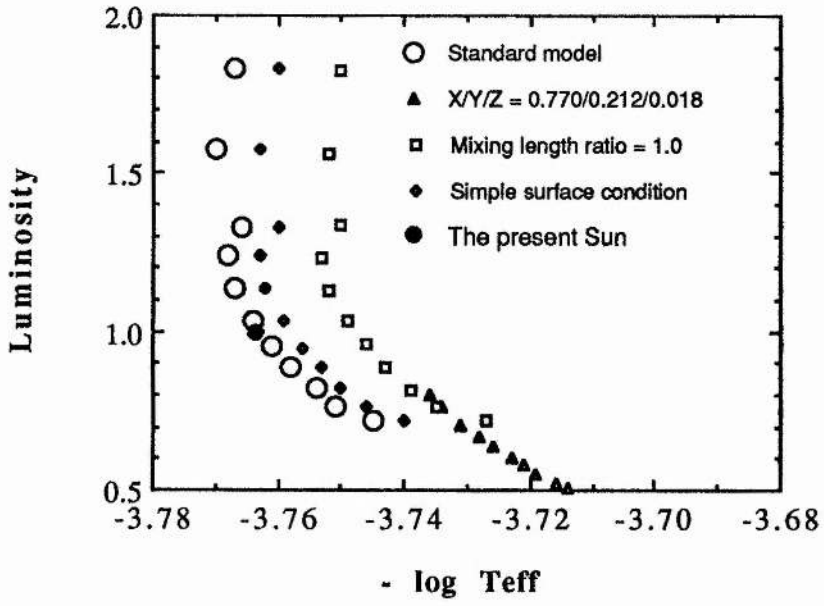

Figure 7.4 : The same as in Figure 7.1, but in the H-R diagram and with a comparison of the present state of the sun.

model has good agreement. This agreement was achieved by our tests of various values of the element abundances and the mixing length ratio before they were used to define the standard solar model.

7.2 Evolution of the LM stars

7.2.1 Evolutionary sequences of the LM stars

In spite of the fact that the LM stars have a very slow evolution over the age of the universe, it is interesting to see how slow their evolution is. The solar evolution has been investigated in the preceding section while in this section we examine the evolution sequences of the models with the masses of 0.8, 0.6, 0.4, 0.2 and 0.1 M_{sun}.

The calculation is performed using the input physics and model parameters for the Standard Pop I (see Section 6.1.2). The photospheric model defines surface condition in order to succeed in the calculation of all low mass models. Like the calculation of the solar evolution model, a period of 10^{10} years is covered and the calculated results are interpolated to give the the evolutionary properties on regular time steps.

The evolutionary properties of the models with the masses 0.8, 0.6, 0.4, 0.2 and 0.1 M_{sun} are listed respectively in Table 7.5, 7.6, 7.7, 7.8 and 7.9. How slowly they evolve is seen by the decreased amount of hydrogen abundance at their centre. After a time of 10^{10} years, the hydrogen abundance is reduced by 0.261, 0.091, 0.039, 0.003 and 0.001 respectively for the models of 0.8, 0.6, 0.4, 0.2 and 0.1 M_{sun}, in contrast to a complete depletion of hydrogen at the solar centre. The evolution of the luminosities and the effective temperatures of the five models are plotted in Figures 7.5 and 7.6. The H-R diagram of their evolution is given in Figure 7.7. We see that the LM star models do not have any obvious change in either the luminosity or the effective temperature, except for the solar model with a distinct evolution in 10^{10} years, and the model of 0.1 M_{sun}.

Table 7.5 : The evolution models for the star with a mass 0.8 M_{sun} of the Standard Population I. The Age is in 10^9 years, the luminosity L and the radius R in solar units, the effective temperature T_{eff} and the central temperature T_c in K, the central density ρ_c in g/cm^3, and the mass fraction of hydrogen at the stellar centre X_c.

Age	log L	log R	log T_e	log T_c	log ρ_c	X_c
0.0	-0.628	-0.132	3.672	7.041	1.888	0.700
1.0	-0.618	-0.128	3.673	7.046	1.905	0.674
2.0	-0.609	-0.125	3.674	7.049	1.920	0.652
3.0	-0.594	-0.121	3.675	7.055	1.945	0.616
4.0	-0.586	-0.119	3.676	7.058	1.957	0.599
5.0	-0.570	-0.115	3.678	7.065	1.984	0.563
6.0	-0.562	-0.113	3.679	7.068	1.997	0.546
7.0	-0.543	-0.109	3.682	7.075	2.026	0.509
8.0	-0.535	-0.107	3.683	7.078	2.040	0.493
9.0	-0.515	-0.102	3.686	7.086	2.072	0.456
10.0	-0.506	-0.100	3.687	7.090	2.087	0.439

Table 7.6 : The evolutionary models of the star with a mass 0.6 M_{sun}, otherwise as in Table 7.5.

Age	log L	log R	log T_e	log T_c	log ρ_c	X_c
0.0	-1.223	-0.237	3.576	6.950	1.852	0.700
1.0	-1.222	-0.235	3.575	6.951	1.857	0.691
2.0	-1.219	-0.234	3.575	6.952	1.863	0.682
3.0	-1.216	-0.233	3.576	6.953	1.869	0.672
4.0	-1.213	-0.232	3.576	6.954	1.875	0.663
5.0	-1.210	-0.231	3.576	6.956	1.881	0.654
6.0	-1.207	-0.230	3.577	6.957	1.886	0.646
7.0	-1.203	-0.229	3.577	6.958	1.893	0.636
8.0	-1.200	-0.228	3.577	6.960	1.900	0.626
9.0	-1.196	-0.227	3.578	6.961	1.905	0.617
10.0	-1.193	-0.226	3.578	6.962	1.911	0.609

Table 7.7 : The evolutionary models of the star with a mass 0.4 M_{sun}, otherwise as in Table 7.5.

Age	log L	log R	log T_e	log T_c	log ρ_c	X_c
0.0	-1.688	-0.427	3.555	6.887	1.838	0.700
1.0	-1.708	-0.424	3.548	6.884	1.838	0.696
2.0	-1.717	-0.422	3.545	6.883	1.839	0.692
3.0	-1.722	-0.421	3.543	6.882	1.841	0.688
4.0	-1.723	-0.421	3.543	6.882	1.843	0.684
5.0	-1.724	-0.420	3.542	6.882	1.845	0.680
6.0	-1.724	-0.420	3.542	6.883	1.847	0.676
7.0	-1.723	-0.420	3.542	6.883	1.849	0.672
8.0	-1.723	-0.420	3.542	6.883	1.853	0.667
9.0	-1.723	-0.419	3.542	6.884	1.854	0.665
10.0	-1.722	-0.419	3.542	6.884	1.856	0.661

Table 7.8 : The evolutionary models of the star with a mass 0.2 M_{sun}, otherwise as in Table 7.5.

Age	log L	log R	log T_e	log T_c	log ρ_c	X_c
0.0	-2.286	-0.637	3.510	6.777	2.142	0.700
1.0	-2.287	-0.636	3.510	6.777	2.142	0.700
2.0	-2.288	-0.636	3.509	6.777	2.141	0.699
3.0	-2.290	-0.636	3.509	6.777	2.141	0.699
4.0	-2.291	-0.636	3.508	6.777	2.140	0.699
5.0	-2.292	-0.635	3.508	6.777	2.139	0.699
6.0	-2.294	-0.635	3.507	6.777	2.139	0.698
7.0	-2.295	-0.635	3.507	6.777	2.138	0.698
8.0	-2.297	-0.635	3.506	6.776	2.137	0.698
9.0	-2.298	-0.634	3.506	6.776	2.137	0.698
10.0	-2.300	-0.634	3.505	6.776	2.136	0.697

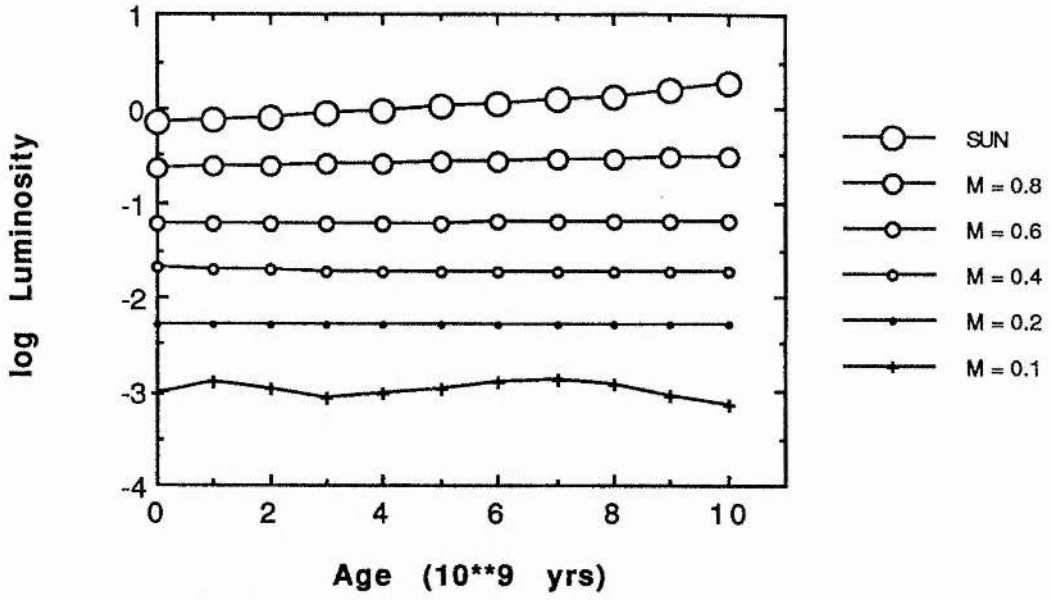

Figure 7.5 : The luminosities (in L_{sun}) of the evolutionary models of the LM stars of the Standard Population I. The mass M is in solar units.

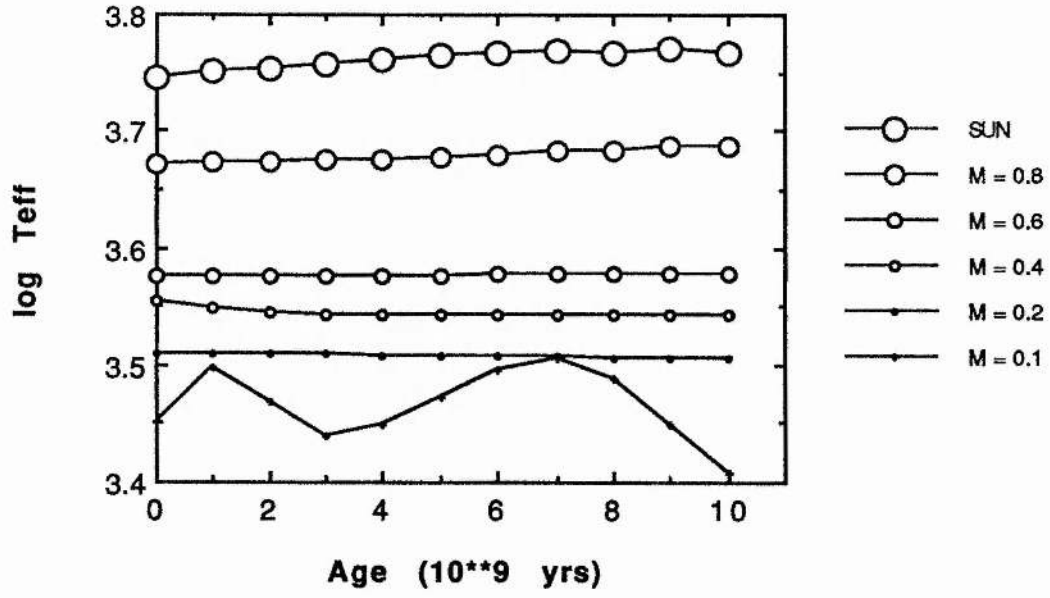

Figure 7.6 : The effective temperatures (Teff in K) of the evolutionary models of the LM stars of the Standard Population I.

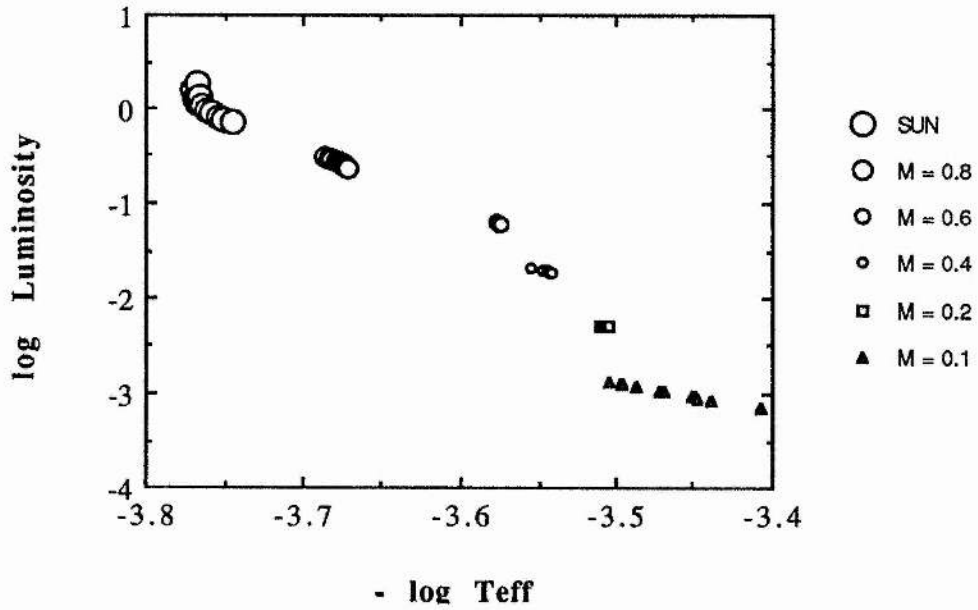

Figure 7.7 : The H-R diagrams of the evolutionary models of the LM stars of the Standard Population I.

Table 7.9 : The evolutionary models of the star with a mass 0.1 M_{sun}, otherwise as in Table 7.5.

Age	log L	log R	log T_e	log T_c	log ρ_c	X_c
0.0	-3.034	-0.892	3.451	6.619	2.602	0.700
1.0	-2.914	-0.925	3.497	6.627	2.699	0.700
2.0	-2.987	-0.903	3.468	6.622	2.635	0.700
3.0	-3.061	-0.882	3.439	6.616	2.571	0.700
4.0	-3.033	-0.889	3.449	6.618	2.591	0.700
5.0	-2.972	-0.904	3.472	6.622	2.637	0.700
6.0	-2.912	-0.919	3.495	6.626	2.682	0.699
7.0	-2.884	-0.925	3.505	6.628	2.703	0.699
8.0	-2.934	-0.915	3.487	6.624	2.671	0.699
9.0	-3.044	-0.891	3.448	6.617	2.600	0.699
10.0	-3.154	-0.868	3.408	6.610	2.530	0.699

7.2.2 Oscillating solutions of evolution of very low mass models

Figures 7.5-7.7 reveal a problem of oscillating solutions for the evolution sequence of the model of 0.1 M_{sun}. This problem has been discovered in Chapter VI in the calculation of the zero age models with the mass near or below 0.1 M_{sun}. We have found that the equation of state is responsible. The problem was removed when a modified EOS is employed instead of the standard EOS.

We performed the evolutionary calculation of the model of 0.1 M_{sun} by using the modified EOS. We indeed found that the use of the modified EOS also removed the problem of the oscillating solutions in the evolutionary sequence. This is shown in Tables 7.10 and 7.11 which list the evolutionary properties of the 0.1 M_{sun} model using, respectively, the standard EOS and the modified EOS.

Table 7.10 : The evolution sequence of 0.1 M_{sun} model with the standard EOS.

Age	L/L_{sun}	R/R_{sun}	$\log T_e$	$\log T_c$	$\log \rho_c$	X_c
0.0	-3.0344	-0.8922	3.4508	6.6194	2.6024	0.7000
1.0	-2.9142	-0.9246	3.4970	6.6269	2.6989	0.6999
3.0	-3.0606	-0.8818	3.4390	6.6162	2.5705	0.6997
7.0	-2.8841	-0.9254	3.5050	6.6277	2.7029	0.6994
11.0	-3.2045	-0.8570	3.3906	6.6071	2.4976	0.6989

Table 7.11 : The evolution sequence of 0.1 M_{sun} model with the modified EOS.

Age	L/L_{sun}	R/R_{sun}	$\log T_e$	$\log T_c$	$\log \rho_c$	X_c
0.0	-3.2921	-0.8741	3.3773	6.6072	2.4685	0.7000
1.0	-3.2923	-0.8741	3.3772	6.6072	2.4686	0.6999
3.0	-3.2921	-0.8741	3.3773	6.6073	2.4688	0.6999
7.0	-3.2917	-0.8740	3.3774	6.6075	2.4692	0.6997
15.0	-3.2909	-0.8740	3.3775	6.6079	2.4701	0.6993

7.2.3 Discussions

The calculated results of the evolutionary models show that the lower main sequence evolves very slowly. The H-R diagram in Figure 7.7 indicates that the evolution of the models with mass below 0.6 M_{sun} cannot be compared with observation since the changes of their properties within 10^{10} years are too small. Nevertheless, Tables 7.5-7.9 indeed indicate their evolution. The variation of the stellar radii shows that all models have their radius increased although the change within 10^{10} years is only $\Delta\log R=0.032$ for the mass 0.8 M_{sun} to $\Delta\log R=0.003$ for the mass 0.2 M_{sun}. The surface luminosities are increased by an amount $\Delta\log L=0.112$ for the mass 0.8 M_{sun} and $\Delta\log L=0.03$ for the mass 0.6 M_{sun}, and decreased by $\Delta\log L=-0.034$ for the mass 0.4 M_{sun} and $\Delta\log L=-0.014$ for the mass 0.2 M_{sun}.

The increment of the surface luminosities is explained by the increment of the central temperatures which is the result of the hydrogen burning. In contrast, the decrease of the

surface luminosities of the models with 0.4 and 0.2 M_{sun} could be due to the state of strong convection of the stellar interiors.

The evolutionary models of the mass 0.1 M_{sun} show solutions oscillating when the standard EOS is employed. The range of the oscillating solutions is logL=(-3.2) to (-2.9) for the surface luminosity and $\log T_{eff}$=3.39 to 3.51 for the effective temperature. The H-R diagram in Figure 7.7 indicates that the oscillation of calculated results cannot be ignored in the comparison with the observation.

Oscillating solutions have also been found in the calculation of the zero age model of 0.1 M_{sun}. The calculations for both the zero age model and the evolutionary models of 0.1 M_{sun} show that the oscillations did not occur when the modified EOS was used instead of the standard EOS. This implies that the nonideal effects in the EOS may be responsible.

Chapter VIII Conclusion

The aim of this thesis is to investigate the effects of the input physics and model parameters on the theoretical models of LM stars. So we would like to conclude our study by summarizing the function of each element one by one.

8.1 Element abundances

The element abundances affect the properties of the stellar models remarkably. The zero age main sequence models of LM stars for three compositions have been calculated and compared in Sections 6.1.2 and 6.2.3. The three compositions have element mass abundances, respectively, of 0.70/0.28/0.02, 0.71/0.289/0.001 and 0.78/0.212/0.018. From our study we conclude the following points.

1> The richer abundances of heavy elements shifts the whole main sequence to cooler effective temperatures in the H-R diagram.

2> The richer abundances of heavy elements decrease the luminosity of the same mass model of relatively massive stars. Their effect on the luminosity weakens for the stars of lower mass.

3> The richer abundance of hydrogen does not significantly shift the position of the main sequence in the H-R diagram. However, it decreases the luminosity and effective temperature of the same mass model of the relatively massive stars (e.g. for $M>0.5M_{sun}$).

We calculated an evolutionary sequence for a star of one solar mass for the two compositions: 0.70/0.28/0.02 and 0.77/0.212/0.018 in Section 7.1.2. and 7.1.3. The calculated results show a considerable difference for using the two compositions. Throughout the whole evolution up to 10^{10} years, the model with the composition 0.77/0.212/0.018 is 500 K cooler than that with 0.70/0.28/0.02, and the luminosity is less by 0.23 L_{sun} to 1.2 L_{sun} less.

8.2 Mixing length ratio

The mixing length ratio was taken as 1.5 for the Standard Pop I and Pop II models of zero age main sequence in Section 6.1.2. In Section 6.2.1, the Standard Pop I models were recalculated but with a mixing length ratio of 0.5. The comparison of the calculated results between using 1.5 and 0.5 as the mixing length ratio shows the following.

1> The reduction of the mixing length ratio does not affect the luminosity of zero age models of lower main sequence.

2> The reduction of the mixing length ratio decreases the effective temperatures of zero age models. This effect weakens as the model mass decreases. The reduction of the mixing length ratio from 1.5 to 0.5 lowers the effective temperature by $\Delta \log T_{eff} = 0.05$ for the solar mass. The effect vanishes for the models with masses near 0.1 M_{sun}.

The solar evolutionary model was calculated using two mixing length ratios, 1.5 and 1.0, with the same input physics and other parameters, in Sections 7.1.2 and 7.1.4 . The comparison shows the same results as above. The luminosity is not affected while a difference of $\Delta \log T_{eff} = 0.02$ in the effective temperature persists during the whole evolution.

8.3 Surface boundary conditions

Two physical models were used as surface conditions in our calculation of lower main sequence models. The photospheric model was employed in the calculation of zero age models of the Standard Pop I and Pop II in Section 6.1.2. It allowed us to calculate the zero age models of LM stars down to the hydrogen burning limiting mass. In Section 6.2.2 we obtained the results calculated for the Standard Pop I models with masses above 0.8 M_{sun} (but using the atmospheric model to obtain the surface condition). Below this mass the calculation failed to achieve convergence.

The reason for the failure could possibly be the sensitive integration in the atmospheric model for lower mass star models. The problem is expected to be removed when the treatment of the surface integration in the atmospheric model is improved. We compared the

calculated results between the two models as surface condition in Section 6.2.2. For the zero age models of masses 1 M_{sun} and 0.8 M_{sun}, the difference is less than $\Delta \log L = 0.002$ in luminosities and less than $\Delta \log T_{eff} = 0.006$ in effective temperatures. In Section 7.1.2 and 7.1.5 the calculated results of the solar evolutionary model only indicates a difference of $\Delta \log T_{eff} = 0.006$ in effective temperatures between the two models.

From our investigation, we conclude that the theoretical models of LM stars are insensitive to the model used for surface condition. Whether the photospheric model or the atmospheric model is used does not make any significant difference in the theoretical models.

8.4 Electron screening effect on nuclear reactions

In the calculation of the Standard Pop I and Pop II models, the electron screening effects have been included by the enhancement factor. In Section 6.2.4 the zero age models were recalculated by excluding the electron screening effects from the Standard Pop I models. The comparison between including and excluding the electron screening effects shows that the difference is less than one percent both in luminosities and effective temperatures. However we found that the calculation excluding the electron screening effects could only be performed for models with mass down to 0.12 M_{sun}. Below this limit the computing convergence is difficult to achieve.

Let us look at the zero age models of 0.12 M_{sun} and 0.09 M_{sun} whose central conditions are given in Table 6.3. Their enhancement factors at the centre are thus found in Figure 4.1 to be $10^{0.1}$ for the 0.12 M_{sun} model and $10^{0.3}$ for the 0.09 M_{sun} model. This implies that the electron screening effects may play a role in the limiting models of the lower main sequence.

We may conclude that the electron screening effects do not affect the LM stars models considerably until mass below 0.12 M_{sun}, but they could affect the determination of the limiting model of LM stars.

8.5 Conductive opacities

The conductive opacities have been included in the calculation of the Standard Pop I and Pop II models. By excluding them from the Standard Pop I, the zero age models were recalculated in Section 6.2.5. The comparison shows that there is little difference in the zero age models between including and excluding the conductive opacities.

In the central conditions of the models with masses below 0.15 M_{sun}, the conductive opacity is smaller than the radiative opacity. This is found from Table 6.3 and Figure 4.3. However the calculated models of LM stars are not affected . So we may conclude that the strong convection in the LM stars makes the state of stellar interiors insensitive to the opacity.

8.6 Radiative opacities

8.6.1 The Carson and Sharp opacities and the calculated opacities

The radiative opacities employed in the Standard Pop I and Pop II come from two sources: the low temperature opacities calculated by Carson and Sharp for $T<10^4$ K and the radiative opacities we calculated for $T>10^4$ K.

We calculated the radiative opacities from the formulation in terms of the hydrogen-like model and the average atom models which are established in Chapter III. The formulation succeeded in giving the radiative opacities data for $T>10^4$ K. We compared the opacities we calculated with those calculated by Carson and Sharp and those calculated by Alexander for temperatures below 10^4 K in Section 4.4.3. The comparisons show good agreement of the calculated opacities with the other two sources at temperatures around 10^4 K. We also see that at temperatures below 10^4 K the calculated opacities can be greater than the Carson and Sharp opacities. The maximum difference can be as big as $\Delta\log\kappa=0.2$ at $\log T=3.8$. From the investigation of the opacity model in Section 3.7 and the data plotted in Figure 3.6 we may think that the formula of negative hydrogen absorption presented by Tsuji (1960)

which we employed could be responsible.

The opacities calculated by Carson and Sharp include the contribution from a great number of molecular absorbers. They were combined with the calculated opacities in terms of a linear combination in Section 4.4.

8.6.2 Alexander opacities

The Standard Pop I and Pop II models were calculated using the Carson and Sharp opacities as the low temperature opacities for $T<10^4$ K. In Section 6.2.6 the Alexander opacities were used to calculated the Standard Pop I models instead of the Carson and Sharp opacities. The comparison of the calculated results indicates no considerable difference between using two sets of opacity data. However the calculation of zero age models could not succeed for the models with masses below 0.15 M_{sun} when using the Alexander opacities.

In Section 4.4.2 and Figure 4.4 the comparison of two sets of opacity data shows that they basically agree with each other at temperatures above logT=3.5. Below this temperature, however, the Alexander opacities start to be greater than the Carson and Sharp opacities, and can be greater by a factor up to 5. The temperature of logT=3.5 is just that below the effective temperature of the zero age model of mass 0.15 M_{sun} below which the use of the Alexander opacities cannot allow us to obtain a convergent solution. We may therefore think that the difference between two sets of opacity data at temperatures below logT=3.5 can affect the limit model of the lower main sequence.

8.6.3 Christy formula opacities

The Christy formula opacities were used to calculate the LM star models with the input physics and other model parameters as the same as those for the Standard Pop I in Section 6.2.7 . The comparison of the calculated results with the Standard Pop I models shows that the zero age models calculated using the Christy formula opacities have lower effective temperatures for the models with masses below 0.5 M_{sun}. The difference in effective

temperatures can be as big as $\Delta \log T_{eff}=0.03$, which is shown in Figure 6.14 and 6.15. However, there is no significant difference in luminosities of the models.

The reason why the Christy formula opacities cause the lower main sequence models to be cooler may be found by the comparison with the Carson and Sharp opacities. Section 4.2.2 and Figure 4.5 show that the Christy formula opacities are mostly greater than the Carson and Sharp opacities for temperatures below logT=3.7. We may therefore conclude that the greater values of low temperature opacities cause cooler effective temperatures of LM star models.

In fact, many studies which use opacities including a molecular contribution have shown that the increase of the low temperature opacities by molecular absorption shifts the lower main sequence to cooler effective temperatures. This agrees with the conclusion we get.

8.7 Equation of state (EOS)

8.7.1 EOS with nonideal effects

The EOS we employed was formulated according to the theory of the grand canonical ensemble in Section 2.4. It includes the general atomic configurations of any elements as well as the molecular hydrogen configurations. The interatomic interactions are simulated by a simple atomic model and are incorporated into the EOS by the occupation probability and the perturbation of electron energy levels.

The interatomic interactions lead to two nonideal effects in the EOS. One is the pressure ionization of bound configurations. At low temperatures below 10^5 K, the pressure of H_2, HI, HeI and HeII occur successively when the mass density increases from 10^{-2} g/cm^3 to 10^2 g/cm^3. The other effect is the nonideal terms of the gas pressure and energy density which are the results of the interatomic interactions. The importance of the nonideal effects on thermodynamic quantities can be seen in Figure 2.5 which shows that the nonideal terms dominate thermodynamic properties of the gas with temperatures below 10^4 K and densities around 1.0 g/cm^3 . The EOS established in Section 2.4 has been used to produce

the thermodynamic quantities for the calculation of the Standard Pop I and Pop II models. We called it the standard EOS.

8.7.2 Modified EOS

In order to investigate the nonideal effects of the EOS on the LM star models, we artificially changed the interatomic interaction model used in the EOS and made another EOS which we called the modified EOS (see Section 2.5). Compared with the Standard Pop I models, the LM star models calculated using the modified EOS have much cooler effective temperatures for masses below 0.4 M_{sun} although the luminosities are not changed considerably. The difference in effective temperatures increases as the model mass decreases and can be as big as $\Delta \log T_{eff}=0.08$ for the model of 0.1 M_{sun}.

The shift of temperature of the lower main sequence stars to be cooler values is due to the depression of pressure ionization in the EOS. The study in Section 2.5.2 and Figure 2.1-2.4 shows that the modified EOS makes pressure ionization occur in the density range from 1.0 g/cm^3 to 10^4 g/cm^3, in contrast to that from 10^{-2} g/cm^3 to 10^2 g/cm^3 calculated by the standard EOS. So we conclude that weaker pressure ionization shifts the LM star models to cooler effective temperatures.

8.7.3 Oscillating solutions of very LM star models

In the calculation of zero age models of the Standard Pop I and Pop II, we found oscillating solutions for the models with masses around 0.1 M_{sun} (see Section 6.1.1). The successive solutions oscillate within a range and probably between two values (see Table 6.2). This may suggest that there could be two solutions for a one mass model of very LM star.

The calculation of 0.1 M_{sun} model by using the modified EOS shows that the oscillating solutions converge to one solution (see Section 6.2.9 and Table 6.15). The difference between the standard EOS and the modified EOS is only the contribution from the nonideal effects. So we may conclude that the nonideal effects in the EOS is responsible for the oscillating solutions of the very LM star models.

The problem of the oscillating solution of the very LM star is quite interesting because it could mean the existence of two solutions for stellar models. In our further study which is not presented in the thesis we found that the nonideal effects in the EOS leads to very unsmoothed derivatives of the pressure and internal energy with respect to the density. This could be the real reason of the existence of oscillating solutions.

8.8 Comparison with observed data

8.8.1 Comparison with the binary stars

The zero age models of the standard Pop I and Pop II were compared with the observed data of some binary stars. The comparisons in the Section 6.1.4 and Figure 6.1-6.4 indicate good agreement for the models with effective temperatures above logT=3.5, which corresponds to the models with masses greater than 0.15 M_{sun}. For the models near the main sequence limit, the observed data are somewhat cooler than the theoretical models. This result has also been found by other studies of LM star models (see Section 6.3 and Figure 6.19). We also found that the uncertainty of the nonideal effects in the EOS can affect the theoretical models considerably.

8.8.2 Solar evolutionary model

The solar mass model in the Standard Pop I has been calculated for its evolution sequence for which the atmospheric model was used as surface condition. The calculated results show that a perfect theoretical model of solar evolution is obtained when the element abundances are chosen to be 0.70/0.28/0.02 and the mixing length ratio to be 1.5. The element abundances were found to be sensitive parameters in the solar evolutionary model.

8.9 Concluding marks

The low temperature opacities and the EOS with nonideal effects are the most important elements of the input physics in the determination of theoretical models of LM stars. Therefore, the agreement of the theoretical models, we calculated, with the observed data

examined the validity of the Carson and Sharp opacity as well as the formulation of our EOS. In addition, the radiative opacities data for $T>10^4$ K that we calculated were also examined in the calculation of the solar evolutionary model. The problem of the oscillating solutions motivates our interest in the study of the nonideal effects in the EOS on the models of the very LM star models.

References

Allen C W, 1973, Astrophysical Quantities (3rd ed, University of London, the Athlone Press).

Alexander D R, 1975, Ap J Suppl 29:363.

Alexander D R, Johnson H R & Rypma R L, 1983, Ap J 272:773.

Baker N & Kippenhahn R, 1962, Z Astrophys 54:114.

Baker N H & Temesvary S D, 1966, Tables of convective stellar envelopes (Goddard Institute for Space Studies).

Bahcall J N & Soneira R M, 1981, Ap J Suppl 357:401.

Bahcall J N, 1984a, Ap J 276:156.

Bahcall J N, 1984b, Ap J 276:169.

Bahcall J N, 1986, in Astrophysics of Brown Dwarfs (Cambridge Univ Press).

Berrington et al, 1987, J Phys B 20:6379.

Berriman G & Reid N, 1987, M N R A S 227:315.

Böhm-Vitense E, 1958, Z Astrophys 46:108.

Bowers R L & Deeming T, 1984, Astrophysics I : Stars (Jones and Bartlett Publisher, INC).

Cameron A G W, 1971, Space Science Reviews 15:121.

Carson T R, 1966, J Quant Spectrosc Radiat Transfer 6:563.

Carson T R & Hollingsworth H M, 1968, M N R A S 41:77.

Carson T R, Mayers D F & Stibbs D W N, 1968, M N R A S 140:483.

Carson T R, 1971, Progress in High Temperature Physics and Chemistry, 3:99 (Oxford and New York : Pergamon).

Carson T R, 1972, in Stellar Evolution (Cambridge, Mass: MIT Press).

Carson T R, 1976, Ann Rev Astron Astrophys 14:95.

Carson T R, 1987, Radiative Properties of Hot Dense Matter III (World Scientific) p372.

Carson T R, 1988a, Astron Ap 189:319.

Carson T R, 1988b, Astron Ap Suppl 75:385.

Carson T R & Sharp C M, 1991, in preparation.

Chandrasekhar S, 1939, Intr. Principles of Stellar Structure (Cambridge).

Clayton D,1968, Principles of Stellar Evolution and Nucleosynthesis (McGraw-Hill).

Chiu H Y, 1968, Stellar Physics, Vol I (Blaisdell Publishing Company).

Copeland H, Jensen J O & Jorgensen H E, 1970, Astron Ap 5:12.

Cox A N 1965, Stars and Stellar Systems, Vol 8 (Univ of Chicago Press).

Cox A N, Stewart J N & Eilers D D, 1965, Ap J Suppl 11:1.

Cox A N & Giuli R T, 1968, Principles of Stellar Structure (Gordon and Breach, Science Publishers).

Cox A N & Tabor J E, 1976, Ap J Suppl 31:271.

Cox A N & Stewart J N, 1970a, Ap J Suppl 19:243.

Cox A N & Stewart J N, 1970b, Ap J Suppl 19:261.

Cox A N, Shaviv G & Hodson S W, 1981, Ap J, 245:L37.

D'Antona, F, & Mazzitelli, I, 1975, Astron Ap 42:165.

D'Antona F & Mazzitelli I, 1982, Astron Ap 113:303.

D'Antona F & Mazzitelli I, 1983, Astron Ap 127:149.

D'Antona F & Mazzitelli I, 1985, Ap J 296:502.

Dappen W, Mihalas D, Hummer D G & Mihalas B W, 1988, Ap J 332:261.

Dimitrijevi M S & Konjevic N, 1987, Astron Ap 172:345.

Dorman B, Nelson L A, Chau W Y, 1989, Ap J, 342:1003.

Doughty N A, Fraser P A & McEachran R P, 1966, M N R A S 132:255.

Doughty N A & Fraser P A, 1966, M N R A S 132:267.

Eggleton P P, 1971, M N R A S 151:351.

Ezer D W & Cameron A G W, 1967, Canadian J Phys 45:3461.

Faber S M & Gallagher J S, 1978, Ann Rev Astron Ap 17:135.

Fermi E, 1924, Z Phys 26:54.

Fontaine G, Van Horn H M, Bohm K M & Grenfell T C, 1975, Ap J 193:205.

Fontaine G, Graboske H C & Van Horn H M, 1977, Ap J Suppl 35:293.

Fowler W A, Caughlan G R & Zimmerman B A, 1967, Ann Rev Astron Astrophys 5:525.

Fowler W A, Caughlan G R & Zimmerman B A, 1975, Ann Rev Astron Astrophys 13:69.

Frank-Kamenetskii D A & Albertovich P, 1962, Physical Processes in Stellar Interiors (Jerusalem : Israel Program).

Gaustad J E, 1963, Ap J 138:1050.

Goldberg A, Rozsnyai B F & Thompson P, 1986, Phys Rev A 34:421.

Goldwire H C, 1968, Ap J Suppl, 17:445.

Graboske H C Jr, Harwood D J & Rogers F J,1969, Phys Rev186:210.

Griem H R, 1961, Phys Rev 5:1490.

Griem H R, Kolb A C & Shen K Y, 1959, Phys Rev 116:4.

Grossman A S & Hays D, 1974, Astron Ap 30:95.

Grossman A S & Graboske H C,1971, Ap J 174:475.

Grossman A S, Hays D & Graboske H C,1974, Astron Ap 30:95.

Harris G, 1975, Introduction to Modern Theoretical Physics : Vol I and Vol II (A wiley-interscience Publication).

Harris M J, Fowler W A, Caughlan G R & Zimmerman B A, 1983, Ann Rev Astro Astrophys 21:165 .

Hayashi C & Nakano T, 1963, Prog Theor Phys, 30:460.

Heitler W, 1954, The Quantum Theory of Radiation (Oxford University Press).

Henyey L G, Wilets L, Bohm K H, et al, 1959, Ap J, 129:628.

Henyey L G, Forbes J E & Gould N L, 1964, Ap J, 139:306.

Hubbard W B & Lampe M, 1969, Ap J Suppl 18:297.

Huebner W F, 1986, Physics of the Sun (Reidel Publishing).

Hofmeister E, Kippenhahn R & Weigert A, 1964, Z Astrophys 59:215.

Humlicek J, J Quant Spectrosc Radiat Transfer 21:309.

Hummer D G & Mihalas D, 1988 Astrophys J 331:749.

Ichimaru S, Tanaka S & Iyetomi H, 1984, Phys Rev 29:2033.

Ichimaru S, 1983, Rev Mod Phys 54:1017.

Iglesias C A & Rogers F J, 1991, Ap J 371:L73.

Jancovici B, 1977, J Stat Phys 17:357.

John T L, 1988, Astron Ap 193:189.

Karzas W L & Latter R, 1961, Ap J Suppl 6:167.

Kippenhahn R, Weigert A & Hofmeister E, 1967, Methods in computational physics, Vol 7 (Academic Press).

Kramers H A, 1923, Phil Mag 46:836.

Kroupa P, Tout C A & Gilmore G, 1990, M N R A S 244:76.

Kumar S S, 1963a, Ap J 137:1121.

Kumar S S, 1963b, Ap J137:1126.

Kumar S S, 1972, Astrophys Space Sci 17:216.

Lamb D Q & Van Horn H M, 1975, Ap J 200:306.

Lampe M, 1968a, Phys Rev 170:306.

Lampe M, 1968b, Phys Rev 170:276.

Lee T D, 1950, Ap J 111:625.

Liebert J & Probst R G, 1987, Ann Rev Astron Astrophys 25:473.

Limber D N, 1985, Ap J 127:387.

Lifshitz E M & Pitaevski L P, 1980, Statistical Physics : Vol I (Oxford : Pergamon Press)

Linden Ven der T J, 1987, Astron Ap 171:87.

Magni G & Mazzitelli I, 1979, Astron Ap 72:134.

Magee N H, Merts Jr A L & Huebner W F, 1984, Ap J 283:264.

Marshak R E, 1941, Ann N Y Acad sci 41:49.

Marcy W M & Benitz H J, 1989, Ap J 344:441.

Mayer H, 1948, Reports LA-647 (AECD-1870), (1947), Los Alamos Scientific Lab.

Menzel D H, 1969, Ap J Suppl 18:221.

Mestel L, 1950, Progs Cambridge Phil Soc 46:331.

Mihalas D, Dappen W & Hummer D G, 1988, Ap J 331:815.

Neece G D, 1984, Ap J 277:738.

Nelson L A, Rappaport S A & Joss P C, 1985, Nature 316:1003.

Nelson L A, Rappaport S A & Joss P C, 1986, Astrophys J, 311:226.

Nelson L A, Rappaport S A & Joss P C, 1986a, Astrophys J, 304:231.

Nelson L A, Rappaport S A & Joss P C, 1986b, Astrophys J, 311:226.

Nelson L A, Rappaport S A & Joss P C, 1986c, in Astrophysics of Brown Dwarfs (Cambridge Univ Press).

Oort J H, 1965, in Stars and Stellar Systems, Vol 5, Galactic Structure (Univ of Chicago Press).

Ostriker J P & Peebles P J E, 1973, Ap J 186:467.

Peytremann E, 1974, Astron Ap 33:203.

Pathria, R K, 1984, Statistical Mechanics (Pergamon Press).

Popper D M, 1980, Ann Rev Astr Astronphys 18:115.

Rappaport S & Joss P C, 1982, Ap J 254:616.

Rappaport S, Verbunt F & Joss P C, 1983, Ap J 275:713.

Rappaport S & Joss P C, 1984, Ap J 283:232.

Reid N & Gilmore G, 1984, M N R A S 206:19.

Roger F J, Phys Rev A 10:2441.

Rosseland S, 1924, M N R A 84:525.

Rozsnyai B F, 1972, Phys Rev A 5:1137.

Rozsnyai B F, 1989, Ap J 341:414.

Salpeter E E, 1955, Ap J 121:161.

Salpeter E E & Van Horn H M, 1969, Ap J 155:183.

Seaton M J, 1987, J Phys B 20:6363.

Seaton M J, 1987, J Phys B 20:6431.

Senden L, Johnson H R & Krupp B M, 1976, Ap J 204:281.

Sienkiewicz R, 1982, Acta Astr 32:275.

Simon N R, 1982, Ap J 260:L87.

Slater J C, 1955, Phys Rev 98:1039.

Tsakiris G D & Eidmann K 1987, J Quant Spectrosc Radiat Transfer 38:353

Tsuji T, 1966, Publ A S Japan 18:127.

Tsuji T, 1971, Publ A S Japan 23:553.

Upgren A R & Weiss E W, 1975, Ap J 197:L53.

VandenBerg D A, Hartwick F D A, Dawson P & Alexander D R , 1983, Ap J 266:747.

Vardya M S, 1960, Ap J Suppl 4:281.

Vardya M S, 1961, Ap J 133:107.

Veeder G J, 1974, Astron J 79:1056.

Yan Y & Seaton M J, 1987, J Phys B 20:6409..

Yan Y, Taylor K T & Seaton M J, J Phys B 20:6399.

Zwicky F, 1983, Helv Phys Acta 6:110.